Phase behavior of mixtures of magnetic colloids and non-adsorbing polymer

Fasegedrag van mengsels van magnetische colloïden en niet-adsorberend polymeer

(met een samenvatting in het Nederlands)

Proefschrift

ter verkrijging van de graad van doctor aan de Universiteit Utrecht op gezag van de Rector Magnificus, prof. dr. H.O. Voorma, ingevolge het besluit van het College voor Promoties in het openbaar te verdedigen op maandag 22 januari 2001 des middags te 14.30 uur

door

Gerard Antonie van Ewijk

geboren op 22 november 1971, te Zeist

Promotor: Prof. dr. A. P. Philipse

Co-promotor: Dr. G. J. Vroege

Beiden verbonden aan de Faculteit Scheikunde van de Universiteit Utrecht.

Contents

1

General introduction on magnetic fluids

1.1   Magnetism

1.1.a   Atomic magnetism, paramagnets and diamagnets [1-3]

Wherever electrical currents flow, magnetic fields are generated. Within atoms, the orbital motions of electrons around the nucleus and protons within the nucleus produce magnetic fields. In addition, the spinning motion of electrons, proton, and neutrons around their axes generate magnetic fields. However, because the contribution to the induced magnetic field of nucleons is typically two thousand times smaller than that of electrons, it is usually neglected.

In case of current loops, the generated magnetic field strength is conveniently written as being proportional to the magnitude (*current*)×(*loop area*) of the magnetic moment **m**, a vectorial quantity. Many atoms have a permanent non-zero magnetic moment, in the order of 10^{-23} A m^2. The net magnetic moment of an assembly of atoms, however, is generally zero due the random orientation of atomic moments within the assembly (see figure 1.1a). The net magnetic moment can be changed by bringing the assembly into an external magnetic field **H**. This effect of **H** can usually be expressed as **M**=χ**H**, where $\mathbf{M} = \sum_i \mathbf{m}_i / V$ is the magnetization (net dipole moment per unit volume), *V* the volume of the system, and χ the susceptibility, describing the strength of the response to an external magnetic field. Microscopically, the effect of the external field is twofold. First, the external field exerts a torque **τ**=**m**×**H** on the atomic moments that forces them to align with **H**. Since Brownian rotation counteracts the alignment, the degree of alignment depends on the magnetic field strength and temperature. The alignment of dipoles with **H** gives a positive contribution to χ, called the *paramagnetic* susceptibility. Second, the external field induces a change in the orbital motion of electrons, thereby producing a magnetic field that opposes the external field. Accordingly, this effect gives a negative contribution to χ, called the *diamagnetic* susceptibility. The diamagnetic susceptibility is independent of temperature, and is present in all atoms, regardless of the presence of a permanent magnetic moment.

Depending on the sign of the total susceptibility, materials are classified as *paramagnets* (χ>0, and of the order of 10^{-5} to 10^{-3}) or *diamagnets* (χ<0, typically -10^{-5}).

1.1.b   Ferromagnets, antiferromagnets and ferrimagnets [1,2]

In the previous section, magnetic materials were treated as systems containing atoms with non-interacting dipoles. In some materials, however, strong dipole-dipole interaction of quantum-mechanical   origin   causes   long   range   orientational   correlations   of
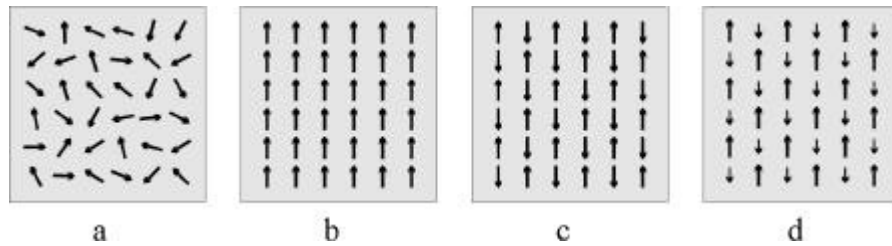
Figure 1.1. *Dipole orientations in four types of magnetic materials: (a) paramagnet; (b) ferromagnet; (c) antiferromagnet; (d) ferrimagnet.*

the permanent atomic dipoles. In metallic iron, for example, dipolar interaction favors parallel alignment of the dipoles (figure 1.1b), hence this material has a net magnetization even in the absence of an external field. Materials with this kind of ordering of dipoles are called *ferromagnets*, and are characterized by a high susceptibility, typically between 10^{-2} and 10^{6}, which, moreover, depends on the field strength. Above the so-called Curie temperature, which is material-specific, the dipolar ordering inside a ferromagnet is lost and the material becomes a paramagnet.

Dipolar interaction does not always lead to net magnetization. In some materials, named *antiferromagnets*, neighboring dipoles are aligned antiparallel (figure 1.1c). Consequently, such materials do not have a net magnetization in the absence of an external field, and have a low susceptibility, generally between 0 and 10^{-2}. At the so-called Néel temperature, a transition from antiferromagnetic ordering to paramagnetic occurs.

Ferrimagnets form a third class of magnetic materials with ordered dipoles. On the microscopic scale, ferrimagnets are similar to antiferromagnets, with antiparallel arrangement of neighboring dipoles. However, because the number (or magnitude) of dipoles pointing in one direction differs from the number pointing in the opposite direction, ferrimagnets have a non-zero magnetization in zero field (figure 1.1d). Thus, ferrimagnets resemble ferromagnets on the macroscopic scale. Due to partial cancellation of dipole moments, the magnetization of ferrimagnets is generally lower than that of ferromagnets. The most well-known ferrimagnetic material is magnetite (Fe_3O_4).

1.1.c Magnetic domains [1,3]

The dipole ordering described in the previous section is long ranged, but usually does not extend over the entire volume of a sample. Rather, a sample of magnetic material is split up into *domains* in which all dipoles are ordered along a preferential direction (figure 1.2). This direction changes from domain to domain, and it is for this reason that bulk magnetic materials may as a whole be unmagnetized, even though they are
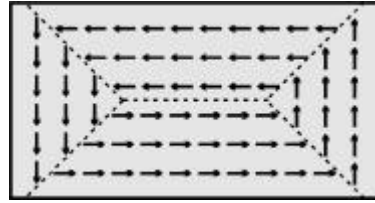
Figure 1.2. *In bulk ferromagnetic materials, dipole alignment is split up into domains.*

magnetized on the length scale of the domains.

In an external magnetic field, the magnetization directions of the domains are forced to align with the field, or domains with favorable magnetization direction will grow at the cost of domains with unfavorable directions. Both mechanisms increase the net magnetization of the bulk material. At infinite magnetic field strength, all dipoles are aligned with the field, and the system has reached its saturation magnetization.

After the field is removed, the magnetization tends to relax into its original state with randomly oriented domains. However, in order to reach that equilibrium state, the system may have to pass unfavorable states that can keep it from actually reaching equilibrium. Materials for which the relaxation to the unmagnetized state is prevented, are called *hard magnetic*, as opposed to *soft magnetic* materials, which demagnetize quickly upon removal of the external field or application of a small field opposing the magnetization.

1.2   Magnetic fluids

1.2.a   Introduction

Unlike paramagnets and diamagnets, which can be gaseous, liquid or solid, ferromagnets are almost exclusively solid[1]. There exist, however, liquids with a susceptibility of roughly 1, not as high as many ferromagnets but still orders of magnitudes higher than that of paramagnets. Moreover, like ferromagnets these liquids can easily approach their saturation magnetization. These so-called *magnetic fluids* or *ferrofluids* are actually two-phase systems, comprised of small solid ferro- or ferrimagnetic particles dispersed in a liquid [6-8]. Because the size of the particles is in the colloidal range, i.e. between about 1 and 1000 nm, these particles are often referred to as magnetic colloids.

Although intensive research on magnetic fluids did not start until the 1960s, the preparation of

---

[1] *Only very few exceptions are known, such as liquid ^{3}He [4] and undercooled, metastable melts of $Co_{80}Pd_{20}$ [5].*

(water-based)   magnetic   fluids   had   already   been   described   in   1938   by
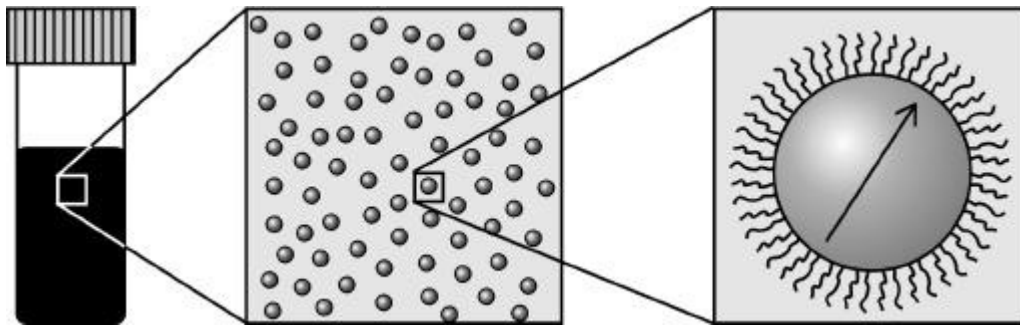

Figure 1.3. Schematic drawing of a ferrofluid on three length scales. On the macroscopic length scale (left), it resembles an ordinary liquid. On the colloidal length scale (middle), the fluid is appears to consist of small solid particles dispersed in a liquid. Each particle consists of a single domain magnetic iron oxide core, and a surface grafted with polymer chains (right).

Elmore [9]. The first ferrofluids were primarily used as a means to study magnetic domain structures in solids. Three decades later, Papell [10] and Rosensweig [11] developed the synthesis of oil-based ferrofluids, which are still used today. The most commonly used ferrofluid contains spherical magnetite particles with a typical size of 10 nm, dispersed in an apolar solvent. Sedimentation of these particles is sufficiently counteracted by their Brownian motion to keep them dispersed for years. A prerequisite for such long-term stability is that particles do not aggregate, since aggregates sediment faster and have slower Brownian motion to compensate for sedimentation. Unfortunately, without special measures magnetite particles will form large clumps that settle quickly. To prevent aggregation, the colloids can be covered with a thin layer of polymer, commonly a monolayer of oleic acid, which makes the particles soluble in many organic solvents. A schematic drawing of a ferrofluid, seen on three length scales, is shown in figure 1.3.

Because of their small size, these magnetic colloids contain a single magnetic domain, and therefore have a permanent magnetic moment proportional to their volume. Although magnetic colloids are ferromagnetic on the molecular scale, they resemble a paramagnet on the colloidal scale, with the major difference that the magnetic moments of magnetic colloids are much larger than the moments in a paramagnet (typical values are 10^{-19} A m^2 for magnetic colloids and 10^{-23} A m^2 for paramagnets). It is for this reason that ferrofluids are sometimes called *superparamagnetic*. In order to be (super)paramagnetic, the dipole moment of each particle must be free to rotate on the time scale of experiments. Two modes of rotation are operative in magnetic colloids. One is Brownian rotation, with a relaxation time

$$\tau_B = \frac{3v\eta_0}{kT} \quad , \tag{1.1}$$

where v the volume of the particle, η_0 the viscosity of the solvent, k the Boltzmann constant and T the temperature. For 10-nm colloids in a solvent with $\eta_0=10^{-3}$ Pa s, τ_B is $4 \ 10^{-7}$ s. The other mode of rotation is Néel rotation, which involves rotation of the magnetization with respect to the crystal lattice of the magnetic colloid. The relaxation time for this process is

$$\tau_N = f_0^{-1} \exp\left[\frac{Kv}{kT}\right] \quad , \tag{1.2}$$

where K is the (material-dependent) anisotropy constant, and f_0 is the Larmor frequency, about 10^9 s^{-1}. Clearly, the Néel relaxation time stronly depends on the particle volume. For example, the τ_N of magnetite colloids (K=1.1 10^4 Jm^{-3} [7]) increases from $4 \ 10^{-9}$ s to $7 \ 10^{-5}$ s upon increasing the particle diameter from 10 nm to 20 nm.

1.2.b   Applications of magnetic fluids

An important property of concentrated ferrofluids is that they are strongly attracted by permanent magnets, while their liquid character is preserved. The attraction can be strong enough to overcome the force of gravity. Many applications of ferrofluids are based on this property [7]. For example, ferrofluids are widely used as lubricating, airtight seals in rotary shafts. A magnetic field gradient keeps the ferrofluid in place, even in case of pressure differences between the two separated compartments. Today, many computer hard disk drives contain a ferrofluid-sealed shaft. Ferrofluids are also used to improve heat dissipation in loudspeaker coils, enabling higher output power.

When non-magnetic objects are immersed in a ferrofluid and subjected to the field gradient of a permanent magnet, the objects will be effectively repelled by the magnet (actually, the ferrofluid is attracted and drives away the object). When combined with a gravitational or centrifugational force opposing the effective magnetic force, this effective repulsion has the same effect as a density gradient in the solvent. This principle is used to separate materials into density fractions, for instance in the mining industry or waste processing [12]. Because the effective 'density' of ferrofluids can be much higher than that of ordinary liquids, density-based separation with ferrofluids is also suitable for high density materials such as metals.

In the aforementioned applications, the ferrofluid was considered to be homogeneous. However, structural changes can occur on a microscopic level when magnetic fluids are subjected to a magnetic field. Because an external field aligns the dipole moments of magnetic colloids, it can increase the average interaction strength between magnetic colloids sufficiently

to induce aggregation of the colloids into concentrated, micron-sized droplets [13]. Because the size of such droplets is comparable to the wavelength of light, the optical properties of ferrofluids depend on the direction and strength of the external field. Optical devices employing the strong magneto-optical effects of magnetic fluids are still in development [7,14,15].

1.2.c   Phase behavior of magnetic fluids

The macroscopic properties of ferrofluids not only depend on the properties of single particles, but also on their mutual interaction. As can be inferred from the previous section, some applications depend on the stability of ferrofluids, others depend on their *in*stability. In addition to the irreversible aggregation mentioned in section 1.2.a, aggregation may also be reversible. Because of the colloid's Brownian motion, the behavior of a magnetic fluid is dictated by thermodynamics, so given the characteristics of the magnetic colloids, the temperature and concentration, the system adapts a state or phase that minimizes its free energy.

The anisotropic nature of magnetic interaction leads to a rich phase behavior of magnetic fluids. For example, because magnetic interaction favors head-to-tail configurations of magnetic colloids, worm-like structures can be expected in dilute solutions of strongly interacting magnetic colloids [16]. In concentrated magnetic fluids, calculations suggest that strong interaction may lead to macroscopic parallel alignment of dipole moments, yielding a liquid permanent magnet [17,18]. These two phases have not yet been found experimentally, and some even question if the spontaneously magnetized liquid exists at all [19]. Another unresolved and actively debated issue is whether magnetic attraction can give rise to gas-liquid separation [20], i.e. spontaneous separation of an initially homogeneous magnetic fluid into two fluids with different concentrations.

Interactions between magnetic colloids can be modified by applying an external field, thereby enriching the phase behavior. The external field will align magnetic moments of colloids along the field, thereby increasing their average strength of interaction. This can also lead to gas-liquid phase separation [17,18], though in this case both fluid phases are magnetized. Field-induced phase separation has been experimentally demonstrated [13], but the factors influencing this type of phase instability of magnetic fluids are only partly understood, both theoretically and experimentally.

1.3   Outline of this thesis

In this thesis, the relation between the microscopic and macroscopic properties of magnetic

fluids is investigated. The subject is dealt with experimentally as well as theoretically. This research on dipolar colloids is an extention of the research previously done at the Van 't Hoff Laboratory on other model colloids, such as spherical [21], rod-like [22] and plate-like [23] colloids.

Chapter 2 describes the synthesis of several types of magnetic colloids, all based on 10-nm magnetite particles. The interaction strength between these colloids ranges from very weak to very strong. Weakly interacting colloids are prepared by covering the magnetic core by a non-magnetic shell. Magnetizable colloids that interact strongly in a magnetic field are obtained by making composite colloids, consisting of large silica spheres covered by many small magnetite particles.

In **chapter 3**, several theories describing the magnetic susceptibility of dipolar hard spheres, a model for magnetic colloids, are tested against measurements on oleic acid stabilized magnetite colloids in cyclohexane. The polydisperse ferrofluid is fractionated by means of partial precipitation, yielding a fraction of large particles with relatively strong dipolar interaction. The concentration dependence of the susceptibility of both the unfractionated and the fractionated ferrofluid deviates from all prevailing theories, though for some of them deviations are not large.

Apart from magnetic interaction, the stability of ferrofluids is also influenced by non-magnetic constituents, such as an excess polymeric stabilizer. Chapters 4 to 6 deal with the phase behavior of magnetic fluids-polymer mixtures, where the non-adsorbing polymer acts as a destabilizing agent. In **chapter 4**, the phase diagram of magnetic colloid-polymer mixtures is treated theoretically by incorporating magnetic interactions into a well-known mean field theory for non-magnetic colloids-polymer mixtures. Calculations with this theory show that the interactions in common ferrofluids are too weak to explain the observed field-induced phase separation. The presence of free polymer, however, may account for the experimentally observed instabilities. Chapters 5 and 6 describe experiments on phase behavior of magnetic colloid-polymer mixtures. Phase instabilities are detected and characterized with a Colpitts oscillator, which is used as a local concentration meter. The principle of operation of this device and its application to the study of the phase behavior of magnetic colloids and polymers in absence of an external magnetic field is described in **chapter 5**. In **chapter 6**, the destabilizing influence of an external field is investigated. It is shown that, contrary to many experimental observations but in line with theoretical prediction, the ferrofluid investigated here is stable at any concentration and field strength. This may be due to the high quality (absence of clusters) of the investigated ferrofluid. In addition, the influence of an applied field on the stability of ferrofluid-polymer mixtures agrees quite nicely with the theory described in chapter 4.

Most interactions between colloids are understood, although not always quantitatively known. For example, in addition to magnetic interaction magnetic colloids experience Van der Waals attraction, the strength of which is often uncertain. Sometimes, however, colloids exhibit unexpectedly strong interaction which can not be explained by the usual theories. In **chapter 7**, experimental evidence is presented for the presence of a strong, anomalous attraction between small magnetite colloids and large silica spheres, leading to irreversible adsorption of magnetite on silica. Textbook theories fail to describe the strength of the interaction and the very slow kinetics of the adsorption process. A proposed proton transfer between the magnetite and silica colloids is consistent with the experiments.

References

1   D. Jiles, 'Introduction to magnetism and magnetic materials', Chapman & Hall, London (1991).

2   D. Craik, 'Magnetism, principles and applications', John Wiley & Sons, Chichester (1995).

3   E. M. Purcell, 'Electricity and magnetism', McGraw-Hill, New York (1963).

4   T. Lang, P. L. Moyland, D. A. Sergatskov, E. D. Adams, and Y. Takano, *Phys. Rev. Lett.* **77**, 322 (1996).

5   D. Platzek, C. Notthoff, D. M. Herlach, G. Jacobs, D. Herlach, and K. Maier, *Appl. Phys. Lett.* **65**, 1723 (1994).

6   R. E. Rosensweig, 'Ferrohydrodynamics', Cambridge University Press, Cambridge (1985).

7   'Magnetic fluids and applications handbook', ed. B. Berkovski and V. Bashtovoy, Begel House Inc., New York (1996).

8   E. Blums, A. Cebers, and M. M. Maiorov, 'Magnetic fluids', Walter de Gruyter, Berlin (1997).

9   W. C. Elmore, *Phys. Rev.* **54**, 309 (1938).

10   S. S. Papell, U.S. Patent 3,215,572 (1965).

11   R. E. Rosensweig, J. W. Nestor, and R. S. Timmins, in 'Mater. Assoc. Direct Energy Convers. Proc. Symp. AIChE-I. Chem. Eng. Ser. 5' (1965), p. 104.

12   J. Shimoiizaka, K. Nakatsuka, T. Fujita, and A. Kounosu, *IEEE Trans. Magn.* **MAG-16**, 368 (1980).

13   R. E. Rosensweig and J. Popplewell, in 'Electromagnetic Forces and Applications', ed. J. Tani and T. Takagi, Elsevier Science Publishers, Amsterdam (1992), p. 83.

14   S. Taketomi, U.S. Patent 4,812,767 (1989).

15   H.-E. Horng, C.-Y. Hong, W. B. Yeung, and H.-C. Yang, *Applied Optics* **37**, 2674 (1998).

16   P. G. De Gennes and P. A. Pincus, *Phys. Cond. Matter* **11**, 189 (1970).

17   A. O. Tsebers, *Magnetohydrodynamics* **18**, 137 (1982).

18   K. Sano and M. Doi, *J. Phys. Soc. Jpn.* **52**, 2810 (1983).

19   L. Onsager, *J. Am. Chem. Soc.* **58**, 1486 (1936).

20   P. I. C. Teixeira, J. M. Tavares, and M. M. Telo da Gama, *J. Phys.* **12**, R411 (2000).

21   A. K. van Helden and A. Vrij, *J. Colloid Interface Sci.* **78**, 312 (1980).

22   P. A. Buining, C. Pathmamanoharan, J. B. H. Jansen, and H. N. W. Lekkerkerker, *J. Am. Ceram. Soc.* **74**, 1303 (1991).

23   F. M. van der Kooij, E. Kassapidou, and H. N. W. Lekkerkerker, *Nature* **406**, 868 (2000).

2

Preparation of magnetic colloids

Abstract

Small Fe_3O_4 or γ-Fe_2O_3 particles with a typical diameter of 10 nm can be used for the preparation of several types of magnetic colloids, each type having distinctive properties. This chapter describes the preparation of three types of magnetic colloids. First, a convenient method for grafting iron oxide particles with fatty acids, in particular oleic acid, is described. Such colloids experience magnetic interaction of intermediate strength, and can be used to study the effect of dipole-dipole interaction on the macroscopic behavior of magnetic fluids. Second, an improved procedure for coating small iron oxide particles with a shielding layer of silica is presented, which yields colloids with weak magnetic interaction. And finally, silica spheres with a typical diameter of 0.5 μm are covered with a thin layer of iron oxide particles, giving magnetizable colloids with a magnetic moment depending on the strength of the magnetic field.

2.1   Introduction

Magnetic dispersions with a variety of magnetic materials and solvents are currently available. This chapter describes the preparation of three kinds of magnetic colloids with different characteristics: small, moderately interacting particles with a permanent magnetic moment (figure 2.1a), larger, weakly interacting magnetic particles (figure 2.1b) and large, magnetizable particles (figure 2.1c).

Oleic acid stabilized magnetite in an organic solvent, by now a classical system, is still widely used. Basically two methods are known to graft magnetite with oleic acid: long term grinding of bulk magnetite in the presence of pure surfactant [1] and grafting of surfactants onto chemically precipitated magnetite in an alkaline aqueous solution. The latter method, described by Khalafalla and Reimers [2,3], is still frequently used to synthesize organophilic magnetite. Here we present a new and convenient laboratory-scale preparation method for this type of fatty acid stabilized ferrofluid. Unlike Khalafalla's method, heating is not required and the grafting step takes only a few minutes to complete.

The second type of colloid we investigate are silica spheres with iron oxide cores [4,5]. They are prepared by hydrolyzing tetraethoxysilane (TES) which subsequently polymerizes as silica on the surface of magnetite particles. Since this reaction is carried out in an alkaline ethanol/water mixture, the point of zero charge (PZC) of magnetite must be lowered before these particles can be dispersed in the reaction mixture. Originally, the PZC was lowered by precipitating a very thin silica layer from a metastable sodium silicate solution [4]. However, the PZC can also be lowered by adsorption of citric acid. This makes the tricky precipitation step obsolete, but still allows further silica growth using TES. Such silica particles with a small magnetic core experience weak magnetic dipole-dipole interaction. Such particles can be used, for example, as magnetic tracers in systems where other tracing methods cannot be used.

Silica spheres can also be *covered* with magnetic material. Because the magnetic moments of individual magnetic particles will be randomly oriented, a decorated silica sphere will not have a magnetic moment. However, upon application of a magnetic field, the magnetic moments will align parallel to the field, giving the silica+magnetite sphere as a whole a large magnetic moment parallel to the field. Large, magnetizable (latex) spheres find widespread use in biochemical research, where they are employed for efficient isolation of specific biological material. In physical research, micron-sized magnetizable spheres have been used to study formation and evolution of strings of particles in an applied field [6,7]. Such research may benefit from silica+magnetite when fluorescent silica [8] is used, for fluorescent labeling allows

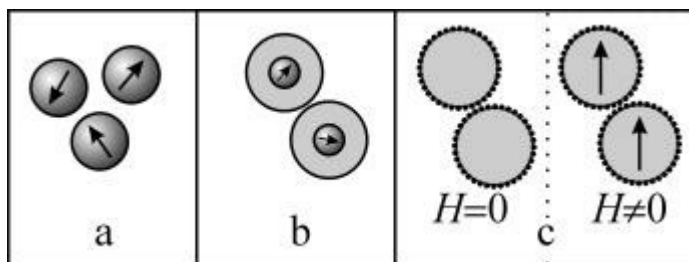such   colloids   to   be

Figure 2.1. *Schematic representation of three types of magnetic colloids. a:small (typically 10 nm) magnetite (Fe_3O_4) particles with permanent magnetic moment; b:like a, but with its magnetic dipole-dipole interaction screened by a layer of silica (SiO_2); c:large (typically 1 μm) magnetizable spheres with a silica core and magnetite shell. Only in a magnetic field will particles of type c have a net magnetic moment.*

investigated with confocal scanning laser microscopy (CSLM). With this technique, three-dimensional images of structures in magnetic dispersions can be investigated [9].

2.2   Experiments

2.2.a   Preparation of maghemite

Magnetite was precipitated by dissolving 2.08 g $FeCl_2$ anh. and 5.22 g $FeCl_3$ anh. in 380 ml demineralized water and adding 20 ml 25% NH_3 to this solution while stirring vigorously [10]. After sedimenting the precipitate with a permanent magnet the supernatant was removed by decantation. 40 ml 2 M HNO_3 was then added to the black sediment and the mixture was stirred for 5 minutes. The oxidation to maghemite was completed by adding 60 ml 0.35 M $Fe(NO_3)_3$ to the mixture and stirring it at its boiling temperature for one hour [10]. After sedimentation and washing with 2 M HNO_3, the reddish yellow sediment was dispersed by adding demineralized water. The resulting black dispersion, coded FF, contained 5.6 g of solid material per liter.

The X-ray diffraction pattern of FF corresponds well to reference patterns for maghemite; other crystalline products could not be detected. The lattice spacing was calculated from the position of the *400*-peak using Bragg's law. This yields a *d*-value of 8.35 Å, which equals the value for colloidal maghemite [11]. From the line broadening of the four most intense diffraction peaks, a particle diameter of 11.5 nm was calculated using Scherrer's equation

[12]. The average diameter $<d>$ can be calculated from this number, knowing that the X-ray diameter equals $<d^3>/<d^2>$ [12]. Using a binomial expansion one can find $<d^n> \cong <d>^n [1+0.5\,n\,(n-1)\,\sigma^2]$. With this approximation a mean particle diameter of 9.0 nm was calculated, assuming σ to have the typical value of 0.4.

2.2.b   *Grafting maghemite with oleic acid*

A typical experiment went as follows. 2 ml FF was diluted by adding 50 ml demineralized water. The sol was flocculated by adding a few drops of 25% NH_3, and sedimented using a permanent magnet. After washing with 50 ml water, 100 ml water was added to the precipitate. Under *mild* mechanical stirring, 2 ml oleic acid was added. Within a few minutes, all magnetic material was transferred to the oil phase. The black oil droplets were separated from the colorless water phase and washed three times with 10 ml ethanol to remove water and excess surfactant. After drying under a gentle nitrogen stream, the particles redispersed easily in cyclohexane. A representative TEM picture of the grafted particles is shown in figure 2.2.

With a small modification, this procedure can also be applied for coating magnetic particles with other fatty acids, such as dodecanoic acid. Since fatty acids with saturated chains are solid at room temperature, the extraction must be performed above the melting temperature of the fatty acid (usually around 50°C). Repeated experiments showed that the amount of water has no noticeable effect on the final product; it merely facilitates stirring. Excessive washing with ethanol did not decrease the stability of the final product. The amount of oleic acid does not play a role as long as it is large; at least 13 ml oleic acid per gram maghemite was needed to extract and stabilize all particles.

The diffuse reflectance IR (DRIFT) spectrum of dried product shows peaks at 1428 and 1531 cm^{-1}, which correspond to the symmetric and asymmetric stretching of carboxylate groups [13]. The presence of carboxylate groups shows that a condensation reaction has occurred between the hydroxylated maghemite surface and the fatty acid. The strong C=O stretching vibration (~1750 cm^{-1}) is absent; apparently washing the precipitate removes all free oleic acid. Thermogravimetry was performed by heating some powder in a nitrogen stream from room temperature to 1200°C at a rate of 10°C min^{-1}. The surface area per oleic acid molecule was calculated from the weight loss at 600-750°C, and amounted to 0.28 nm^2, which agrees with other work [14,15].
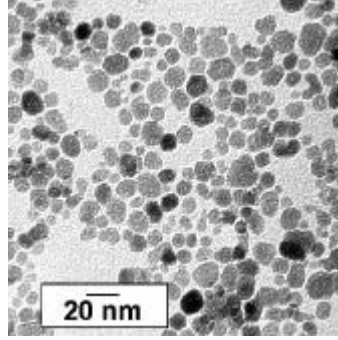
Figure 2.2. *TEM picture of maghemite grafted with oleic acid.*

2.2.c   Silica deposition from a TES solution

The PZC of FF was lowered by adding a 0.01 M citric acid solution [10] to 45 ml FF until flocculation was visible. The precipitate was redispersed by increasing the pH to 7 with tetramethylammonium hydroxide. Of the resulting dispersion 1 ml was added to a mixture of 75 ml ethanol, 20 ml water and 5 ml 25% NH_3. While stirring, 0.1 ml TES was added, and after a day, an additional amount of 0.2 ml TES was added.

TEM photo's show particles similar to those in earlier work [4,5]. The average particle radius is 39.0±8.1 nm. This radius is corrected for the shrinkage of approximately 5% of these particles in the electron microscope. Most of the silica particles contain clusters of magnetic particles; these clusters were also present in the magnetic silica spheres prepared before [4]. An estimate of the number of magnetic particles per silica sphere was made using

$$C = \frac{V_{\text{Fe2O3,total}} / \langle V_{\text{Fe2O3,grain}} \rangle}{V_{\text{m-SiO2,total}} / \langle V_{\text{m-SiO2,grain}} \rangle} = \frac{V_{\text{Fe2O3,total}}}{kV_{\text{TES}} + V_{\text{Fe2O3,total}}} \left(\frac{\langle d^3_{\text{m-SiO2}} \rangle}{\langle d^3_{\text{Fe2O3}} \rangle} \right) \tag{2.1}$$

where d and V indicate diameter and volume, respectively, and $k = V_{\text{SiO2}}^{\text{mol}} / V_{\text{TES}}^{\text{mol}} = 0.1422$. The lower density of TES-hydrolyzed silica is taken into account in the calculation of k. V_{Fe2O3} was calculated from the total mass of γ-Fe_2O_3 and its density. The subscript 'm-SiO2' denotes a magnetic silica particle. Taking $\langle d^3 \rangle \approx \langle d \rangle^3 (1+3\sigma^2)$, an average cluster size of 13 is found. This is roughly twice as large as the estimated cluster size in [4]. Clusters of this size are also thought to be present in other ferrofluids [16].

How silica is linked to the surface of magnetic particles is not resolved, but it is probably anchored on spots where no citric acid is adsorbed. Since gold particles stabilized with citric acid are 'vitreophobic' [17], attachment of silica to citric acid itself seems unlikely.

2.2.d   Adsorption of maghemite on silica spheres

At pH values between the PZC's of silica (PZC≈2) and maghemite (PZC≈7) in water, silica and maghemite are oppositely charged, and upon mixing, adsorption of maghemite on silica due to Coulomb forces is likely to occur. The principle of electrostatic adsorption was employed here to prepare magnetizable silica spheres.

A dispersion of silica spheres with a mean diameter of 460 nm, prepared according to Stöber *et al.* [18], was transferred from the water/ethanol/ammonia mixture it was prepared in to an aqueous nitric acid solution with pH=3.5 by means of centrifugation/redispersion. This procedure was repeated until the pH of the supernatant was 3.5 and remained constant. The pH of an acidic maghemite dispersion was raised to a value of 3.5 by dialysis against a nitric acid solution. The concentrations of the separate silica and maghemite dispersions were diluted to 40 gl^{-1}.

Mixtures with several compositions (see Table 2.1) were prepared by adding silica to maghemite under mechanical stirring. Non-adsorbed maghemite was removed by centrifugation/redispersion of the silica+maghemite spheres. After repeated purification steps, the sediment color was still brown, indicating that maghemite indeed adsorbed on the silica spheres. This can be seen more directly on the TEM picture in figure 2.3, which shows a silica sphere homogeneously covered with the much smaller maghemite particles.

Adsorption of maghemite was also evident from the change in ζ-potential of the silica spheres. Table 2.1 contains the results of electrophoretic measurements performed on a Coulter Delsa 440 SX. For bare silica spheres and silica spheres with 1wt-% maghemite added, the ζ-potential is negative. In the other mixtures, the coverage of maghemite on the silica surface was apparently high enough to change the sign of the ζ-potential.

Although at pH=3.5 maghemite particles were irreversibly bound to silica, raising the pH, and thereby changing the surface potential of maghemite from positive to negative, led to desorption of maghemite from the silica surface. Deposition of silica from a TES solution according to the procedure described in section 2.2.c will therefore fail for silica+maghemite spheres, because this reaction is carried out at high pH. Such a surface coating was attempted because it may improve the stability of the magnetic silica particles. Even though the particles were initially stable, it was noticed that flocculation occurs during prolonged storage. The reason for this instability is not yet resolved, but it was verified that it is not due to a drift of the pH.
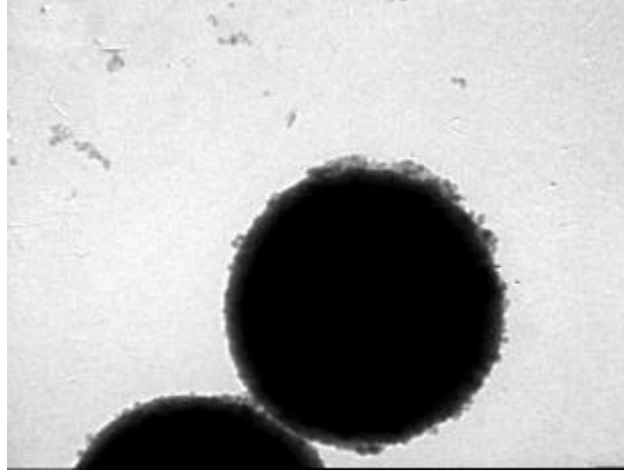
Figure 2.3. *TEM picture of a 460-nm silica sphere covered with ~10-nm maghemite particles.*

Table 2.1. Compositions of mixtures for the preparation of silica+maghemite spheres and surface potential of the products.

Volume of SiO_2 dispersion	Volume of γ-Fe_2O_3 dispersion	ζ-potential /mV
1.00	0.00	-45
1.00	0.01	-40
1.00	0.10	+47
1.00	1.00	+58
0.10	1.00	

The dipolar interaction between decorated silica spheres depends on the strength of the applied field. At infinite field strength, a sphere with diameter d covered with a maghemite layer of thickness δ will have a magnetic moment $m \approx \pi d^2 \delta M_{sb}$ (M_{sb} is the saturation magnetization bulk maghemite). At closest distance, the attractive energy between two fully magnetized silica+maghemite spheres is approximately

$$U_{dd} = -\frac{1}{2}\pi\mu_0 d\delta^2 M_{sb}^2 \qquad (2.2)$$

For the spheres prepared here, $U_{dd} \approx -5000\,kT$ if the surface is completely covered with maghemite ($\delta = 10$ nm, $M_{sb} = 4.8\ 10^5$ Am^{-1}). Of course, the interaction strength will be less at finite field strengths, but the number calculated here demonstrates that dipolar interactions between the particles described here can be very strong.

2.3   Conclusions

Several different types of magnetic colloids, with magnetic interaction ranging from weak to strong, were prepared from 10-nm iron oxide particles. Weakly interacting particles were prepared by covering the iron oxide particles with layer of silica. Iron oxide particles were also grafted with fatty acid, resulting in magnetic colloids with intermediate interaction that could be dispersed in a variety of non-polar solvents. And large magnetic colloids with strong and tunable interaction strength were obtained by adsorbing iron oxide particles on large silica spheres.

Acknowledgements

References

1   S. S. Papell, U.S. Patent 3,215,572 (1965).

2   G. W. Reimers and S. E. Khalafalla, U.S. Patent 3,843,540 (1974).

3   S. E. Khalafalla and G. W. Reimers, *IEEE Trans. Magn.* **MAG-16**, 178 (1980).

4   A. P. Philipse, M. P. B. van Bruggen, and C. Pathmamanoharan, *Langmuir* **10**, 92 (1994).

5   L. N. Donselaar, 'Silica-magnetite colloids and magnetic fluids - Synthesis and particle interaction', PhD Thesis, Utrecht University (1998).

6   A. T. Skjeltorp and G. Helgesen, in 'Phase Transitions in Soft Condensed Matter', ed. T. Riste and D. Sherrington, Plenum Press, New York (1989), p. 23.

7   M. Fermigier and A. P. Gast, *J. Colloid Interface Sci.* **154**, 522 (1992).

8   A. van Blaaderen and A. Vrij, *Langmuir* **8**, 2921 (1992).

9   A. van Blaaderen, *Progr. Colloid Polym. Sci.* **104**, 59 (1997).

10 A. Bee and R. Massart, *J. Magn. Magn. Mater.* **122**, 1 (1990).

11 J. P. Jolivet and E. Tronc, *J. Colloid Interface Sci.* **125**, 688 (1988).

12 V. Cabuil and R. Perzynski, in 'Magnetic Fluids and Applications Handbook', ed. B. Berkovski, Begell House, New York (1996).

13 A. D. Buckland, C. H. Rochester, and S. A. Topham, *J. Chem. Soc. Far. Trans. I* **76**, 302 (1980).

14 C. Rocchiccioli-Deltcheff, R. Franck, V. Cabuil, and R. Massart, *J. Chem. Res. (S)*, 126 (1987).

15 A. Wooding, M. Kilner, and D. B. Lambrick, *J. Colloid Interface Sci.* **144**, 236 (1991).

16 V. M. Buzmakov and A. F. Pshenichnikov, *J. Colloid Interface Sci.* **182**, 63 (1996).

17 L. M. Liz-Marzán, M. Giersig, and P. Mulvaney, *Langmuir* **12**, 4329 (1996).

18 W. Stöber, A. Fink, and E. Bohn, *J. Colloid Interface Sci.* **26**, 62 (1968).

Interactions between magnetic colloids

Abstract

In this chapter, measurements of the concentration dependence of magnetic susceptibility of two high-quality ferrofluid samples are presented. One sample contains polydisperse particles with an average core size of 9.1 nm; the other sample contains particles with a mean core size of 15 nm, obtained by size-selective precipitation from the former sample. Susceptibilities, measured over a large concentration range, deviate from all prevailing theories, but are most accurately described by Onsager's theory, the Mean Spherical Model and perturbation theory.

3.1   Introduction

The macroscopic behavior of ferrofluids can in principle be modelled by a fluid of dipolar hard spheres. However, accounting for dipolar interactions has proven to be a difficult problem, which is most evident from the ongoing discussion on the possibility of a gas-liquid transition in dipolar fluids [1-5].

Interactions in ferrofluids can be experimentally investigated with magnetic susceptibility measurements. Various models of dipolar fluids have been directly tested against such measurements. Much effort has been put in the measurement of the temperature-dependence of the susceptibility [6,7]. Central in some investigations [8-11] is the question if ferrofluids have, just as ferromagnets, a Curie temperature, i.e. the temperature below which a sample becomes spontaneously magnetized. Elsewhere [12,13], models for the susceptibility are quantitatively compared with experimental data. Unfortunately, temperature-dependent measurements must be corrected for expansion of the solvent and the decrease of magnetic moment with increasing temperature. In view of the crudeness of such corrections over large temperature ranges and, in addition, the uncertain effect of temperature variation on the effectiveness of the steric stabilization layer, one may question whether such measurements are valid tests for the theoretical models. These corrections and uncertainties are avoided in measurements of the concentration dependence of magnetic susceptibility [12-14].

In this chapter, interaction models for dipolar fluids are studied using concentration dependent susceptibility measurements of oleic acid grafted Fe_3O_4 particles in cyclohexane. A high quality, cluster-free ferrofluid is used which has a lower polydispersity than normally reported. This ferrofluid is fractionated by means of size-selective precipitation, to give stable ferrofluids containing particles with mean diameters ranging from 8 to 15 nm and low polydispersity. To the best of our knowledge, such large and strongly interacting particles have not been investigated before. The susceptibility measurements deviate from most theories, such as Weiss' theory [15], Onsager's theory [16] and the Mean Spherical Model [17]. Before discussing theory and measurements of the susceptibility, the interaction between two magnetic particles is briefly discussed.

3.2   Theory

3.2.a   Interactions between magnetic colloids

The magnetic colloids used here consist of roughly spherical Fe_3O_4 particles with a diameter of

approximately 10 nm. All particles have oleic acid (9-Z-octadecanoic acid) grafted onto their surfaces which makes them soluble in organic solvent such as cyclohexane.

Since these particles are ferrimagnetic and consist of single domains [18], they can be considered as point dipoles with a magnetic moment $m = (\pi/6)M_{s,b}d_m^3$ located at the center of spherical particles ($M_{s,b}$ denotes the bulk saturation magnetization, approximately 4.8×10^5 Am^{-1} for Fe_3O_4, and d_m the diameter of the magnetic core). The magnetic interaction between two particles magnetic moments m_1 and m_2 at a distance r_{12} (see figure 3.1) is

$$U_{dd} = \frac{\mu_0 m_1 m_2}{4\pi r_{12}^3}\left[\hat{m}_1 \cdot \hat{m}_2 - 3\left(\hat{m}_1 \cdot \hat{r}_{12}\right)\left(\hat{m}_2 \cdot \hat{r}_{12}\right)\right] \tag{3.1}$$

where the hat above symbols denotes a unit vector. In the energetically most favorable configuration, the magnetic moments point in the same direction and lie head-to-tail.

In addition to magnetic interaction, magnetic colloids also experience (isotropic) London-Van der Waals attraction. The Van der Waals attraction between the Fe_3O_4 cores is [19]

$$U_{VdW} = -\frac{A}{12}\left[\frac{1}{s^2-1}+\frac{1}{s^2}+2\ln\left(\frac{s^2-1}{s^2}\right)\right] \tag{3.2}$$

with A the Hamaker constant (approximately 4×10^{-20} J for iron oxides in a solvent [19,20]) and $s = r_{12}/d$.

Both types of interaction are plotted in figure 3.2 for particles with a 10-nm core as a function of their distance r. The thickness of the grafted layer has not yet been conclusively determined, but a value of 2 nm is often assumed. Figure 3.2 shows that at closest approach (r=14 nm) Van der Waals attraction is small (-0.1 kT), whereas dipole-dipole interaction is significant (-1.1 kT). Moreover, the range of dipole-dipole interaction is much larger than that of Van der Waals interaction.

For other particle sizes, the Van der Waals and dipole-dipole interaction strength between touching particles is plotted in figure 3.3. The plot shows the weak dependence of Van der Waals attraction and strong dependence of dipolar interaction on particle size. Even for the largest particles, with a 15-nm core, Van der Waals attraction remains weak (-0.27 kT). One must bear in mind, however, that the Van der Waals energies calculated here are based on an assumed value for the grafting layer thickness. If this layer is in fact thinner, Van der Waals attraction will be much stronger than the estimated values.
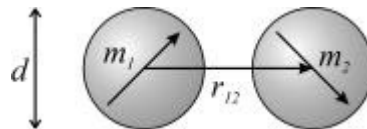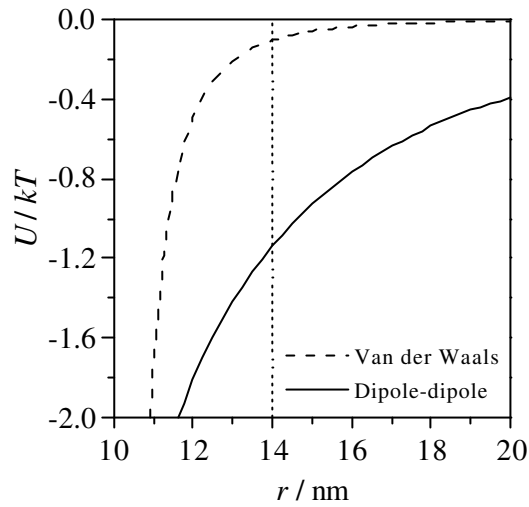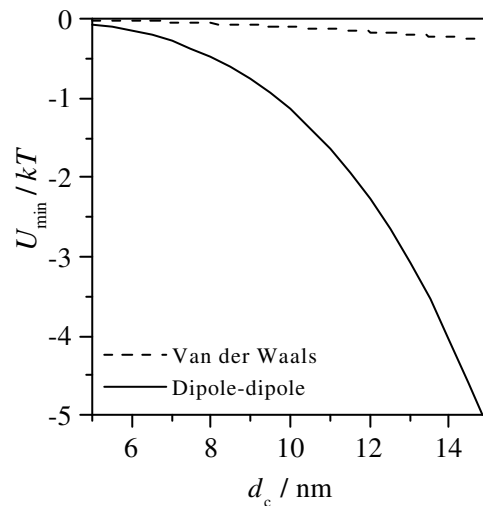
Figure 3.1. *Interaction between two magnetic colloids.*

Figure 3.2. *Distance-dependence of Van der Waals and maximum dipole-dipole interaction between two magnetic particles with a core diameter of 10 nm. The dotted line indicates the distance of closest approach.*

Figure 3.3. *Size-dependence of Van der Waals and maximum dipole-dipole interaction between two touching magnetic particles. d_c is the diameter of the Fe_3O_4 core. The thickness of the oleic acid layer is taken 2 nm.*

3.2.b   Susceptibility

It is reasonable to model dilute ferrofluids with a paramagnetic, or rather *super*paramagnetic

gas. 'Super' in 'superparamagnetic' refers to the large dipole moment of individual particles, which is generally more than three orders of magnitude larger than that of atomic dipole moments in paramagnets.

When a magnetic field H is applied to a sample containing particles with magnetic dipole moments m, these dipoles will tend to align with the magnetic field, thereby lowering their energy $U = -\mu_0 mH\cos\theta$ (μ_0 is the permeability of vacuum, θ the angle between field and dipole). If dipole-dipole interaction is neglected, the average component of m along the direction of the field can be found by calculating the Boltzmann average of $\cos\theta$ [18,21]. The result is known as the Langevin equation $L(\alpha)$:

$$L(\alpha) = \langle\cos\theta\rangle = \coth\alpha - \frac{1}{\alpha} \quad ; \quad \alpha = \frac{\mu_0 mH}{kT} \tag{3.3}$$

Thus, the magnetization M of a system of non-interacting particles is given by

$$M(H) = M_s L\left(\frac{\mu_0 mH}{kT}\right) \tag{3.4}$$

where $M_s = nm$ is the magnetization at infinite field strength (n=particle number density).

At low field strength, $L(\alpha)$ can be Taylor expanded, resulting in a linear relation between M and H with slope

$$\chi_i = \left(\frac{\mathrm{d}M}{\mathrm{d}H}\right)_{H\to 0} = \frac{\mu_0 nm^2}{3kT} = \chi_L \quad , \tag{3.5}$$

where χ_i is called the 'initial susceptibility'. Eqn. (3.5) is specific for non-interacting dipoles, and is often called 'Langevin susceptibility', χ_L.

Dipole-dipole interaction in a ferrofluid is of the order of $1\,kT$ (see previous section), and will affect the susceptibility of concentrated ferrofluids. Accounting for dipolar interactions is an long-standing problem, which was already studied in 1907 by Weiss [15] to explain ferromagnetism and the existence of the Curie temperature. His theory is based on the idea that each dipole experiences an effective field H, which is composed of the externally applied field H_0 plus a field κM due to all other dipoles. In liquids, the value of κ is determined by the shape of the imaginary cavity in which each dipole is thought to reside. The susceptibility according to this model is

$$\chi_i = \frac{\chi_L}{1-\kappa\chi_L} \tag{3.6}$$

where χ_L is given by Eq. (3.5). For a spherical cavity κ is 1/3. A result equivalent to (3.6) was obtained by Debye in 1912 for the dielectric constant of polar materials [22] (because electric

and magnetic dipoles are analogous, expressions for the dielectric constant ε can be easily translated into its magnetic counterpart, the magnetic permeability $\mu = \chi + 1$).

According to (3.6) χ_i diverges at $\chi_L \to 3$, a phenomenon neither observed in dielectric materials nor in ferrofluids. By decomposing the effective field into a 'cavity field' parallel to the external field and a 'reaction field' parallel to the central dipole, Onsager was able to show that the predicted spontaneous polarization is a result from the incorrect assumption that the reaction field exerts a torque on the central dipole [16]. In Onsager's theory, divergence of the dielectric constant is absent, in accordance with experience. The susceptibility following from this model is

$$\chi_i = \frac{3}{4}\left(\chi_L - 1 + \sqrt{1 + \frac{2}{3}\chi_L + \chi_L{}^2} \right) \tag{3.7}$$

Kirkwood later generalized Onsager's theory [23], and Wertheim solved Kirkwood's result within the mean spherical model (MSM) [17]. The susceptibility within the MSM is

$$\chi_i = \frac{q(2\xi) - q(-\xi)}{q(-\xi)} \quad ; \quad q(\xi) = \frac{(1 + 2\xi)^2}{(1 - \xi)^4} \tag{3.8}$$

where the parameter ξ can be found by solving $\chi_L = q(2\xi) - q(-\xi)$.

A more recent expression for the dielectric constant of a dipolar fluids was obtained by Kalikmanov using a statistical mechanical perturbation approach [24]. The result, called the 'algebraic perturbation theory' (APT), is

$$\chi_i = \chi_L\left[1 + \frac{1}{3}\chi_L + \frac{5}{48}\left(1 + a_1\phi + a_2\phi^2\right)\chi_L{}^2 \right] \tag{3.9}$$

with the coefficients $a_1 = 0.036$ and $a_2 = 0.372$.

All theories, except Langevin's theory, coincide at small values of χ_L:

$$\left(\chi_i\right)_{\chi_L = 1} \approx \chi_L\left[1 + \frac{1}{3}\chi_L \right] \tag{3.10}$$

Eqn. (3.10) is the exact result of a simple perturbation theory [25], yet despite its simplicity, the deviation with the more advanced MSM is as small as 10% even at $\chi_L = 5$.

3.3   Experimental

3.3.a   Characterization

The physical diameter of the core of Fe_3O_4 particles, d_c, was obtained from transmission electron microscopy pictures, taken on a Philips CM10 microscope, and analyzed with IBAS, an electronic image analysis system.

Magnetization measurements were performed on a MicroMag 2900 AGM (Alternating Gradient Magnetometer, Princeton Measurements Corp.). Samples were contained in small glass cups with internal dimensions of $4 \times 3 \times 0.4$ mm, which were sealed by gluing a small cover glass over the open end. All measurements were performed at room temperature. The saturation magnetization and diamagnetic susceptibility were determined by fitting the magnetization curve at high fields (up to $1.2 \ 10^6 \ Am^{-1}$) with the Langevin function[18,21] and an added diamagnetic contribution:

$$M = M_s \left\{ \coth(\alpha) - \frac{1}{\alpha} \right\} + \chi_{dia} H \quad ; \quad \alpha = \frac{\mu_o m H}{kT} \qquad (3.11)$$

where M_s is the saturation magnetization of the sample, χ_{dia} the diamagnetic susceptibility, H the applied field strength, m the magnetic moment of particles, μ_o the permeability of vacuum and kT the thermal energy. The initial susceptibility χ_i was calculated from at least ten points measured at applied fields below $10^3 \ Am^{-1}$. These points invariably lay on a straight line. The magnetic core size of particles was calculated using the low-field approximation of Eq. (3.11):

$$\chi_i = M_s \frac{\mu_o m}{3kT} + \chi_{dia} = M_s \frac{\mu_o M_{s,Fe3O4} \pi d_M^3}{18kT} + \chi_{dia} \qquad (3.12)$$

with $M_{s,Fe3O4}$ the saturation magnetization of bulk Fe_3O_4 ($4.8 \ 10^5 \ Am^{-1}$) and d_M the average magnetic core diameter. To minimize the influence of magnetic interaction between magnetite particles, Eq. (3.12) was only used for measurements on dilute samples, having a concentration of magnetic material below $10 \ gl^{-1}$. It should be noted that the diameter d_M can deviate significantly from the physical diameter d_c obtained with TEM. One reasons is that d_M^3 actually equals $<d_m^6>/<d_m^3>$ [26,27] (d_m is the core size of one particle), so polydispersity strongly increases the diameter found with Eq. (3.12). A second reason is that the surface of particles may be non-magnetic[18,27].

Small angle X-ray scattering (SAXS) experiments were carried out at the DUBBLE beamline (BM26) at the European Synchrotron Radiation Facility in Grenoble. Scattering experiments were conducted on dilute samples ($\phi < 1\%$). The radius of gyration, R_g, was calculated using the low q approximation of the scattering intensity of a dilute dispersion[28]: $\ln[I(q)/I(0)] = -R_g^2 q^2/3$, where $q = (4\pi/\lambda_0)\sin(\theta/2)$ is the scattering vector, θ is the scattering

angle and λ_0 the wavelength of incident radiation.

The mass density ρ of a dispersion was measured with an Anton Paar DMA 5000 densitometer. Combined with the mass concentration c this yields the density of dry particles ρ_{dry},

$$\rho_{dry} = \frac{c\rho_{solvent}}{c + \rho_{solvent} - \rho} \quad , \tag{3.13}$$

which is used to calculate volume fractions of samples with known weight concentration.

3.3.b   Fractionation

A high quality ferrofluid, coded FFR, was fractionated by size-selective precipitation, using pentanol as a bad solvent. This ferrofluid consists of Fe_3O_4 colloids, grafted with purified oleic acid and dispersed in cyclohexane. Unreacted oleic acid was removed by repeated precipitation and redispersion. Clustered particles were taken away by magnetic filtration. No sediment developed within a period of two years. The characteristics of FFR are summarized in Table 3.1.

In the first fractionation step, FFR with a particle concentration of about 10% by volume was destabilized by stepwise addition of pentanol. After each addition, the sample was ultrasonicated for five minutes and left undisturbed for at least four hours to let aggregates settle. The two fractions were separated when the magnetic susceptibility of the top layer indicated that about half of the particles were flocculated. Both top and bottom layer, coded FFR-S and FFR-L respectively, were fractionated once more by adding pentanol or cyclohexane.

Pentanol was removed by precipitating and washing all four fractions with ethanol. After drying in a nitrogen stream, the products were redispersed in cyclohexane.

3.3.c   Susceptibility measurements

The concentration dependence of susceptibility was measured on a Kappabridge KLY-3 susceptibility meter (Agico). The KLY-3 applies a homogeneous field of 300 Am^{-1}, oscillating at a frequency of 875 Hz. All measurements were done at 296.65 ± 0.2 K.

Ferrofluid samples were contained in 300 μl cylindrical tubes with a length/diameter ratio of 9. With the field applied along the long axis of the sample, demagnetization effects [29] can be neglected, as was experimentally confirmed by measuring samples with higher length/diameter ratios. It was also verified that the instrument's readout
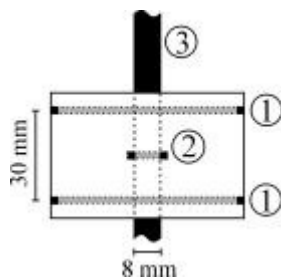
Figure 3.4. *Schematic drawing of mutual induction coils. 1: Helmholtz coils, generating a homogeneous magnetic field of 100 Am⁻¹; 2: secondary coil, measuring χ_i; 3: sample tube. The susceptibility meter consists of a measuring coil and a compensation coil, both of the type shown here.*

value depends linearly on the susceptibility of the sample.

The concentration dependent susceptibility of FFR-LL was also measured in a home-made setup using mutually inducting coils. Two coils in Helmholtz configuration (figure 3.4) generate a homogeneous magnetic field of 100 Am⁻¹, oscillating at a frequency of 875 Hz. The oscillating field produces an oscillating voltage difference over a small, thin pickup coil, positioned halfway between the Helmholtz coils (see figure 3.4). The pickup signal is compensated by a second pair of Helmholtz and pickup coils, and measured with a lock-in amplifier. When a sample tube is inserted in one of the pickup coils, the voltage difference changes proportionally to the susceptibility of the sample.

In this setup, a concentration series was measured by drying some FFR-LL in a long 8-mm wide sample tube, and measuring the susceptibility after successive dilutions with cyclohexane. After each dilution, the sample was weighed and left to equilibrate for at least 15 minutes before the susceptibility was measured. The concentration was calculated afterwards from the weights of dry material and dispersion and the densities of dry material and cyclohexane.

3.4 Results and discussion

3.4.a Fractionation

Precipitation of FFR started at a pentanol volume fraction of 50% and complete precipitation was found at 90%. These percentages were, however, strongly affected by small temperature variations.

Table 3.1 shows the characteristics of the four ferrofluid fractions. Both TEM (figure 3.5) and magnetization measurements (figure 3.6) yield significant differences between the mean diameters and hence the maximum strength of dipole-dipole interactions in the

Table 3.1. Characteristics of magnetic fluids.

Sample	d_c /nm [a]	σ_c /nm [a]	d_M /nm [b]	ρ_{dry} /kg m^{-3}	$U_{dd,min}$ / kT
FFR	9.1	2.3	11.3	2900	-0.8
FFR-SS	7.9	1.3	7.7		-0.5
FFR-SL	9.7	2.6	9.9		-1.1
FFR-LS	11.4	2.8	11.7		-2.0
FFR-LL	15.0	2.8	15.22	3630	-5.4

[a] Determined from TEM pictures

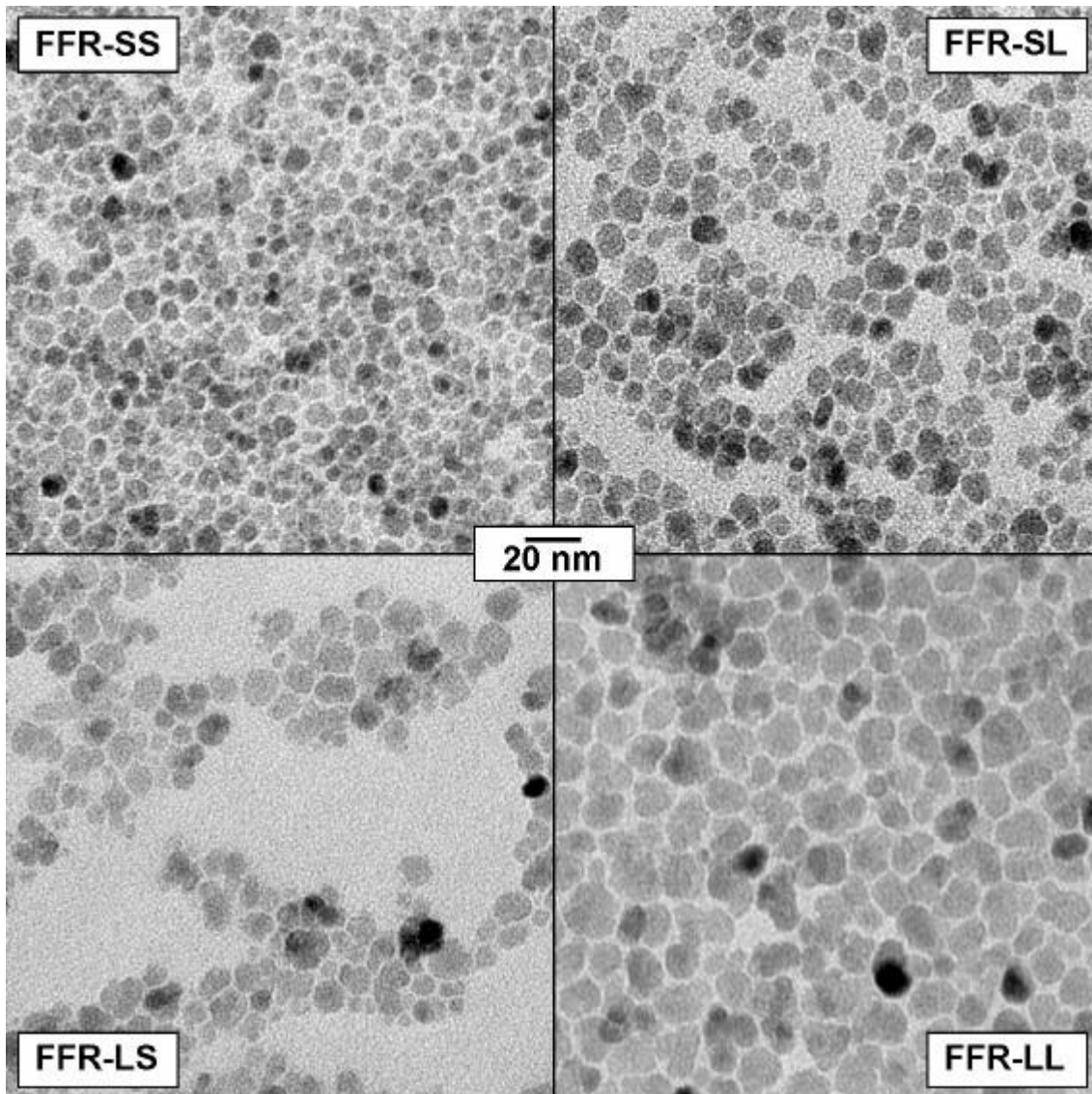[b] Obtained from magnetization measurements

Figure 3.5. *Electron micrographs of the four ferrofluid sample obtained by size-selective precipitation. See table 3.1 for characteristics.*
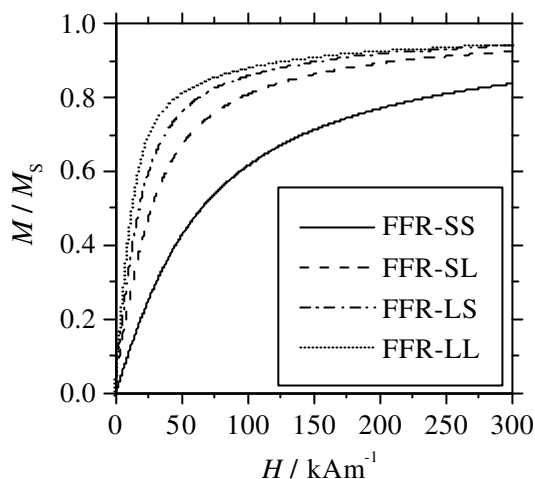
Figure 3.6*. Magnetization measurements of the four ferrofluid fractions. The difference in particle sizes between samples is evident from the difference in initial slope.*

fractions. Fraction FFR-LL is especially interesting, for it contains large particles of a size not reported before. Dipole-dipole interaction is strong in this system: values for U_{dd} (Eqn. (3.1)) can reach -5.4 kT. Despite its strong attraction, FFR-LL is stable at volume fraction up to 35%, possibly higher. Conversely, adding cyclohexane to dried FFR-LL does not give an 'instant ferrofluid', not even an immediate coloration of the solvent, whereas the other fractions are easily redispersible from the dried state. For FFR-LL it takes about ten hours before redispersion is complete. Apparently, strong interaction makes redispersion difficult, but can still lead to a stable ferrofluid.

Unfortunately, the polydispersity is only slightly reduced by fractionation. Similar behavior was found in fractionation studies on aqueous ferrofluids [3,30], where size sorting resulted in different mean sizes but almost the same polydispersity. Still, the polydispersity of all samples used here is lower than the polydispersity of 40% that is often reported in literature. The fractionation method described here can perhaps be improved upon by varying the temperature to modify the solvent quality of the pentanol/cyclohexane mixture. In this way, a more homogeneous precipitation can be achieved, possibly yielding fractions with lower polydispersity.

3.4.b   SAXS measurements

Figure 3.7 shows the Guinier plot of a dilute sample of FFR at small scattering vectors. A straight line fits the scattering curve well and gives a radius of gyration of 6.5 nm. For spherical

particles, the physical particle diameter $d = 2R_g\sqrt{5/3}$=16.8 nm. The difference between

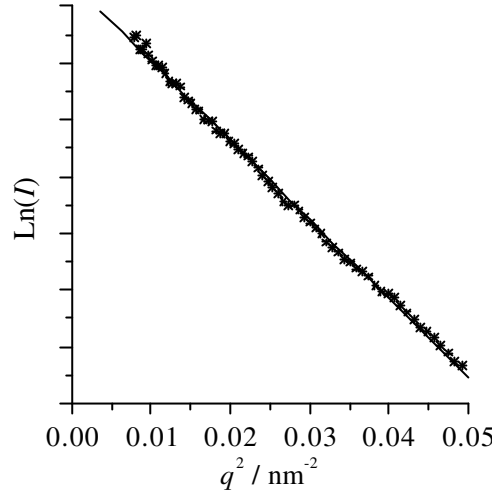SAXS   diameter   and   TEM   diameter   can   be   largely   attributed   to

Figure 3.7. *Guinier plot of SAXS measurement of FFR. The linearity up to small q indicates that clusters are absent.*

polydispersity. If particle sizes are log-normally distributed, then [26]

$$\frac{d_{\mathrm{SAXS}}}{d_{\mathrm{TEM}}} = \frac{\sqrt{\langle d^8 \rangle / \langle d^6 \rangle}}{\langle d \rangle} = \frac{\exp\left(7\sigma^2\right)}{\exp\left(\sigma^2 / 2\right)} \tag{3.14}$$

Substituting σ =0.26 and <d>=9.1 (see Table 3.1) in (3.14) yields d_{SAXS}=14.1 nm.

The linearity of the Guinier plot up to the smallest q-value is the strongest indication we have for the absence of clusters. Absence of a sediment in ferrofluid samples is insufficient to conclude that clusters are absent [31]: sediments only form when the gravitational length [32] $l_g=kT/Nmg$ (N=number of particles in a cluster, m=mass of a single particle$\approx$3 10^{-21} kg, g=earth's gravity constant) is less than, say, a millimeter. This condition is only satisfied for clusters of about 100 particles or more; smaller clusters remain dispersed because their thermal energy is larger than their gravitational energy.

The absence of clusters is in agreement with dichroism and rheological measurements done with the same kind of ferrofluid [33].

3.4.c   Susceptibility measurements

For the samples FFR and FFR-LL, susceptibility measurements are shown in figures 3.8 and 3.9. The ordinate values χ_L were calculated from the concentration c with $\chi_L=k\,c$, where the proportionality constant k was obtained by fitting measurements on dilute samples with the low

concentration expansion (eqn. (3.10)). This approximation differs less than 2% of the exact values at χ_L<0.3. The difference in figure 3.9 between data obtained with the two different techniques can be solely attributed to a small difference
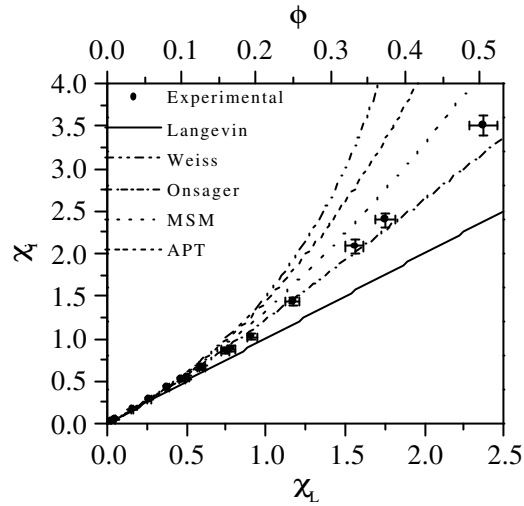

Figure 3.8. *Concentration dependent susceptibility of FFR (mean core diameter is 9.1 nm, maximum attraction -1 kT), measured with the Agico KLY-3. Horizontal error bars refer to error in χ_L.*
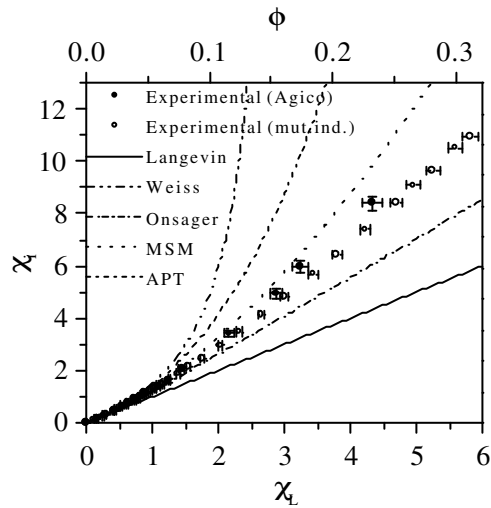
Figure 3.9. *Concentration dependent susceptibility of FFR-LL (mean core diameter is 15 nm, maximum magnetic attraction -5 kT), measured with the Agico KLY-3 and the mutual induction bridge. Horizontal error bars refer to error in χ_L.*

between proportionality constants; plots of the same data as a function of concentration agree very well. The volume fraction ϕ, calculated from the mass concentration c and the density ρ_{dry}

(Table 3.1), is also indicated in graphs.

The concentration dependent susceptibility of FFR-LL is of particular interest, because the polydispersity in particle sizes is relatively low, the mean magnetic dipole moment (hence also dipole-dipole interaction) is higher than reported anywhere else for Fe_3O_4, and the susceptibility is measured over a large range of Langevin susceptibilities. Despite the difference in particle size and dipolar interaction, the susceptibility curves of FFR and FFR-LL in figures 3.8 and 3.9 are in good agreement: the maximum relative difference in χ_i between the two curves amounts to 14%.

As expected, dipolar interactions lead to non-Langevin behavior at high concentrations (figures 3.8 and 3.9). Surprisingly, none of the theories described in section 3.2.b appears to describe the data very well. Only Onsager's theory [16], the MSM [17] and the perturbation theory [25] come close to the experimental values, the other theories largely overestimate the susceptibility at high concentrations.

Weiss' theory can be made to fit the data reasonably well if κ in Eq. (3.6) is used as a fitting parameter. For a value of κ of 0.12, the theoretical curve lies slightly below the experimental data at low concentrations, and above the data at high concentrations (not shown in figure). The low value for κ means that the imaginary cavities in which magnetic particles reside are elongated parallel to the field. However, although such a cavity shape may be conceivable for elongated magnetic particles, it is not for the nearly spherical particles used here. So Weiss' theory can be made to fit the measurements, but then its physical meaning is unrealistic.

3.5   Conclusions

The main type of interaction between oleic acid grafted magnetite particles with a core diameter around 10 nm is dipolar interaction; Van der Waals attraction between particle cores is probably small, even if somewhat larger particles are considered. In contrast, dipolar interaction strongly depends on particle size.

In this chapter, it has been shown that a polydisperse ferrofluid can be separated by means of size-selective precipitation into fractions with mean core diameters ranging from 8 to 15 nm. Because of the strong size-dependence of dipolar interaction, this fractionation leads to samples with a large range of maximum interaction energies, namely from 0.5 to 5 kT. Despite their strong mutual attraction, the largest particles still form stable dispersions up to high concentrations.

The effect of dipolar interactions on the macroscopic behavior of ferrofluids has been investigated by means of concentration dependent susceptibility measurements. Experimental

data clearly show that dipolar interaction increases the susceptibility above the susceptibility of a (imaginary) system of the same particles, but without dipolar interaction. The increase however, is less than predicted by most theories. Only one theory, due to Onsager, underestimates our data. Though not accurately described by any of the theories discussed in this chapter, the data lie closest to predictions from the Mean Spherical Model, a perturbation theory and Onsager's theory.

Acknowledgements

References

1   A. O. Tsebers, *Magnetohydrodynamics* **18**, 137 (1982).

2   K. Sano and M. Doi, *J. Phys. Soc. Jpn.* **52**, 2810 (1983).

3   J.-C. Bacri, R. Perzynski, D. Salin, V. Cabuil, and R. Massart, *J. Colloid Interface Sci.* **132**, 43 (1988).

4   M. E. van Leeuwen and B. Smit, *Phys. Rev. Lett.* **71**, 3991 (1993).

5   P. J. Camp, J. C. Shelley, and G. N. Patey, *Phys. Rev. Lett.* **84**, 115 (2000).

6   F. Söffge and E. Schmidbauer, *J. Magn. Magn. Mater.* **24**, 54 (1981).

7   K. O'Grady, J. Popplewell, and S. W. Charles, *J. Magn. Magn. Mater.* **39**, 56 (1983).

8   K. O'Grady, A. Bradbury, S. W. Charles, S. Menear, J. Popplewell, and R. W. Chantrell, *J. Magn. Magn. Mater.* **31-34**, 958 (1983).

9   J. Popplewell, B. A. Aisheh, and N. Y. Ayoub, *J. Appl. Phys.* **64**, 5852 (1988).

10 M. Holmes, K. O'Grady, and J. Popplewell, *J. Magn. Magn. Mater.* **85**, 47 (1990).

11 H. D. Williams, K. O'Grady, S. W. Charles, and K. J. Davies, *J. Magn. Magn. Mater.* **122**, 134 (1993).

12 Y. I. Dikanskii, *Magnetohydrodynamics* **18**, 237 (1982).

13 A. F. Pshenichnikov, A. V. Lebedev, and K. I. Morozov, *Magnetohydrodynamics* **23**, 31 (1987).

14 P. C. Fannin, B. K. P. Scaife, and S. W. Charles, *J. Phys. D: Appl. Phys.* **23**, 1711

(1990).

15 P. Weiss, *J. Phys. Radium* **4**, 661 (1907).

16 L. Onsager, *J. Am. Chem. Soc.* **58**, 1486 (1936).

17 M. S. Wertheim, *J. Chem. Phys.* **55**, 4291 (1971).

18 R. E. Rosensweig, 'Ferrohydrodynamics', Cambridge University Press, Cambridge (1985).

19 P. Scholten, *J. Magn. Magn. Mater.* **39**, 99 (1983).

20 D. Y. C. Chan, D. Henderson, J. Barojas, and A. M. Homola, *IBM. J. Res. Develop.* **29**, 11 (1985).

21 I. S. Jacobs and C. P. Bean, in 'Magnetism, a treatise on modern theory and materials', vol. III, ed. G. T. Rado and H. Suhl, Academic Press (1963).

22 P. Debye, *Physik. Z.* **13**, 97 (1912).

23 J. G. Kirkwood, *J. Chem. Phys.* **7**, 911 (1939).

24 V. I. Kalikmanov, *Phys. Rev. E* **59**, 4085 (1999).

25 Y. A. Buyevich and A. O. Ivanov, *Physica A* **190**, 276 (1992).

26 V. Cabuil and R. Perzynski, in 'Magnetic Fluids and Applications Handbook', ed. B. Berkovski, Begell House, New York (1996).

27 A. F. Pshenichnikov, V. V. Mekhonoshin, and A. V. Lebedev, *J. Magn. Magn. Mater.* **161**, 94 (1996).

28 G. Porod, in 'Small Angle X-ray Scattering', ed. O. Glatter and O. Kratky, Academic Press, Lodon (1982), p. 17.

29 H. Dijkstra, in 'Selected topics in solid state physics', ed. E. P. Wohlfarth, North-Holland Publishing Co. (1967).

30 V. Cabuil, R. Massart, J.-C. Bacri, R. Perzynski, and D. Salin, *J. Chem. Res. (S)*, 130 (1987).

31 P. C. Scholten, *Chem. Eng. Comm.* **67**, 331 (1988).

32 V. Degiorgio, R. Piazza, and T. Bellini, in 'Observation, prediction and simulation of phase transitions in complex fluids', ed. M. Baus, L. F. Rull, and J.-P. Ryckaert, Kluwer Academic Publishers, Dordrecht (1995).

33 L. Vékás, M. Rasa, and D. Bica, *J. Colloid Interface Sci.* **231**, 247 (2000).

4

Phase behavior of magnetic colloids-polymer mixtures:

mean field calculations

Abstract

The phase behavior of mixtures of magnetic colloids and non-adsorbing polymer has been investigated using a mean field theory. The polymer in this mixture causes an effective isotropic attraction ('depletion attraction') between the magnetic colloids, the range and strength of which can be varied independently from the (anisotropic) dipole-dipole interaction.

Calculations within this mean field approximation show that, even in the absence of a magnetic field, a magnetic colloid-polymer mixture may phase separate into a polymer-rich colloidal gas and a polymer-poor colloidal liquid. Upon application of a magnetic field, the minimum amount of polymer needed to destabilize the mixture is reduced. However, for a dipole-dipole interaction strength typical for real ferrofluids, this reduction is insufficient to give phase coexistence in a polymer-free ferrofluid.

At higher interaction strength and in zero-field, three phase coexistence was found between an isotropic gas, isotropic liquid and a magnetized liquid.

The theory also suggests that free oleic acid, which is present in many ferrofluids, may decrease a ferrofluid's stability in the same way a polymer does.

4.1   Introduction

The dipolar hard sphere is the simplest model for polar molecules and magnetic colloids. The phase behavior of dipolar sphere fluids has been studied extensively for nearly twenty years now [1,2], and is still a matter of debate [3]. One of the attractive aspects of dipolar systems is that magnetic or electric fields may affect, for example, their phase behavior. Polar molecules are not expected to be much influenced by an electric field. Because the energy of a molecular dipole in a large electric field is typically $10^{-3} \, kT$ (k is Boltzmann's constant, T is temperature), the direction of molecular dipoles is nearly unaffected by electric fields.

For magnetic colloids the situation may be very different. The most widely used ferrofluids (as dispersions of magnetic colloids are sometimes called) contain spherical particles of ferrimagnetic magnetite (Fe_3O_4) with a typical diameter of 10 nm. Because of their single domain nature, these particles bear a permanent magnetic dipole. The energy of one such dipole in the field of a strong permanent magnet (~1 MAm^{-1}) is about $100 \, kT$, large enough to align these dipoles almost completely with the field. Moreover, the magnetic attraction energy between two magnetic particles is approximately $1 \, kT$, so magnetic interaction is expected to have a noticeable influence on the phase behavior of ferrofluids. In fact, phase instabilities in ferrofluids have been observed experimentally. For example, Rosensweig [4] observed the separation of a sterically stabilized ferrofluid into a dilute (colloidal 'gas') and a concentrated (colloidal 'liquid') phase upon application of a magnetic field. Aqueous, charge stabilized ferrofluids at high salt concentrations show gas-liquid coexistence even in the absence of a magnetic field [5,6], but under such conditions (isotropic) London-Van der Waals attraction probably has a significant influence on thermodynamic stability [6,7].

The role of isotropic interaction on the phase behavior of dipolar spheres has been studied both theoretically [2,8,9] and by computer simulation [10]. Although these studies give a broader understanding of the stability of dipolar fluids in general and of ferrofluids in particular, they are hard to verify experimentally. A major obstacle is that, normally, isotropic attraction between magnetic colloids can not be changed independently from magnetic attraction. However, by using the concept of 'depletion attraction', independent variation of isotropic attraction can be achieved experimentally. Asakura and Oosawa [11] and Vrij [12] have shown theoretically that the presence of a non-adsorbing polymer in a colloidal dispersion causes an effective attraction between the colloids. They reasoned that, if two colloidal particles have a surface-to-surface distance smaller than the diameter of polymer coils, polymer is excluded from the region in between the particles. The resulting imbalance in osmotic pressure pushes the colloidal particles together. This effective attraction can lead to phase separation into a polymer-rich colloidal gas and a polymer-poor colloidal liquid, as experiments have

demonstrated [12,13]. The phase behavior of non-magnetic colloid-polymer mixtures can be well described by simple theories [14,15].

In this paper, we adapt the mean field theory by Lekkerkerker *et al.* for the phase behavior of colloid-polymer mixtures [15] to the case of magnetic colloids. The influence of magnetic interaction is taken into account using two different approaches: a self-consistent mean field theory [1] and a perturbation theory [16]. Although formation of structures, strings in particular [17,18], is ignored in these theories, we think its use is justified for most ferrofluids because mutual magnetic interaction is only of moderate strength and strings are probably absent [19]. This is supported by experiments which show almost quantitative agreement between experimental magnetization curves at high field strength and mean field predictions [20].

Calculations with this mean field theory on systems with a magnetic interaction strength comparable to, or somewhat higher than in typical real ferrofluids, show that, contrary to reported experimental findings [4,21-24], field-induced phase separation does not occur in polymer-free ferrofluids. With sufficient polymer present, the system exhibits gas-liquid separation even in zero-field. Moreover, phase separation is promoted by application of a magnetic field. As a final note, it is shown that removing free surfactant from oleic acid-stabilized ferrofluids may prove beneficial for the stability of these ferrofluids.

4.2   Theory

The principle of depletion attraction can be exemplified by considering two colloidal spheres with diameter *d*, immersed in a solution containing polymer coils with diameter d_p. The polymers are interpenetrable with respect to each other, but hard repulsive towards the colloids. Therefore, each colloid is surrounded by a 'depletion zone', which is free of polymer. If the colloids are at a distance at which their depletion zones overlap (figure 4.1), polymer is absent in between the colloids, resulting in an osmotic pressure difference Π_p pushing these colloids together. This effective attraction energy has a range of $(d+d_p)$ and a magnitude of $-\Pi_p V_{overlap}$, thus depending on the polymer concentration.

In this chapter, the phase behavior of mixtures of *magnetic* colloids and polymer is considered. Therefore, the interaction between the magnetic dipole moments **m** embedded in the colloids and the interaction of these dipoles with an external magnetic field **H** must also be taken into account. The total potential energy of the system containing *N* colloidal particles and N_p polymer coils is

$$U = \frac{1}{2}\sum_i^N \sum_{j\neq i}^N u_{hs}\left(r_{ij}\right) + \frac{1}{2}\sum_i^N \sum_{j\neq i}^N u_{dd}\left(\mathbf{r}_{ij}, \mathbf{U}_i, \mathbf{U}_j\right) + \sum_i^N u_m\left(\mathbf{U}_i\right) + \sum_i^N \sum_j^{N_p} u_{cp}\left(\tilde{r}_{ij}\right) \qquad (4.1)$$
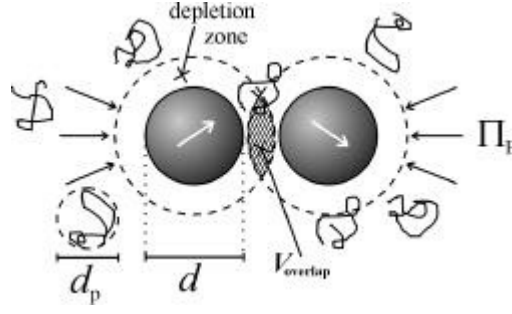
Figure 4.1. *Two magnetic colloids at close distance experience an effective isotropic attraction, induced by the surrounding polymers.*

where $u_{hs}(r_{ij})$ is the hard-sphere pair potential between two colloids at distance r_{ij} and $u_{dd}(\mathbf{r}_{ij}, \mathbf{\Omega}_i, \mathbf{\Omega}_j)$ is the interaction between two dipoles $\mathbf{m}_i = \mathbf{m}(\mathbf{\Omega}_i)$ and $\mathbf{m}_j = \mathbf{m}(\mathbf{\Omega}_j)$ connected by the vector $\mathbf{r}_{ij} = \mathbf{r}_j - \mathbf{r}_i$:

$$\beta u_{dd}\left(\mathbf{r}_{ij}, \mathbf{\Omega}_i, \mathbf{\Omega}_j\right) = -\lambda \frac{d^3}{r_{ij}^3}\left[3(\hat{\mathbf{m}}_i \cdot \hat{\mathbf{r}}_{ij})(\hat{\mathbf{m}}_j \cdot \hat{\mathbf{r}}_{ij}) - \hat{\mathbf{m}}_i \cdot \hat{\mathbf{m}}_j\right]$$

(4.2)

$$\lambda = \beta \frac{\mu_0 m^2}{4\pi d^3}$$

where $\beta = (kT)^{-1}$, λ is a dimensionless parameter measuring the dipole-dipole interaction strength between two colloids at closest distance, μ_0 is the permeability of vacuum, and m is the dipole strength. Hats denote unit vectors. The interactions of a dipole with an external field is described by

$$\beta u_m\left(\mathbf{\Omega}_i\right) = -\alpha \hat{\mathbf{m}}_i \cdot \hat{\mathbf{H}} \quad ; \quad \alpha = \beta \mu_0 m H$$

(4.3)

The expressions for λ and α in (4.2) and (4.3) are only valid in the SI unit system. However, the choice for the SI system has no consequences for the remainder of this section.

The polymer coils are regarded as non-additive hard spheres, i.e. they experience no interaction with other polymer coils, but behave as hard spheres towards colloids. The colloid-polymer interaction is given by $u_{cp}\left(\tilde{r}_{ij}\right)$ and depends on the colloid-polymer distance $\tilde{r}_{ij} = \left|\tilde{\mathbf{r}}_j - \mathbf{r}_i\right|$.

The phase diagram of the magnetic colloid-polymer mixture is calculated under constant volume restriction. The configuration integral for the system is

$$Z = \int..\int \exp\left[-\beta U\left(\mathbf{r}^N, \mathbf{\Omega}^N, \tilde{\mathbf{r}}^{N_p}\right)\right] d\mathbf{r}^N d\mathbf{\Omega}^N d\tilde{\mathbf{r}}^{N_p}$$

(4.4)

$$d\mathbf{\Omega}_i = (4\pi)^{-1} \sin\theta_i d\theta_i d\phi_i$$

Because of the non-additivity of the polymer coils, each integral over a coil center $\tilde{\mathbf{r}}_i$ can be evaluated individually, each giving the volume accessible to polymer at a certain magnetic colloid configuration, $V_{\text{free}}(\mathbf{r}^N,\mathbf{\Omega}^N)$. As an approximation, the configuration dependent $V_{\text{free}}(\mathbf{r}^N,\mathbf{\Omega}^N)$ is replaced by its mean value $<V_{\text{free}}>_0$, calculated by averaging over all configurations of a pure hard sphere fluid. Thus the influence of polymers and dipolar interactions on the free volume is neglected. With this, eqn. (4.4) becomes

$$Z = [fV]^{N_p} \int .. \int \exp\left[-\beta\frac{1}{2}\sum_{i,j\neq i}^{N} u_{\text{hs}}(r_{ij}) - \beta\frac{1}{2}\sum_{i,j\neq i}^{N} u_{\text{dd}}(\mathbf{r}_{ij},\mathbf{\Omega}_i,\mathbf{\Omega}_j) - \beta\sum_{i}^{N} u_{\text{m}}(\mathbf{\Omega}_i)\right] d\mathbf{r}^N d\mathbf{\Omega}^N \quad (4.5)$$

where the integral in (4.5) is the configuration integral Z_{DHS} of a pure dipolar hard sphere system, and $fV=<V_{\text{free}}>_0$ so f is the fraction of the entire volume V accessible to polymer. The Helmholtz free energy $F=F^{\text{id}}-kT\ln(Z/V^{N+N_p})$ derived from (4.5) is the sum of a dipolar hard sphere part F_{DHS} and a polymer part F_p:

$$F = F_{\text{DHS}} + N_p kT \ln\frac{\phi_p}{f} \quad , \quad (4.6)$$

where ϕ_p is the polymer "volume fraction" $N_p(\pi/6)d_p^3/V$. The free volume fraction f can be obtained using Scaled Particle Theory [25], yielding

$$f = (1-\phi_c)\exp\left[-A\left(\frac{\phi_c}{1-\phi_c}\right) - B\left(\frac{\phi_c}{1-\phi_c}\right)^2 - C\left(\frac{\phi_c}{1-\phi_c}\right)^3\right] \quad , \quad (4.7)$$

where $\phi_c=N(\pi/6)d^3/V$ is the colloid volume fraction, $A=3q+3q^2+q^3$, $B=9q^2/2+3q^3$, $C=3q^3$, and q is the polymer-to-colloid size ratio: $q=d_p/d$.

In order to calculate Z_{DHS}, some approximation for the magnetic interaction must be made. Two approximations are employed here: the self-consistent field theory (SCFT) [1] and the perturbation theory (PT) [16].

Self-consistent field theory

The interaction of a single dipole at position $\mathbf{r}_i$ with all other dipoles is equivalent to the the interaction of that dipole with the local magnetic field $\mathbf{H}_L$ at $\mathbf{r}_i$ produced by all other dipoles. The magnetic part of the eqn. (4.1) can therefore be written as

$$\frac{1}{2}\sum_{i}^{N}\sum_{j\neq i}^{N} u_{\text{dd}}(\mathbf{r}_{ij},\mathbf{\Omega}_i,\mathbf{\Omega}_j) + \sum_{i}^{N} u_{\text{m}}(\mathbf{\Omega}_i) = -\sum_{i}^{N} \mu_0 \mathbf{m}_i \cdot \left[\frac{1}{2}\mathbf{H}_L(\mathbf{r}_i,\mathbf{\Omega}^{N-1}) + \mathbf{H}\right] \quad (4.8)$$

As a mean field assumption, $\mathbf{H}_L$ is replaced by its mean $<\mathbf{H}_L>$, averaged over all configurations $(\mathbf{r}_j,\mathbf{\Omega}_j)$ of the dipoles $\mathbf{m}_{j\neq i}$, pointing in the same direction as the external field $\mathbf{H}$. Because in this assumption every dipole experiences the same *effective* field

$H_e=H+<H_L>$ [1], the right-hand side of eqn. (4.8) can be replaced by the angular average

$$U_{\mathrm{m}} = -\sum_i^N \mu_0 \mathbf{m}_i \cdot \left[\frac{1}{2}\langle \mathbf{H}_{\mathrm{L}} \rangle + \mathbf{H} \right] = -N\!\int p\left(\theta\right)\mu_0 m\left(\frac{1}{2}\langle H_{\mathrm{L}} \rangle + H \right)\cos\theta\,d \qquad , \qquad (4.9)$$

where $p(\theta)$ is the normalized angular distribution function

$$p\left(\theta\right) = \frac{\alpha_{\mathrm{e}}}{\sinh\alpha_{\mathrm{e}}}\exp\left[\alpha_{\mathrm{e}}\cos\theta\right] \quad ; \quad \alpha_{\mathrm{e}} = \beta\mu_0 m H_{\mathrm{e}} \qquad (4.10)$$

If the spatial distribution of dipoles around dipole $\mathbf{m}_i$ is spherically symmetric, $<H_L>$ equals the Lorentz field κM (κ=1/3), a well-known result in solid state physics[26], where the magnetization $M=nmL(\alpha_e)$, n is the particle number density and $L(\alpha_e)=<\cos\theta>_{p(\theta)}=\coth(\alpha_e)-\alpha_e^{-1}$ is the Langevin function for paramagnetism[27]. Because M depends on $p(\theta)$, which in turn depends on M, the effective field is determined self-consistently:

$$\alpha_{\mathrm{e}} = \alpha + 24\kappa\lambda\phi_{\mathrm{c}}L\left(\alpha_{\mathrm{e}}\right) \qquad (4.11)$$

Note that in the absence of an external magnetic field (α=0), eqn. (4.11) has a non-zero solution for $8\kappa\lambda\phi_c\geq1$, corresponding to a state of spontaneous magnetization [1].

Although above κ was said to be 1/3, its value in fact depends on the *macroscopic* shape of the system [26], even for infinitely large systems. Macroscopically, this can be understood as the result of excess magnetic "surface charges" present on the poles of the sample, which produce a magnetic field (the so-called "demagnetizing field" [26]) counteracting the external field and lowering κ. In accordance with other authors [1,8,16], we consider a needle-shaped system with the long axis parallel to the field, so that the ratio of pole surface to system volume is small and consequently the demagnetizing field can be neglected.

The magnetic part of the potential energy, eqn. (4.3), no longer depends on the particle positions, and is therefore independent of the hard-sphere part. Eqn. (4.6) can therefore be written as:

$$\begin{aligned} F &= F_{\mathrm{HS}} + F_{\mathrm{P}} + \left[U_{\mathrm{m}} - TS_{\mathrm{m}}\right] \\ &= F_{\mathrm{HS}} + NkT\ln\frac{\phi_{\mathrm{p}}}{f} - NkT\ln\frac{\sinh\alpha_{\mathrm{e}}}{\alpha_{\mathrm{e}}} + 12\,NkT\kappa\lambda\phi_{\mathrm{c}}L^2\left(\alpha_{\mathrm{e}}\right) \end{aligned} \qquad (4.12)$$

where S_{m} is the orientational entropy of N dipoles with their orientations distributed according to (4.10):

$$S_{\mathrm{m}} = -Nk\!\int p\left(\theta\right)\ln p\left(\theta\right)d\Omega \qquad (4.13)$$

Phase equilibria can be located by finding compositions with equal pressure and chemical potentials of colloids and polymers. Expressions for the chemical potentials μ_c and μ_p and the pressure P can be derived from the free energy (4.12), taking (4.11) into account:

$$\frac{\mu_c - \mu_c^0}{kT} = \ln\frac{\phi_c}{1-\phi_c} + 7\frac{\phi_c}{1-\phi_c} + \frac{15}{2}\left(\frac{\phi_c}{1-\phi_c}\right)^2 + 3\left(\frac{\phi_c}{1-\phi_c}\right)^3 - \frac{\phi_p}{f}\left(\frac{df}{d\phi_c}\right)q^{-3} - \ln\frac{\sinh\alpha_e}{\alpha_e} \quad (4.14)$$

$$\frac{\mu_p - \mu_p^0}{kT} = \ln\frac{\phi_p}{f} \quad (4.15)$$

$$\frac{Pv_c}{kT} = \frac{\phi_c\left(1+\phi_c+\phi_c^2\right)}{\left(1-\phi_c\right)^3} + \frac{\phi_p}{f}\left(f - \phi_c\frac{df}{d\phi_c}\right)q^{-3} - 12\kappa\lambda\phi_c^2 L^2\left(\alpha_e\right) \quad (4.16)$$

where v_C is the volume of a colloid particle. The hard-sphere parts in (4.14)-(4.16) are taken from Scaled Particle Theory [25].

According to (4.15), the volume fraction of polymer in the *available* volume, ϕ_p/f, is the same for two phases in equilibrium. Finding the composition for two coexisting phases I and II therefore comes down to solving $\mu_c^I(\phi_c^I,\phi_p/f,\alpha_e^I)=\mu_c^{II}(\phi_c^{II},\phi_p/f,\alpha_e^{II})$ and $P^I(\phi_c^I,\phi_p/f,\alpha_e^I)=P^{II}(\phi_c^{II},\phi_p/f,\alpha_e^{II})$ at a given α and ϕ_p/f. The true polymer concentration in each phase follows from the imposed ϕ_p/f and f for each phase.

Perturbation theory

If dipole-dipole interactions are weak compared to kT, the part of Z_{DHS} containing dipole-dipole interactions can rewritten in terms of Mayer functions $\Phi_{dd}(ij)=\exp[-\beta u_{dd}(\mathbf{r}_{ij},\mathbf{\Omega}_i,\mathbf{\Omega}_j)]-1$ and the product of all $(\Phi_{dd}(ij)+1)$ can be expanded:

$$Z_{DHS} = \int..\int\exp\left[-\beta\frac{1}{2}\sum_{i,j\neq i}^N u_{hs}\left(r_{ij}\right) - \beta\sum_i^N u_m(\mathbf{\grave{U}}_i)\right]\left[1+\frac{1}{2}\sum_{i,j\neq i}^N\Phi_{dd}(ij)+...\right]d\mathbf{r}^N d\mathbf{\grave{U}}^N \quad (4.17)$$

Since the integration volumes are the same for all dipole pairs, the sum of Mayer functions gives $N(N-1)$ identical terms $\Phi_{dd}(12)$, hence integration over the orientations $\mathbf{\Omega}_3$ to $\mathbf{\Omega}_N$ can be carried out immediately, resulting in one term $\sinh(\alpha)/\alpha$ for each dipole. By integrating over the positions $\mathbf{r}_3$ to $\mathbf{r}_N$, the (hard sphere) pair distribution function $g^{(2)}(\mathbf{r}_{12})$ [28] can be introduced into (4.17):

$$Z_{DHS} = Z_{HS} \left(\frac{\sinh\alpha}{\alpha} \right)^{N} \left[1 - N\phi G\left(T,H\right) \right] \tag{4.18}$$

$$G\left(T,H\right) = \frac{1}{2v_{c}} \left(\frac{\alpha}{\sinh\alpha} \right)^{2} \int .. \int \Phi_{dd}\left(12\right) g^{(2)}\left(\mathbf{r}_{12}\right) \exp\left[-\beta u_{m}\left(\dot{\mathbf{U}}_{1}\right) - \beta u_{m}\left(\dot{\mathbf{U}}_{2}\right) \right] d\mathbf{r}_{12} d\dot{\mathbf{U}}^{2}$$

Combined with (4.6) and provided $G(T,H)$<<1, eqn. (4.18) gives the total free energy of the magnetic colloids-polymer mixture:

$$F = F_{HS} + NkT\ln\frac{\phi_{p}}{f} - NkT\ln\frac{\sinh\alpha}{\alpha} - NkT\phi G\left(T,H\right) \tag{4.19}$$

In order to calculate $G(T,H)$, the Mayer function is Taylor expanded and only the linear and quadratic term are retained. Integration over some of the angular coordinates can be evaluated without assumptions, giving

$$G\left(T,H\right) = \frac{1}{2v_{c}} L^{2}\left(\alpha\right) \iiint \lambda \frac{d^{3}}{r_{12}^{3}} \left(3\cos^{2}\theta_{r} - 1 \right) g_{0}\left(r_{12}\right) r_{12}^{2} dr_{12}\, d\theta_{r}\, d\phi_{r}$$

$$+ \frac{1}{2v_{c}} \frac{1}{3} \left\{ \frac{6}{5} - \frac{6}{5}\frac{L\left(\alpha\right)}{\alpha} + \frac{9}{5}\left[\frac{L\left(\alpha\right)}{\alpha}\right]^{2} \right\} 4\pi \int_{d}^{\infty} \left(\lambda \frac{d^{3}}{r_{12}^{3}} \right)^{2} g_{0}\left(r_{12}\right) r_{12}^{2} dr_{12} \tag{4.20}$$

It is important to note that in the first (multiple) integral, integration of ($3\cos^{2}\theta_r$-1) over the surface of a sphere gives 0 [8]. Consequently, only the outer regions of the system, where integration is not performed over the entire surface of a sphere, give non-zero contributions. And since $g_0(r_{12}) \to 1$ as $r_{12} \to \infty$, the integral does not depend on the actual structure of the colloidal particles, but does depend on the macroscopic shape of the system. As in the self-consistent field theory, we consider a needle-shaped sample here. The second integral does depend on $g_0(r_{12})$. Here, the low concentration approximation $g_0(r_{12})$=1 for $r_{12} \geq d$ is used.

Under the given conditions, $G(T,H)$ becomes

$$G\left(T,H\right) = 4\lambda L^{2}\left(\alpha\right) + \frac{4}{3}\lambda^{2} \left[\frac{6}{5} - \frac{6}{5}\frac{L\left(\alpha\right)}{\alpha} + \frac{9}{5}\left(\frac{L\left(\alpha\right)}{\alpha}\right)^{2} \right] \tag{4.21}$$

From (4.19), the chemical potential and pressure can be derived

$$\frac{\mu_{c} - \mu_{c}^{0}}{kT} = \ln\frac{\phi_{c}}{1-\phi_{c}} + 7\frac{\phi_{c}}{1-\phi_{c}} + \frac{15}{2}\left(\frac{\phi}{1-\phi_{c}}\right)^{2} + 3\left(\frac{\phi_{c}}{1-\phi_{c}}\right)^{3} - \frac{\phi_{p}}{f}\left(\frac{df}{d\phi_{c}}\right)q^{-3}$$

$$- \ln\frac{\sinh\alpha}{\alpha} - 2\phi G\left(T,H\right) \tag{4.22}$$

$$\frac{Pv_{c}}{kT} = \frac{\phi_{c}\left(1+\phi_{c}+\phi_{c}^{2}\right)}{\left(1-\phi_{c}\right)^{3}} + \frac{\phi_{p}}{f}\left(f - \phi_{c}\frac{df}{d\phi_{c}} \right)q^{-3} - \phi_{c}^{2}G\left(T,H\right) \tag{4.23}$$

and with (4.15), (4.22) and (4.23) the phase diagram can be calculated as explained in the section on the self-consistent field theory, with the exception that the μ_c does not depend on the self-consistent α_e here but on the external field α.

Note that when the λ^2 term in (4.21) is neglected, the free energies of the self-consistent field theory and perturbation theory are equal at infinite field strength.

4.3 Results and discussion

All phase diagrams are calculated for a polymer/colloid size ratio q=0.5 and at three different field strengths: α=0, α=2 (achievable by a small electromagnet) and α=10^6 (approaching the situation of complete alignment). Because each phase is defined by both density and magnetization, we can expect several types of phases. The isotropic (unmagnetized) fluid, gas and liquid phases are denominated IF, IG and IL, respectively. The magnetized fluid, gas and liquid phases are denoted by MF, MG and ML, respectively.

4.3.a Phase diagrams for λ=0.5

Self-consistent field theory (SCFT)

Figure 4.2 shows the phase diagrams of a system with λ=0.5, i.e. the magnetic interaction at closest distance is -1 kT, typical for the commonly used oleic acid grafted magnetite colloids. At zero field (α=0), the self-consistency relation (4.11) gives α_e=0 at all concentrations. Magnetic interaction is therefore absent and the phase diagram is that of a system of hard spheres with added polymer [15], exhibiting only IG-IL coexistence. At non-zero fields, the binodal obviously defines the region of MG-ML coexistence. Because magnetic interaction increases the effective attraction, a magnetic field shifts the binodal to lower ϕ_p/f or ϕ_p. Over the entire ϕ_c range, phase instabilities can be found at roughly 7% (α=2) or 17% (α=10^6) lower ϕ_p.

Perturbation theory (PT)

If λ is small, the Taylor expansion of eqn. (4.12) equals (4.19) up to order λ. It is therefore not surprising that the phase diagrams in figure 4.3 closely resemble those in figure 4.2. The (small) difference is due to the λ^2 term, which signifies a nearly field-independent attraction. Because of the λ^2 term, PT positions the binodals at slightly lower polymer concentrations than SCFT does.
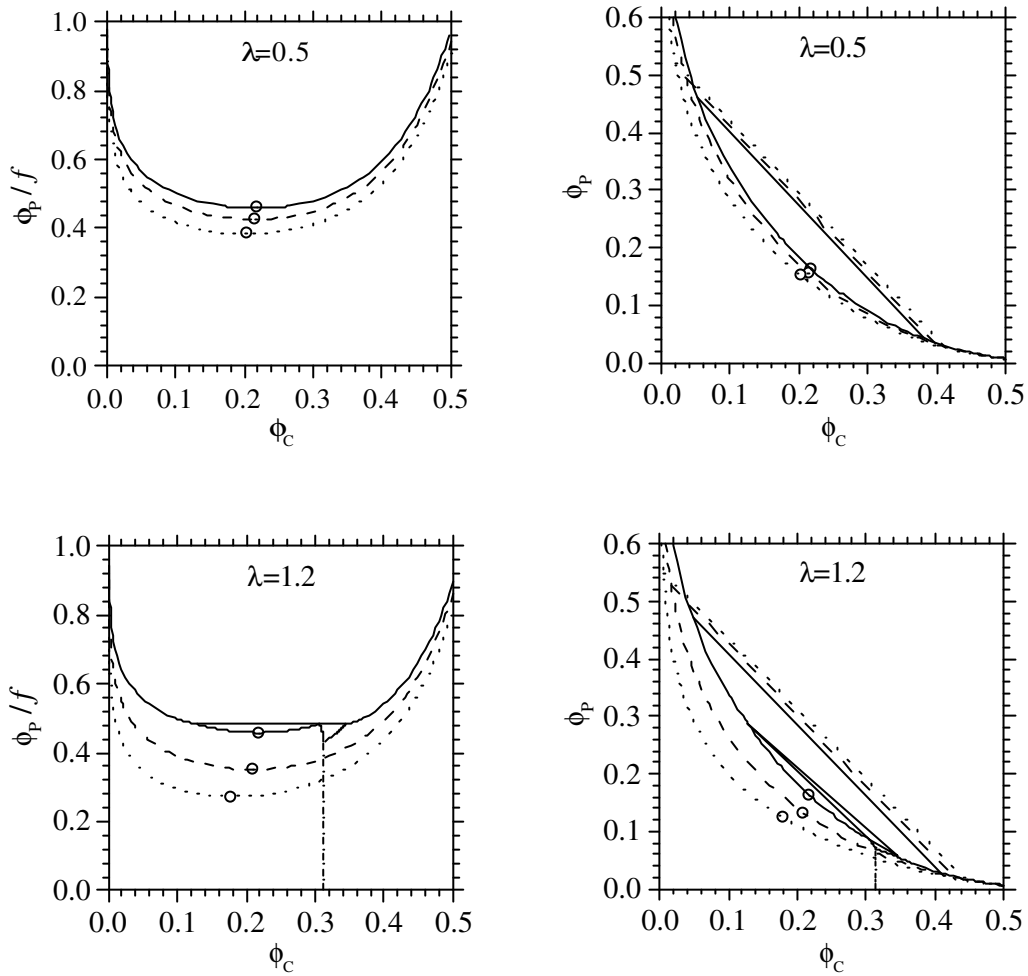
Figure 4.2. *Gas-liquid binodals for a system of magnetic colloids+non-adsorbing polymer, calculated with the self-consistent field theory for q=0.5, λ=0.5 (top) and λ=1.2 (bottom), and α=0 (solid line), α=2 (dashed line) and α=10⁶ (dotted line). Critical points are indicated by open circles. The vertical dash-dotted line is the Curie line, separating the isotropic fluid region from the spontaneously magnetized fluid region. The straight lines in the ϕ_c,ϕ_p diagrams represent are nodelines. For λ=1.2, the horizontal line in the left diagram and the trianglular region in the right diagram correspond to three phase coexistence at α=0.*

4.3.b   Phase diagrams for λ=1.2

Self-consistent field theory

At higher interaction strength (λ=*1.2*), the phase diagram calculated with SCFT gets a different appearance (see figure 4.2). At zero field, the IG-IL coexistence is still present, but in addition, the non-zero solution of (4.11) at ϕ_c>0.313 gives rise to IG-ML
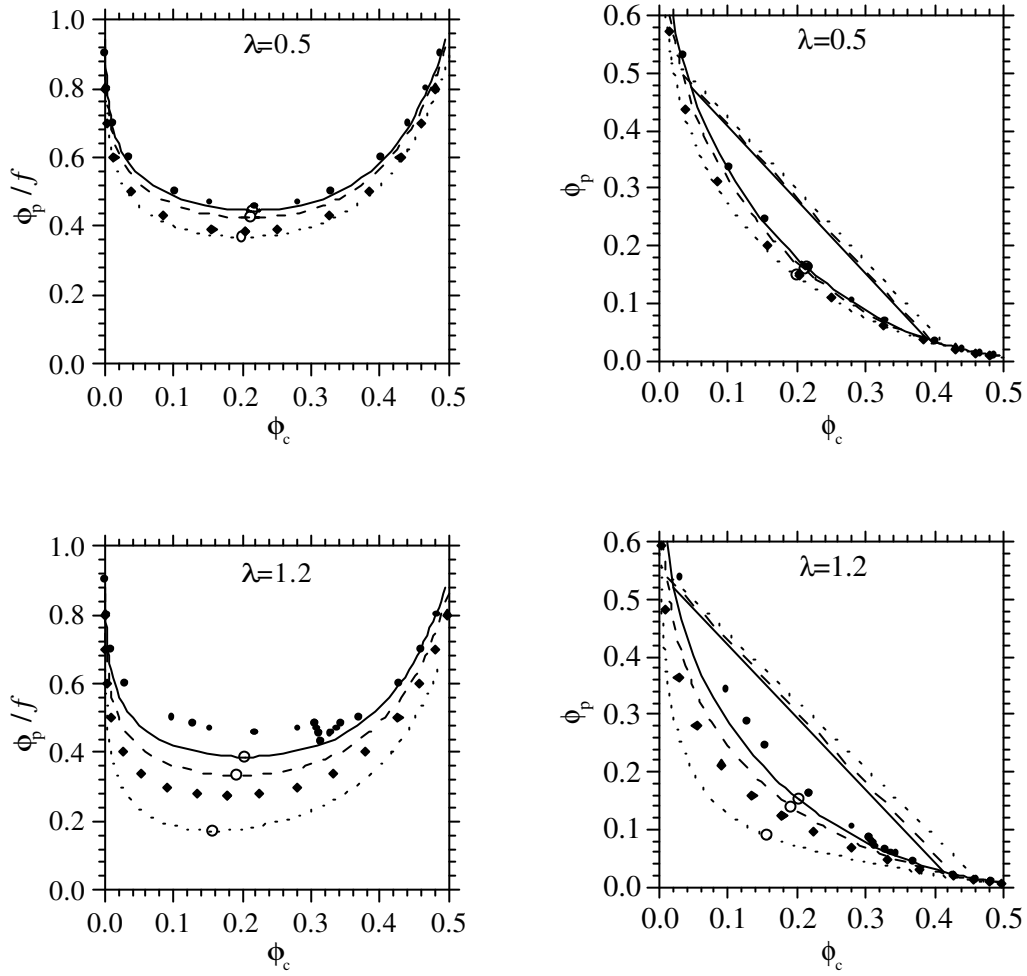
Figure 4.3. *Gas-liquid binodals for a system of magnetic colloids+non-adsorbing polymer, calculated with the perturbation theory for q=0.5, λ=0.5 (top) and λ=1.2 (bottom), and α=0 (solid line), α=2 (dashed line) and α=10⁶ (dotted line). Critical points are indicated by open circles. The straight lines in the diagrams in ϕ_c, ϕ_p representation are nodelines. The diagrams also contain some points calculated with self-consistent field theory for the same λ and q, and for α=0 (circles) and α=10⁶ (diamonds).*

coexistence. The IG-ML coexistence region ends in the so-called "tricritical point" [8], where the first order transition changes over to a second order transition (the Curie line). The two coexistence regions meet in the triple point, where IG, IL and ML are in equilibrium. In the ϕ_c, ϕ_p plot, this three phase coexistence appears as a three phase triangle (also shown in figure 4.2).

Upon application of a magnetic field, the isotropic phases vanish, leaving only MG-ML coexistence. The binodal is shifted towards lower polymer concentrations: about 20% lower ϕ_p at α=2 and 40% lower ϕ_p at α=10⁶.

The zero-field phase diagram in figure 4.2 shows qualitative resemblance to the diagram calculated by Zhang and Widom [8]. Their diagram of a Van der Waals fluid with added

magnetic interaction also exhibits a critical point, triple point and tricritical point. It is questionable, however, whether the tricritical point and triple point are realistic. Up to now, no experiments of spontaneously magnetized ferrofluids have been reported [7], and computer simulations only find spontaneous magnetization at high densities and very strong interaction (e.g. ϕ_c=0.42 and λ=5.3 for dipolar hard spheres [29], ϕ_c=0.31 and λ=6.7 for dipolar soft spheres [30]).

Perturbation theory

At λ=1.2, the phase diagrams obtained with PT and SCFT are clearly different (see figure 4.3). First, PT does not yield the spontaneously magnetized phase that SCFT does. Second, according to SCFT, magnetic interaction is absent in unmagnetized phases, whereas in PT dipoles always experience attraction (described by the λ^2 term in (4.21)). Consequently, the gas-liquid binodals obtained with PT lie below those obtained with SCFT. However, the lowering of the binodal upon application of an external field, 17% for α=2 and 47% for α=10^6, is comparable to the SCFT result.

4.3.c   Critical and tricritical point at various λ

The critical point, in particular ϕ_p/f, depends on both the strength of the external field and the strength of dipole-dipole interaction. The shift of the critical point towards lower ϕ_p/f upon increasing α and/or λ was already evident from figures 4.2 and 4.3, but is explicitly plotted as a function of λ in figure 4.4. In zero field, magnetic interaction hardly influences the position of the critical point, e.g. at λ=0.7, ϕ_p/f is lowered by merely 5%. At (nearly) infinite field strength, the influence of dipolar interaction is much more pronounced: now, λ=0.15 already suffices to lower ϕ_p/f by 5% (this is true for both SCFT and PT).

At ϕ_p/f=0, the critical points correspond to the critical points of pure dipolar hard sphere fluids. In the absence of a magnetic field, PT predicts the possibility of IG-IL coexistence at λ>2.83. The problem whether dipolar fluids can phase separate in zero field is still not resolved; in the past thirty years, theoretical and simulation results both in favor [31-33] and against it [10,34,35] have been reported. The result found with perturbation theory certainly does not clarify this question, because λ is clearly out of the range where the expansions described in the theory section are valid. In absence of polymer, SCFT only predicts IG-ML separation at λ>3.21. Although IG-ML coexistence is also found in the dipolar lattice gas model [2] and predicted by density functional theory [36], it has to our knowledge never been observed in computer simulations nor in experiments.
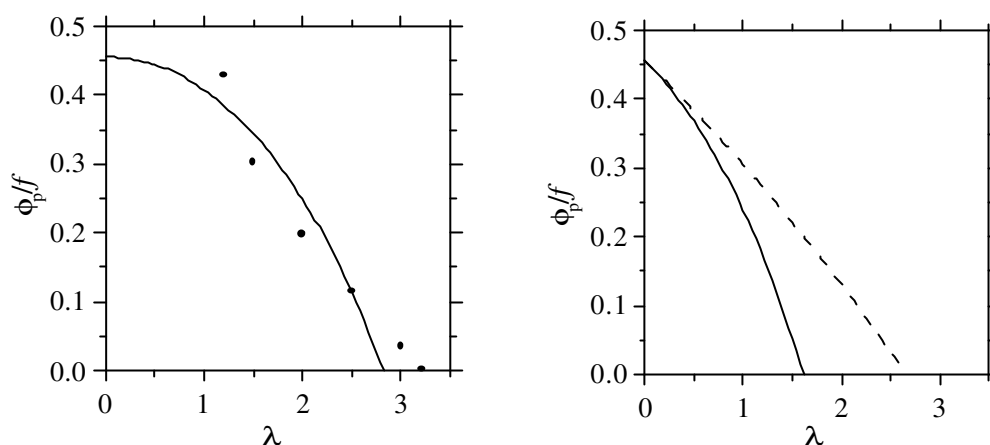
Figure 4.4. *Critical point according to perturbation theory (solid line) and self-consistent field theory (dashed line) at $\alpha=0$ (left graph) and $\alpha=10^6$ (right graph), for q=0.5. The left graph also displays the tricritical points (circles).*

At infinite field strength and in the absence of polymer, the critical values of λ for MG-ML coexistence are 1.62 and 2.66, according to PT and SCFT, respectively. The values differ significantly and are both much higher than the $\lambda > 0.95$ for magnetic lattice gas model [2]. They are, on the other hand, much lower than the limit of $\lambda > 5.6$ found by Monte Carlo simulations [37]. It should be noted, however, that the aforementioned theories poorly describe the behavior of strongly interacting particles ($\lambda > 1$).

In contrast, several authors have reported on field-induced phase separation in magnetite-based ferrofluids [4,21-24]. Even a very optimistic estimate, taking a core diameter 12 nm, a surfactant thickness of 2 nm and neglecting the non-magnetic surface layer, gives a λ of only 1.1. This is too small to explain the observed field-induced instabilities theoretically. Rather, these instabilities must be attributed to polydispersity [38], the presence of small aggregates [39-41], Van der Waals attraction[42], the influence of free oleic acid (dimers) which may act as a small depletion-inducing polymer, or a combination thereof. In some papers, the described procedure for preparing magnetic fluids does not include removal of unreacted oleic acid, thereby making the presence of free oleic acid in those samples likely. If we consider magnetite+free oleic acid as a colloid+non-adsorbing polymer mixture with $q=1/7$, and take a typical ϕ_c value of 0.2, we find phase separation above $\phi_p=0.22$ ($\alpha=0$), corresponding to a free oleic acid concentration of only 24 gl^{-1}. This indicates the importance of removing free oleic acid to obtain stable ferrofluids.

4.4 Conclusions

Using two different theories, namely the self-consistent theory and perturbation theory, we investigated the phase behavior of mixtures of magnetic colloids and non-adsorbing polymers at several magnetic field strengths. The polymer induces isotropic attraction between colloids, the strength and range of which can be modified independently from magnetic interaction.

For colloids with magnetic interaction comparable to that in commonly used magnetite-based ferrofluids (minimal energy -1 *kT*), both theories predict phase coexistence only in the presence of polymer. Application of a magnetic field promotes phase separation, but at infinite field strength the phase boundary shifts to only 17% lower polymer concentrations.

At stronger interaction (minimal energy -2.4 *kT*), the self-consistent field theory shows phase coexistence between an isotropic gas, isotropic liquid and a magnetized liquid in zero field. Application of an infinitely strong magnetic field shifts the phase boundary to approximately 40% lower polymer concentrations. No phase coexistence was found in systems without polymer.

The theories described may hint at the effect of unreacted surfactant in oleic acid-stabilized ferrofluids. It was estimated that a concentration of 24 gl^{-1} oleic acid may already destabilize a ferrofluid with a volume fraction of 20%.

Appendix I. Comparison of zero field free energies.

The free energy expression following from the perturbation theory, eqn. (4.19), is formally only valid for $\lambda \ll 1$ and small ϕ, but may in practice be accurate for larger λ and ϕ as well [16]. In order to assess the applicability of (4.19) for larger values of λ and ϕ, we compare it with the free energy according to the mean spherical model [43] (MSM), which can be used at $\lambda < 5$ and $\phi < 0.2$ [44]. Because the free energy within the MSM is only known for zero field, we limit our comparison to this case. In zero field, the magnetic contribution to the free energy is

$$F_{\mathrm{m}} = -\frac{4}{3} NkT\phi\lambda^2 \tag{4.24}$$

for the perturbation theory, and

$$F_{\mathrm{m}} = -8NkT\phi^{-1}\xi^2 \left[\frac{(1+\xi)^2}{(1-2\xi)^4} + \frac{(2-\xi)^2}{8(1+\xi)^4} \right] \quad , \tag{4.25}$$

for the MSM, where ξ in eqn. (4.25) is the solution of

$$8\lambda\phi = q(2\xi) - q(-\xi) \;\; ; \;\; q(\xi) = \frac{(1+2\xi)^2}{(1-\xi)^4} \tag{4.26}$$

The agreement between the simple perturbation theory and the more advanced MSM is reasonably good (see figure 4.5): even at $\lambda=5$ and $\phi=0.2$, eqn. (4.24) is less then two times as large as eqn. (4.25). This is due to the fact that neglecting local structure formation in concentrated fluids, i.e. taking $g_0(r>2a)=1$, partly cancels the overestimation made by cutting off the expansion of the Mayer function after the λ^2 term. This can be demonstrated by modifying eqn. (4.24) so that it takes local structurization around a central particle into account. At moderate concentrations, $g_0(r)$ can be approximated by [45]

$$g_0(r>d) = 1 + 8\phi\left[1 - \frac{3}{4}\frac{r}{d} + \frac{1}{16}\left(\frac{r}{d}\right)^3\right] \tag{4.27}$$

with which eqn. (4.24) becomes

$$F_m = -\frac{4}{3}NkT\phi\lambda^2\left[1 + \phi\left(\frac{1}{4} + \frac{3}{2}\ln 2\right)\right] \tag{4.28}$$

This modified free energy is larger then that in eqn. (4.24), and its deviation with the MSM is larger (see figure 4.5).
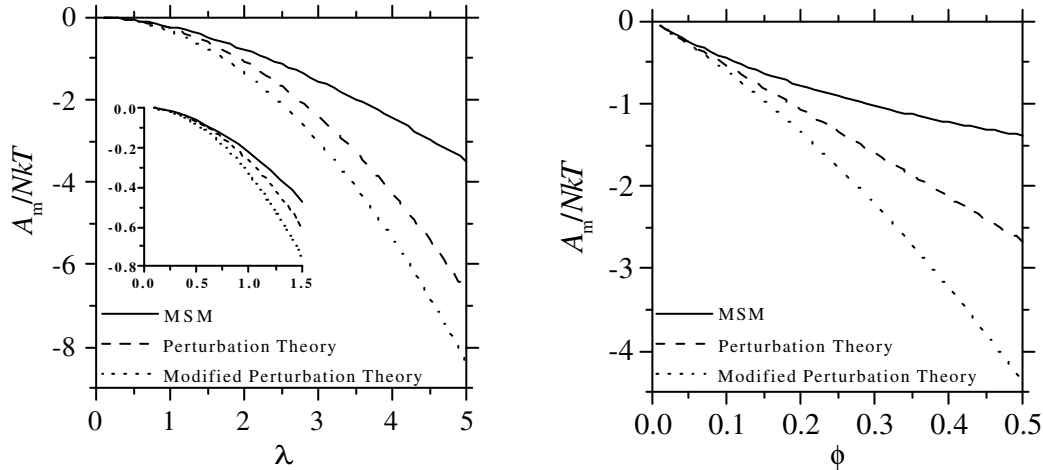

Figure 4.5. *Comparison of zero field free energies at fixed $\phi=0.2$ (left) and at fixed $\lambda=2$ (right). Even at $\phi=0.2$ and $\lambda=5$, MSM (eqn. (4.25)) and perturbation theory (eqn. (4.24)) differ only by a factor two.*

References

1   A. O. Tsebers, *Magnetohydrodynamics* **18**, 137 (1982).

2   K. Sano and M. Doi, *J. Phys. Soc. Jpn.* **52**, 2810 (1983).

3   P. I. C. Teixeira, J. M. Tavares, and M. M. Telo da Gama, *J. Phys.* **12**, R411 (2000).

4   R. E. Rosensweig and J. Popplewell, in 'Electromagnetic Forces and Applications', ed. J. Tani and T. Takagi, Elsevier Science Publishers, Amsterdam (1992), p. 83.

5   J.-C. Bacri, R. Perzynski, D. Salin, V. Cabuil, and R. Massart, *J. Colloid Interface Sci.* **132**, 43 (1988).

6   E. Dubois, V. Cabuil, F. Boue, J.-C. Bacri, and R. Perzynski, *Progr. Colloid Polym. Sci.* **104**, 173 (1997).

7   See chapter 3 of this thesis.

8   H. Zhang and M. Widom, *Phys. Rev. E* **49**, 3591 (1994).

9   J. M. Tavares, M. M. T. d. Gama, and M. A. Osipov, *Phys. Rev. E* **56**, 6252 (1997).

10   M. E. van Leeuwen and B. Smit, *Phys. Rev. Lett.* **71**, 3991 (1993).

11   S. Asakura and F. Oosawa, *J. Chem. Phys.* **22**, 1255 (1954).

12   A. Vrij, *Pure & Appl. Chem.* **48**, 471 (1976).

13   B. Vincent, J. Edwards, S. Emmett, and R. Croot, *Colloids Surf.* **31**, 267 (1988).

14   A. P. Gast, C. K. Hall, and W. B. Russel, *J. Colloid Interface Sci.* **96**, 251 (1983).

15   H. N. W. Lekkerkerker, W. C.-K. Poon, P. N. Pusey, A. Stroobants, and P. B. Warren, *Europhys. Lett.* **20**, 559 (1992).

16   Y. A. Buyevich and A. O. Ivanov, *Physica A* **190**, 276 (1992).

17   P. G. de Gennes and P. A. Pincus, *Phys. kondens. Materie* **11**, 189 (1970).

18   D. Levesque and J. J. Weis, *Phys. Rev. E* **49**, 5131 (1994).

19   L. N. Donselaar, P. M. Frederik, P. Bomans, P. A. Buining, B. M. Humbel, and A. P. Philipse, *J. Magn. Magn. Mater.* **201**, 58 (1999).

20   A. F. Pshenichnikov, *J. Magn. Magn. Mater.* **145**, 319 (1995).

21   A. F. Pshenichnikov and I. Y. Shurubor, *Izv. Akad. Nauk SSSR, Ser. Fiz.* **51**, 1081 (1987).

22   H. Wang, Y. Zhu, C. Boyd, W. Luo, A. Cebers, and R. E. Rosensweig, *Phys. Rev. Lett.* **72**, 1929 (1994).

23   C.-Y. Hong, I. J. Jang, H. E. Horng, C. J. Hsu, Y. D. Yao, and H. C. Yang, *J. Appl. Phys.* **81**, 4275 (1997).

24   H.-E. Horng, C.-Y. Hong, W. B. Yeung, and H.-C. Yang, *Applied Optics* **37**, 2674 (1998).

25   J. L. Lebowitz, E. Helfand, and E. Praestgaard, *J. Chem. Phys.* **43**, 774 (1965).

26   C. Kittel, 'Introduction to Solid State Physics', John Wiley & Sons, New York (1953).

27   R. E. Rosensweig, 'Ferrohydrodynamics', Cambridge University Press, Cambridge (1985).

28   J. P. Hansen and I. R. McDonald, 'Theory of Simple Liquids', Academic Press Ltd., London (1986).

29   J. J. Weis, D. Levesque, and G. J. Zarragoicoechea, *Phys. Rev. Lett.* **69**, 913 (1992).

30   D. Wei and G. N. Patey, *Phys. Rev. Lett.* **68**, 2043 (1992).

31   G. S. Rushbrooke, G. Stell, and J. S. Høye, *Mol. Phys.* **26**, 1199 (1973).

32   K.-C. Ng, J. Valleau, G. Torrie, and G. Patey, *Mol. Phys.* **38**, 781 (1979).

33   P. J. Camp, J. C. Shelley, and G. N. Patey, *Phys. Rev. Lett.* **84**, 115 (2000).

34   J.-M. Caillol, *J. Chem. Phys.* **98**, 9835 (1993).

35   R. P. Sear, *Phys. Rev. Lett.* **76**, 2310 (1996).

36   B. Groh and S. Dietrich, *Phys. Rev. E* **55**, 2892 (1997).

37   M. J. Stevens and G. S. Grest, *Phys. Rev. Lett.* **72**, 3686 (1994).

38   A. O. Ivanov, *Colloid Journal* **57**, 321 (1995).

39   S. W. Charles, *Chem. Eng. Comm.* **67**, 145 (1988).

40   P. C. Scholten, *Chem. Eng. Comm.* **67**, 331 (1988).

41   V. M. Buzmakov and A. F. Pshenichnikov, *J. Colloid Interface Sci.* **182**, 63 (1996).

42   P. Scholten, *J. Magn. Magn. Mater.* **39**, 99 (1983).

43   J. W. H. Sutherland, G. Nienhuis, and J. M. Deutch, *Mol. Phys.* **27**, 721 (1974).

44   L. Verlet and J.-J. Weiss, *Mol. Phys.* **28**, 665 (1974).

45   J. A. Barker and D. Henderson, *Rev. Mod. Phys.* **48**, 587 (1976).

Phase behavior of magnetic colloids-polymer mixtures:

a magnetic sensing coil study

Abstract

The theory and application of a magnetic sensing coil is described, which is used to study the phase behavior of mixtures of magnetic colloids, in this case oleic acid grafted magnetite, and non-adsorbing polymer. The coil measures the local susceptibility in a ferrofluid+polymer sample, from which magnetite concentrations in the separate phases of a phase separated sample can be obtained. It is also shown that the concentration of polymer in each phase can be obtained by combining measurements on different samples.

Experimental results obtained with the sensing coil show all features that were theoretically expected. However, a shortcoming of this technique was also evident: the polydispersity of the magnetic colloids caused size fractionation in a phase separated sample. Because the susceptibility not only depends on concentration, but also strongly on particle size, the true colloid concentration could not be obtained from susceptibility measurements. This in turn made a correct determination of polymer concentrations in separate phases impossible. Still, the magnetic sensing coil has proven to be a valuable tool in obtaining accurate quantitative information on the stability of ferrofluids.

5.1   Introduction

Ferrofluids are colloidal dispersions of (mostly) spherical ferro– or ferrimagnetic particles in a non-magnetic solvent. Because of its monodomain nature, each particle has a permanent magnetic dipole moment. Ferrofluids are therefore frequently used as model systems for dipolar sphere fluids.

Theoretically, the phase behaviour of such systems is still controversial. On the one hand, various theories such as mean field theories [1-3], mean spherical approximation [4] and perturbation theories [5] predict the existence of a gas-liquid equilibrium even in the absence of a magnetic field. On the other hand, computer simulations [6,7] fail to find such an equilibrium, except when isotropic attraction is present in addition to dipolar interaction [6].

Experimentally, phase equilibria in ferrofluids have been found under various circumstances. In zero field, aqueous magnetic fluids become thermodynamically unstable when the ionic strength exceeds a critical value [8-10]. Sterically stabilized magnetic colloids can be made to phase separate by reducing the solvent quality [11] or adding a non-adsorbing polymer [12]. All instabilities probably involve a significant amount of isotropic attraction, either in the form of Van der Waals attraction in aqueous ferrofluids [10] and ferrofluids in a poor solvent, or depletion attraction in mixtures of magnetic particles and free polymer [13].

The stability of magnetic fluids is mostly studied using optical microscopy, which directly reveals the nature of the coexisting phases. Moreover, in principle microscopy also allows determination of the interfacial tension and the difference in susceptibility between dilute and concentrated phase [14]. Another technique that has been employed is the use of a magnetic sensing coil [15-18] which allows the direct determination of the susceptibility at any height in a sample tube with high accuracy. This instrument gives information about the volumes and susceptibilities of all phases in a non-destructive way.

In this chapter we report on the stability of mixtures of magnetic particles and non-adsorbing polymer, measured with a magnetic sensing coil. Variation of the polymer concentration leads to modification of the isotropic attraction between magnetic particles without altering their other properties. After describing the operation of the sensing coil and interpretation of measurements, a method is described for constructing a phase diagram, including nodelines. This method is subsequently applied to data obtained with the sensing coil.

Part I: Susceptibility meter

5.2 Introduction

The initial susceptibility χ_i , which represents the change in magnetization upon applying a small external field, is proportional to the concentration of magnetic colloids if they have negligible mutual magnetic interactions. More specifically, the initial susceptibility (denoted here as 'susceptibility' or 'χ') is

$$\chi \equiv \left(\frac{\partial M}{\partial H}\right)_{H=0} = n\frac{\mu_o}{3kT}\left\langle m^2 \right\rangle \tag{5.1}$$

where n is the particle number density, μ_o the permeability of vacuum, m the particle dipole moment and k and T are Boltzmann's constant and the absolute temperature, respectively. The brackets $< >$ denote a number average. The experimental setup used here to measure concentration profiles is similar to the one described by Peterson *et al.* [15].

5.3 Description and theory

A scheme of the experimental setup is depicted in figure 5.1. Ferrofluid samples were held in cylindrical tubes with 6 mm internal diameter, which were sealed with a screwcap. A susceptibility profile is measured by moving a tube in 1 mm steps through a sensing coil. This coil is part of a Colpitts oscillation circuit, which in turn is connected to a frequency counter (HAMEG HM8021-3), and a DC power supply. The coil produces an oscillating magnetic field with an amplitude of about 100 A m^{-1} and a frequency that depends on the self-inductance L. When no ferrofluid is inserted the circuit oscillates at a basic frequency f_o which is close to 1 MHz for the circuit used here. The frequency changes with an amount Δf when the presence of a ferrofluid changes the self-inductance of the coil. To understand how L is changed, we calculate ΔL for the case of a sample with a height dependent susceptibility $\chi(Z)$ that is inserted into the coil as shown in figure 5.1. The change of self-inductance is, by definition, proportional to the change of flux $\Delta\Phi$ through the coil. The contribution of an imaginary thin ferrofluid disc to ΔL depends on the position (z-Z) with respect to the coil and is proportional to the susceptibility $\chi(Z)$. The sum of contributions of all 'discs' that the sample consists of, is the convolution integral

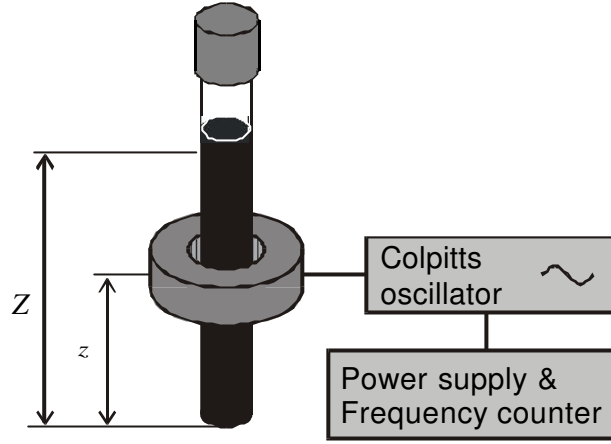$$\Delta L(z) \propto \int_{-\infty}^{+\infty} \chi(Z)r(z-Z)dZ \tag{5.2}$$

Figure 5.1. *Schematic drawing of the susceptibility meter setup.*

where $r(z\text{-}Z)$ is a response function which only depends on the geometry of the coil. This equation implies that sharp changes in the susceptibility profile are 'smeared out' when measured with the oscillator.

Using $L \propto f^{-2}$ for this oscillator [18], we can derive

$$\Delta L(z) \propto F(z) \equiv \left(\frac{f_o}{f_o + \Delta f(z)} \right)^2 - 1 = \int_{-\infty}^{+\infty} \chi(Z)\, r(z - Z) dZ \tag{5.3}$$

For the simple case of a height independent susceptibility eqn. (5.3) reduces to $\Delta L \propto \chi$ which was used in earlier publications [15,18].

The response function can be measured using a long cylinder of ferrofluid with a flat bottom. The susceptibility is constant inside the cylinder and zero outside. Eqn. (5.3) now becomes

$$F(z) = \chi \int_0^{\infty} r(z - Z) dZ \tag{5.4}$$

from which we can derive

$$r(z) = \frac{1}{\chi} \frac{dF(z)}{dz} \tag{5.5}$$

In principle, $\chi(z)$ can be obtained by Fourier transforming eqn. (5.3),

$$\chi(\omega) = \frac{F(\omega)}{r(\omega)} \quad , \tag{5.6}$$

followed by inverse Fourier transformation of $\chi(\omega)$ to $\chi(z)$. But in practice small errors in the high frequency part of $r(\omega)$ result in a very noisy susceptibility profile.

5.4   Experiments

The detection limit, defined here as twice the level of fluctuations, was determined by comparing *F* of a dilute ferrofluid sample with the susceptibility measured with a commercial apparatus (Agico Kappabridge KLY-3). The relation $\chi=7.30\,F$ was thus found. Fluctuations in Δf were about 2 Hz, making the detection limit $\chi=5.84\ 10^{-5}$.

The response function of the sensing coil was measured using the method described in the previous section. The result (figure 5.2) shows that the response function is almost symmetrical, as it should be for a symmetrical coil, and that 95% of the response comes from the area within 7 mm from the center of the coil.

Later we will use an empirical expression for the response function, or rather its derivative. A sigmoidal curve of the form

$$F(z)=\frac{A}{1+\exp\left[\pm\dfrac{(z-z_o)}{w}\right]}, \tag{5.7}$$

where *A* is the height of the step, z_o its position and *w* the extent of smearing, describes a convoluted concentration step very well (see figure 5.3). Note that *w* (which is 1.76) is constant and only depends on the geometry of the coil.
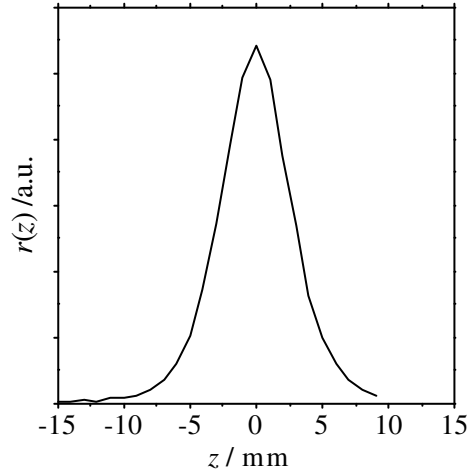

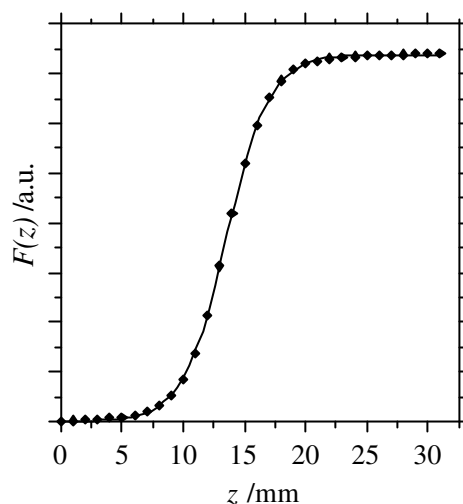***Figure 5.2.*** *Measured response function of the sensing coil.*

Figure 5.3. *Convoluted step profile. (♦) measurements;(———) fit with eqn. (5.7).*

Part II: Phase separation experiments

5.5   Background

The interaction potential between sterically stabilized magnetite particles contains three contributions. At short distance an almost hard sphere repulsion dominates the interaction. At distances beyond the hard sphere diameter particles experience dipole-dipole (anisotropic) interaction and Van der Waals (isotropic) attraction. In addition, adding small amounts of non-adsorbing polymer can further increase the isotropic attraction. When two magnetic particles are at close distance, polymer coils are expelled (depleted) from the space in between these particles. The absence of polymer between particles results in a net osmotic force pushing particles together. This can be modeled as an effective attraction, called 'depletion attraction' [19].

Depletion attraction can induce fluid-crystal and gas-liquid phase separation [20]. Figure 5.4 shows a general phase diagram of a mixture of colloids and polymer [13]; c_{col} and c_{pol} refer to the concentrations of colloids and polymers, respectively. A mixture having a composition C or any other composition on the nodeline will demix into two phases G and L, G being poor in colloids, rich in polymer and L rich in colloids, poor in polymer. Such a colloidal gas-liquid coexistence is expected for polymer/colloid size ratios larger than 0.3 [20].

The susceptibility meter can in principle measure the concentration of magnetic particles in each phase, but not the concentration of polymer. Therefore, in an
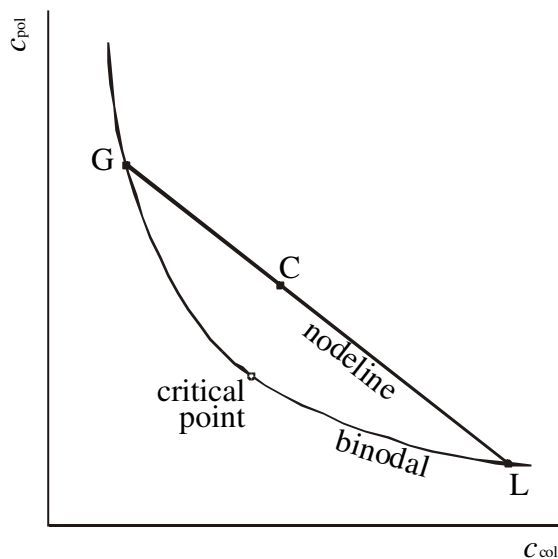
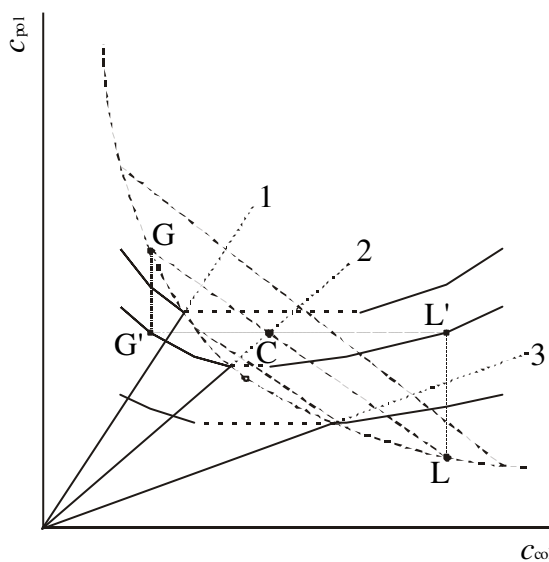***Figure 5.4****. General phase diagram of colloid-polymer mixtures.*

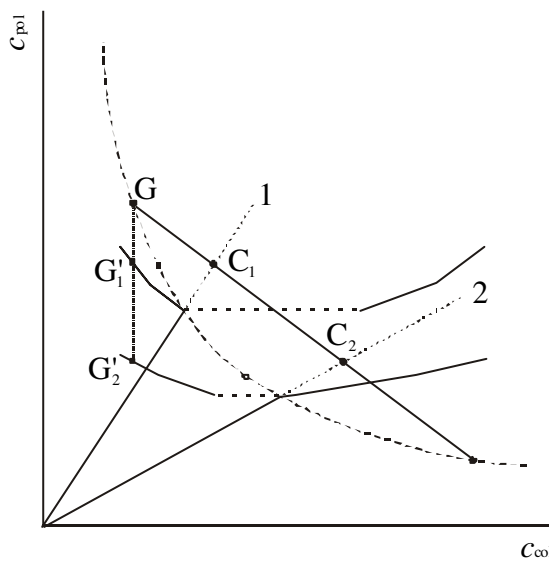***Figure 5.5****. Experimental phase diagram of colloid-polymer mixtures.*

Figure 5.6*. Reconstruction of the phase diagram and nodelines.*

experimental diagram the *overall* polymer concentration must be plotted on the vertical axis. In figure 5.5, such an experimental diagram is constructed from the general phase diagram. The lines labeled '1', '2' and '3' are three samples whose concentrations are varied by adding or removing solvent. This changes the overall composition but leaves the colloid/polymer ratio unaffected; hence, the concentration lines are straight lines through the origin. Beyond the coexistence curve, phase separation takes place and a concentration line splits into a gas line and a liquid line. Depending on the position with respect to the critical point, there is a discontinuous transition from the concentration line to either the gas or the liquid line, and a continuous transition to the other line. As an example, the construction of two points in the experimental diagram is shown in figure 5.5. A sample with initial composition C demixes into two phases having compositions G and L. In the experimental diagram G and L are shifted vertically to G' and L' such that their polymer concentration equals the overall polymer concentration, i.e. the polymer concentration in C.

The construction method described above can also be reversed. The real coexistence curve and nodelines can be reconstructed by combining two experimental gas lines or liquid lines. Consider, as illustrated in figure 5.6, two points G_1' and G_2' on the gas lines of samples 1 and 2. If the colloid concentrations on G_1' and G_2' are equal, both these points correspond to the end of one nodeline. Therefore, their initial compositions C_1 and C_2 must also be part of that same nodeline. Knowing this, the point G can be located on the intersection between the line through G_1' and G_2' and the nodeline through C_1 and C_2.

The reconstruction method described here contains no assumptions and can be applied to any two-component mixture where the concentration of only one of the components can be determined directly.

5.6   Experimental

5.6.a   Preparation of magnetic fluids

Two ferrofluids were used in these experiments, both containing iron oxide particles stabilized with oleic acid and dispersed in cyclohexane. One ferrofluid, coded FOC1, was prepared according to a method described elsewhere [21]. In summary, magnetite was precipitated from an aqueous solution, washed and extracted into pure oleic acid. Excess oleic acid and water was then removed by washing with dry ethanol. After drying the sample easily dispersed in cyclohexane. The other ferrofluid, FFR, was prepared in the group of L. Vekas at Universita Politehnica in Timisoara, Romania.

5.6.b   Characterization

TEM photographs were taken on a Philips CM10 electron microscope and analyzed with IBAS (an electronic image analysis system).

Magnetization measurements were performed on a MicroMag 2900 alternating gradient magnetometer (Princeton Measurements Corporation) in fields up to $1.2 \ 10^6 \ \text{Am}^{-1}$ (see chapter 2 for details). The diameter d_M of the magnetic core was calculated with

$$\tilde{\chi} \equiv \frac{\chi}{M_s} = \frac{\mu_o}{3kT} \frac{\langle m^2 \rangle}{\langle m \rangle} = \frac{\mu_o}{3kT} M_{sbulk} \frac{\pi}{6} d_M^3 \tag{5.8}$$

using a bulk saturation magnetization $M_{s,bulk} = 4.8 \ 10^5 \ \text{Am}^{-1}$.

The mass density ρ of a dispersion was measured with an Anton Paar DMA 5000 densitometer. Combined with the mass concentration c this yields the density of dry particles ρ_{dry}:

$$\rho_{dry} = \frac{c\rho_{solvent}}{c + \rho_{solvent} - \rho} \tag{5.9}$$

5.6.c   Calibration of the susceptibility meter

The relation between concentration and F (eqn. (5.3)) was measured for a range of concentrations. A certain amount of dispersion was dried in the sample tube under flowing nitrogen gas. The remaining solid was weighed and dissolved in cyclohexane. This dispersion was then concentrated stepwise by evaporation of the solvent, followed by vigorous shaking. The weight and susceptibility were measured after each step.

5.6.d   Phase separation experiments

Colloid-polymer mixtures were prepared similar to the method described in the previous section: a certain amount of magnetic fluid was dried under flowing nitrogen and weighed. Before adding the solvent pure poly(dimethylsiloxane) (ACBR, MW=41500 g mole^{-1}, radius of gyration ≈ 8.5 nm) was added and weighed as well. Finally, the mixture was dissolved in cyclohexane.

Each sample was stepwise concentrated and mixed thoroughly after which it was left to stand for at least one day. The sample was then weighed and a concentration profile was recorded by moving the sample in 1-mm steps through the coil and measuring F after each such step. The position of the interface was found by fitting the concentration profile with a sum of convoluted step functions (eqn. (5.7)), one such function for each concentration step.

5.6.e   Size fractionation

Because our samples are polydisperse, the size of magnetic particles in demixed samples is expected to be different in both phases. Therefore, size fractionation in phase separated samples was examined after the phase separation experiments. Starting from their most concentrated state, samples were stepwise diluted by adding cyclohexane, and left to stand for at least one day. After each dilution step, the size of particles in the upper phase was measured by taking about $5\,\mu l$ of that phase, diluting it with cyclohexane, and analyzing it using magnetometry (see Characterization section above).

5.7   Results

5.7.a   Characterization

Characterization results are summarized in Table 5.1. The diameter d_{TEM} is the average diameter of particle cores and σ_{TEM}/d_{TEM} is the relative error therein. Note that $d_M^3=\langle d^6\rangle/\langle d^3\rangle$, so d_M is larger than $\langle d\rangle$ even if a small non-magnetic layer is present.

Table 5.1. Ferrofluid characteristics.

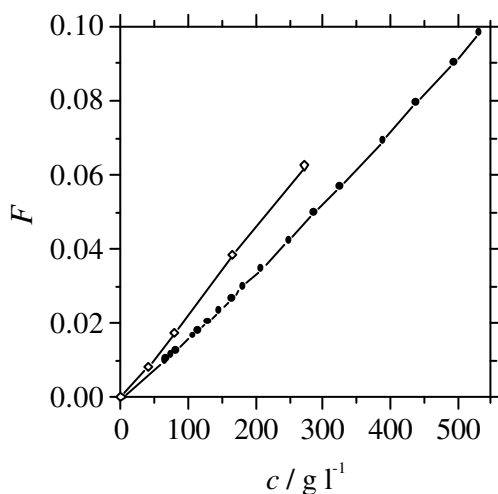| Sample	d_M/nm	d_{TEM}/nm	σ_{TEM}/d_{TEM}	ρ_{dry}/kg m^{-3}
FOC1	11.9	9.1	0.31	
FFR	11.3	9.1	0.26	2900

Figure 5.7. *Calibration curve of susceptibility meter. (   ) FOC1; (   ) FFR.*

5.7.b Calibration

The susceptibility as a function of concentration is shown in figure 5.7. The data show a small but consistent deviation from a linear relation owing to mutual magnetic interaction between the colloids.

5.7.c Phase separation experiments

Figures 5.8 and 5.9 show the experimental diagrams of FOC1 and FFR mixed with PDMS. The concentration of magnetic particles, c_{col}, was calculated from F and the calibration curve 5.7. The average polymer concentration (vertical axes) is calculated from the masses and densities of all three components. Of some samples the concentration line was also measured in the opposite direction, i.e. by diluting the sample. These measurements coincided exactly with the points measured by concentrating. This shows that the instability is reversible and reproducible. We also checked whether added polymer affects the susceptibility. If this is the case, the curves of F vs. c_{col} of colloid/polymer mixtures should deviate from the calibration curve in figure 5.7. Figure 5.10 shows that curves with different colloid/polymer ratios overlap nicely, so adding polymer does not influence the susceptibility noticeably.
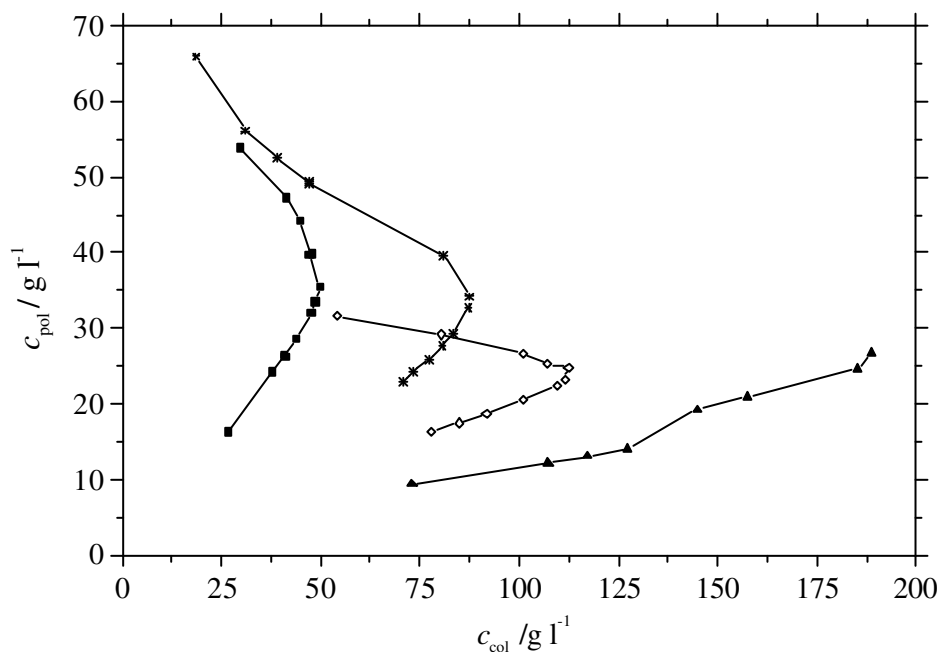

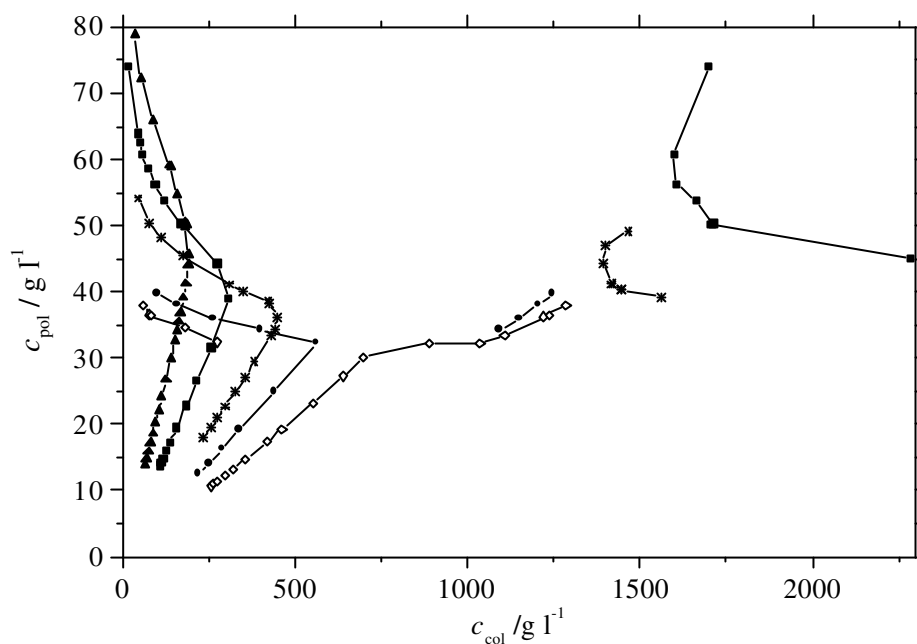***Figure 5.8.** Experimental phase diagram of FOC1.*

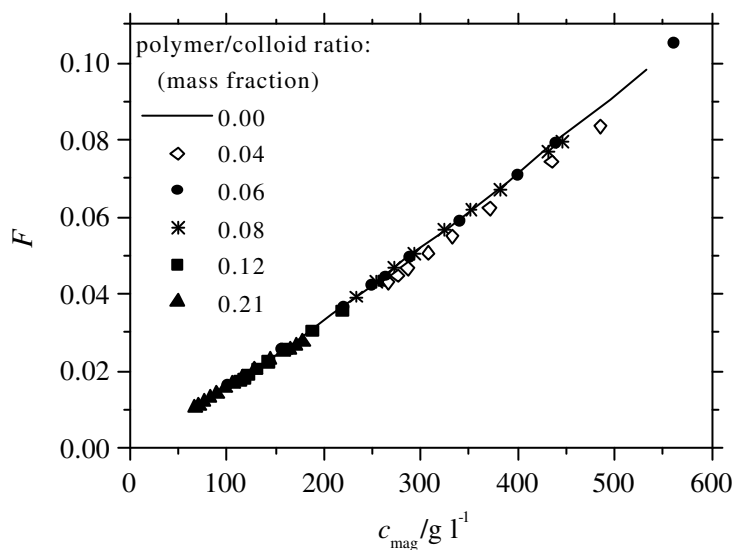**Figure 5.9.** *Experimental phase diagram of FFR..*

Figure 5.10. *Calibration curves, showing that polymer has negligible influence on the susceptibility.*

A typical susceptibility profile and a fit with the sum of two convoluted step profiles are shown in figure 5.11. The dotted lines represent the positions of the bottom of the tube and the phase boundary. Measurements and the fitted curve are in excellent agreement, suggesting that the phase boundary is sharp. Susceptibility profiles never showed significant changes after one day, so it is probably an equilibrium state we are
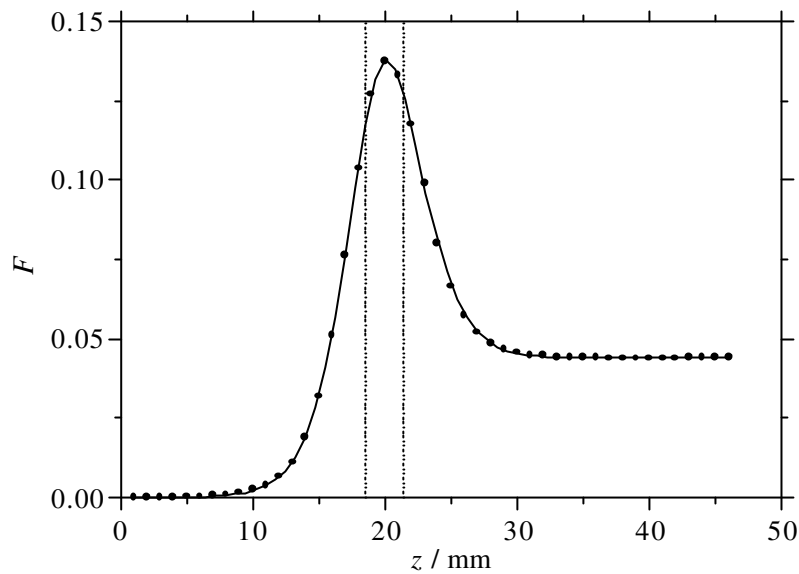
Figure 5.11. *Typical susceptibility profile of a phase separated sample.*
(●) measurements; (———) fitted profile; (……) positions of concentration steps.

observing. In most samples the dilute phase occupied the largest part of the sample volume. The susceptibility of this phase could therefore be measured directly without interference from the phase boundary and the sample meniscus. The concentrated phase was in many cases so thin and concentrated that demagnetization was expected to hinder the direct determination of the susceptibility. Therefore, the concentration of magnetic particles was obtained indirectly from the thickness of this phase. Conservation of mass states that $M_{total}=M_{gas}+M_{liq}$; this gives us the magnetic particle concentration in the concentrated phase:

$$c_{liq} = \frac{M_{total} - c_{gas}V_{gas}}{V_{liq}}$$

(5.10)

All points on the liquid lines where calculated this way.

The experimental diagrams (figures 5.8 and 5.9) contain several features that were expected based on the derivation in section 5.5. The discontinuity in going from the concentration line to either the gas or the liquid line is found both theoretically and experimentally. The critical point of FFR should be close to the point where the sample with the second lowest polymer/colloid ratio becomes unstable, i.e. around $c_{col}=550$ gl^{-1} and $c_{pol}=32$ gl^{-1}.

Deviations from the expected behavior are also present. In samples with high polymer/colloid ratios, a gradual transition from the concentration line to the gas line is found, whereas a sharp transition was expected. Also, the liquid lines of these samples show a peculiar feature, namely a decreasing colloid concentration with increasing

polymer concentration. At this moment, we can not explain this behavior.

The difference between the experimental diagrams of FOC1 and FFR is also noteworthy. Despite the fact that the mean particle size in the same in both samples, FOC1 phase separates at a much lower polymer concentration than FFR does: at c_{col}=100 gl^{-1}, FFR phase separates at a polymer concentration of about 60 gl^{-1}, whereas FOC1 is already destabilized at c_{pol}=25 gl^{-1}. The difference may be due to particle clustering [22-24]. FFR has been freed from clusters by magnetic filtration, which is experimentally confirmed by the SAXS measurements described in chapter 2. FOC1 was not filtered, and presumably contains clusters which are small enough to remain dispersed (see chapter 2), but large enough to give a somewhat larger 'magnetic' radius (Table 5.1).

5.7.d   Size fractionation

Figure 5.12 shows the low concentration part of the phase diagram of FFR (figure 5.9), with the magnetic particle diameter d_M in the gas phase at several points on the gas lines. It is obvious that phase separation causes significant fractionation.

Fractionation will cause a discrepancy between the true colloid concentration $c_{col,true}$ and the 'experimental' colloid concentration $c_{col,exp}$ calculated from the susceptibility χ_i. To see how c_{col} is affected, we first write it as $c_{col}=n<M_p>$, where $n=N/V$ is the number density of particles and $<M_p>$ is the number average mass of a single particle. Because of the high mass density ρ_m of magnetite, $<M_p>$ will be mainly determined by the magnetite core: $M_p \approx <V_m>\rho_m \sim <d_m^3>$ (V_m and d_m are the core volume and diameter, respectively). In the low concentration regime, eqn. (5.1) holds and the number density is $n \sim \chi_i/<m^2> \sim \chi_i/<d_m^6>$. Note that the physical diameter is taken to be equal to the diameter of the magnetic core, which implies that the presence of a magnetically 'dead' surface layer is neglected. The colloid concentration therefore depends on χ_i as

$$c_{col} = k\chi_i \sim d_M^{-3}\chi_i \quad , \qquad (5.11)$$

where we have used $d_M^3 = \left\langle d_m^6 \right\rangle / \left\langle d_m^3 \right\rangle$ (see eqn. (5.8)). It is clear from eqn. (5.11) that the proportionality constant k strongly depends on the particle size distribution. However, in the experiments k is only determined from unfractionated samples, and is taken constant. The relation between the experimental and true concentration is therefore

$$c_{col,true} = k\chi_i = \frac{d_{M,0}^3}{d_M^3} k_0\chi_i = \frac{d_{M,0}^3}{d_M^3} c_{col,exp} \quad , \qquad (5.12)$$
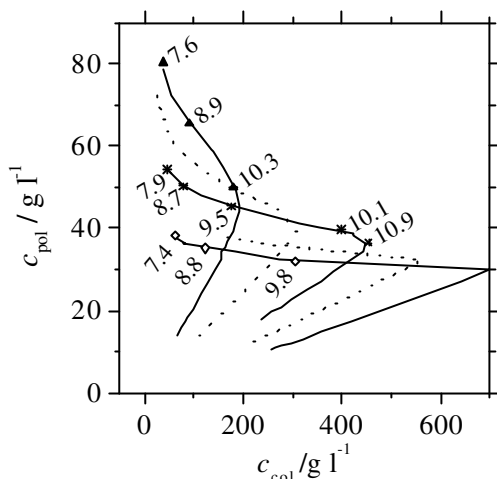
Figure 5.12. *Fractionation upon phase separation. Numbers in plot area represent particle sizes in nanometers, measured with magnetization measurements (eqn. (5.8)). The particle size in the unfractionated ferrofluid is 11.3 nm.*

where k_0 and $d_{M,0}$ denote the values obtained from unfractionated samples. Eqn. (5.12) is directly related to figure 5.12, where d_M is displayed for phase separated samples. It can be seen that the true colloid concentration can be as much as 3.5 times as high as the experimental concentration ($d_{M,0}/d_M$=11.3/7.4).

5.7.e   Reconstruction of the phase diagram

Straightforward application of the reconstruction method, as described in the theory section, does not lead to satisfying results. Firstly, because nodelines, obtained by combining two experimental gas lines at several colloid concentrations, cross each other within the two phase region. This is, of course, unphysical. And secondly, all nodelines determined at a certain colloid concentration should overlap. This is not the case: such nodelines are not even parallel. The main reason is that size fractionation causes a drastic change in the relation between F and c_{col}, which was assumed to be constant (see previous section). Since particles in the dilute phase are smaller than average, the colloid concentration calculated from F is smaller than the true concentration. In some cases, the difference is as high as a factor of 3. Furthermore, since fractionation is different for each sample, two gaslines are combined at different colloid concentrations (but at equal F's). And finally, the reconstruction method cannot be applied to systems with polydisperse components, because in such systems the two-phase region is separated from the homogeneous mixture by a coexistence *surface* rather than a curve.
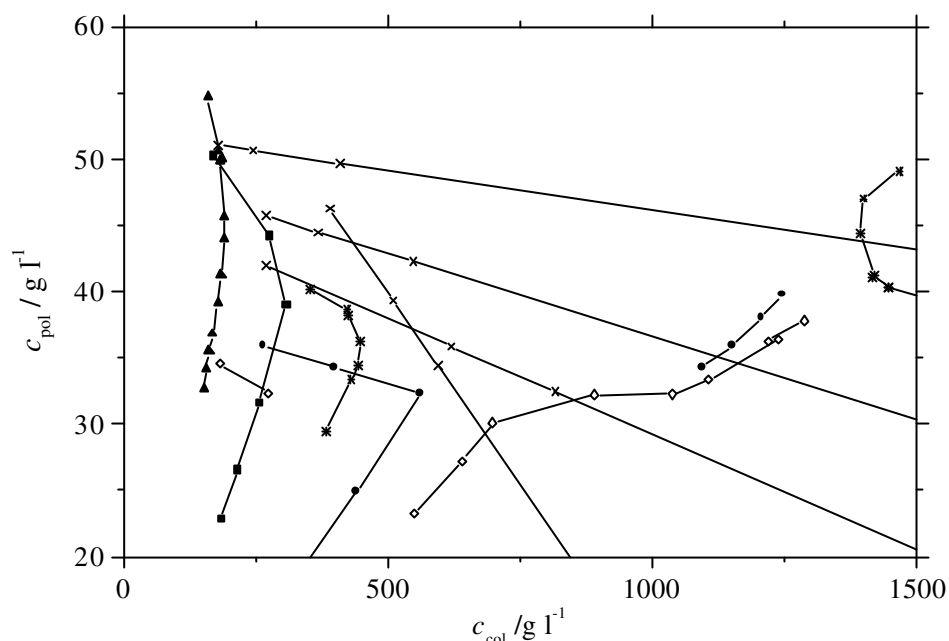
Figure 5.13. *Phase diagram of FFR, with nodelines.*

To minimize the influence of polydispersity, we focussed on those parts of the gaslines where the least fractionation was found, i.e. close to the coexistence curve. Therefore, only combinations of samples with comparable polymer/colloid ratios were used for reconstruction. Points in between measurements were found by cubic spline interpolation. The results in figure 5.13 show that three out of four nodelines do not cross within the two-phase region, but one nodeline has a slope which differs significantly from the others and crosses all others nodelines.

5.8   Conclusions

In this chapter, a susceptibility meter based on a Colpitts oscillator has been described and tested. With this instrument, phase instabilities of magnetic fluids containing free polymer were investigated. By increasing the amount of polymer, phase separation can be induced without a magnetic field. Furthermore, an exact method for reconstructing the coexistence curve and nodelines was described and tested. Although size fractionation hampered the reconstruction of nodelines, the experimental phase diagram qualitatively agrees with expectations.

Acknowledgements

Appendix I. Technical description of the Colpitts oscillator

The Colpitts oscillator

A Colpitts oscillator has fairly good frequency stability and is easy to tune. In a Colpitts oscillator (figure 5.14), the positive feedback condition for oscillation is established by a network of 2 capacitors (C_1 and C_2), separated by an inductor (L_1) that forms in this case the sensing coil. The transistor, used as an amplifier, fulfills the condition to make the closed loop gain equal to 1. When the quality factor of the resonance circuit is high the resonance frequency f is given by:

$$f \approx \frac{1}{2\pi} \sqrt{\frac{1}{L_1 C_v}}$$

with C_v the series capacitance of C_1 and C_2. Oscillation is initiated by random noise. Because the self-inductance L_1 of the sensing coil is proportional the the susceptibility of, for example, a ferrofluid sample inserted into the coil, the oscillation frequency of the Colpitts oscillator is a measure for the concentration of ferromagnetic particles in the sample.
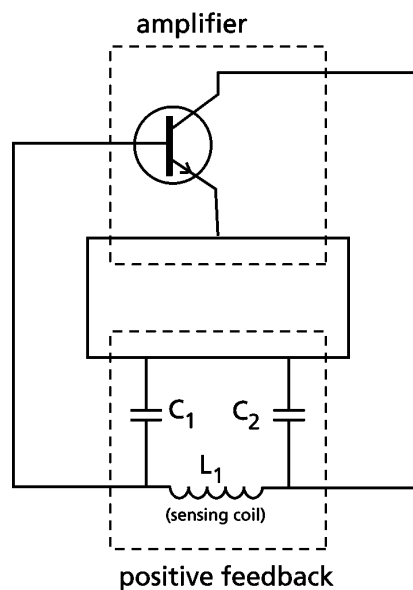

Figure 5.14. Principle of a Colpitts oscillator.

The sensing coil

The coil is wound around a cylinder with an 10-mm outer diameter and 5-mm length, made from Delrin. The coil itself consists of 34 turns of 0.2-mm copper wire. This diameter is a compromise between a low copper wire resistance and low eddy currents. To minimize interference, the connection wires are twisted and the leads from the Colpitts oscillator to the sensing coils are shielded. The shield is connected on one side to the common of the Colpitts oscillator circuit.

The electric characteristics of the coil were measured with a HP 4192A-LF impedance-analyzer at a frequency of 1 MHz. The self-inductance of the coil without ferrofluid inside is 20 µH.

The current through the coil is adjusted to give a maximum magnetic field strength of $100 \, Am^{-1}$.

Materials and electronic circuit

The circuit diagram of the Colpitts oscillator is shown in figure 5.15. The silicon NPN high frequency transistor T_1 is used in the common-emitter configuration. The frequency meter, a Hameg counter HM 8021-3 in our case, is connected to the collector of the transistor T_1. To perform initiation of the oscillation, the transistor is adjusted in the so-called class A mode. When the oscillation has been started the DC set point is shifted automatically to perform amplitude stabilization.

The supply voltage to the Colpitts oscillator limits the AC voltage swing over the collector resistor R_c. In this way, the AC peak current through the sensing coil L_1 is established. To maintain a good DC set point of the transistor T_1 at low supply voltages, an extra diode D_1 in series with resistor R_2 is used. The silicon diode has to be capable of carrying a forward current of at least 10 mA.
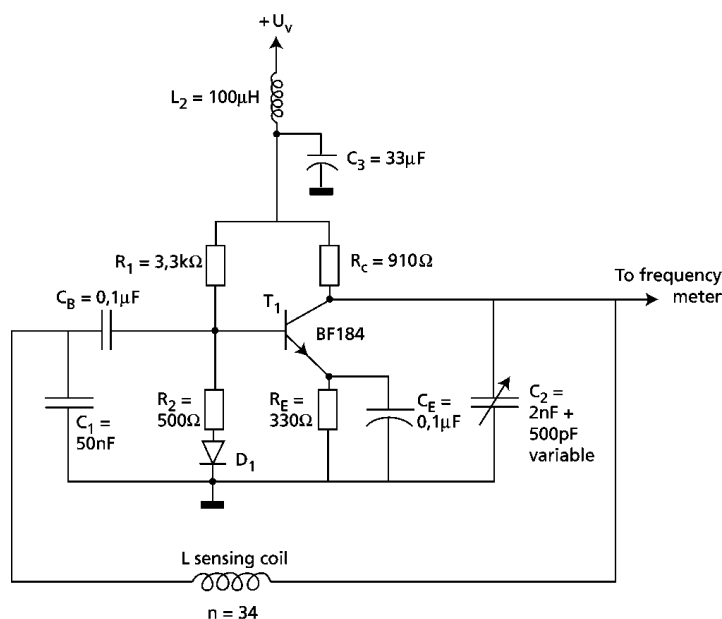

Figure 5.15. *Electronic circuit diagram of the Colpitts oscillator.*

To accomplish stability for C_1 and C_2, silvered mica capacitors are used. Parallel to capacitor C_2, a variable capacitor is connected to enable modification of the resonance frequency. The resonance frequency of the Colpitts oscillator is by default tuned to 1 MHz.

The quality factor Q of the resonance circuit has to be large for a pure sinusoidal waveform, i.e. less harmonics and noise, and less energy dissipation. To accomplish this, the loss factors such as the resistance of the coil wires were as low as possible.

The stability and accuracy of the oscillator were further optimized by the following implementation details. The printing circuit board was shielded with an aluminum cabinet, which is effective in this frequency range. To maintain a stable resonance frequency, mechanical vibrations of the frequency determining components were reduced by filling the cabinet with cotton wool. Stiff wires were used to keep the impedance of the leads constant. Fluctuations in the input voltage were suppressed by a low pass filter comprised of L_2 and C_3.

Appendix II. Complex magnetic susceptibility Meter based on mutual coupling

Introduction

The use of the Colpitts oscillator described in Appendix I is limited to magnetic fluids that have a negligible imaginary part of the complex susceptibility at 1 MHz. This condition is satisfied for the ferrofluids used here, but the technique will not be suitable for, for example, cobalt ferrite based ferrofluids. A susceptibility meter with much wider applicability is described here. Although it is not used in the described experiments, its design is included for future use.

The susceptibility meter contains two physically separated primary/secondary coil pairs (see figure 5.18). The primary coils (figure 5.16) are supplied with an alternating current, which is constant in amplitude to keep magnitude of the magnetic field amplitude constant. The two identical secondary coils are electrically connected in series to each other and in opposite. A tube containing the ferrofluid sample forms the mutual coupling between the primary and secondary coil of one branch of the balanced transformer. The other branch forms the reference, where for example a tube with solvent can be inserted. The difference in magnitude as well as the phase of the secondary voltages is measured with a dual channel Lock In Amplifier (LIA). By triggering the LIA with the synchronization pulse of the AC current source the frequency component of interest is measured. This setup can measure the complex susceptibility at frequencies between 10 Hz and 120 kHz.
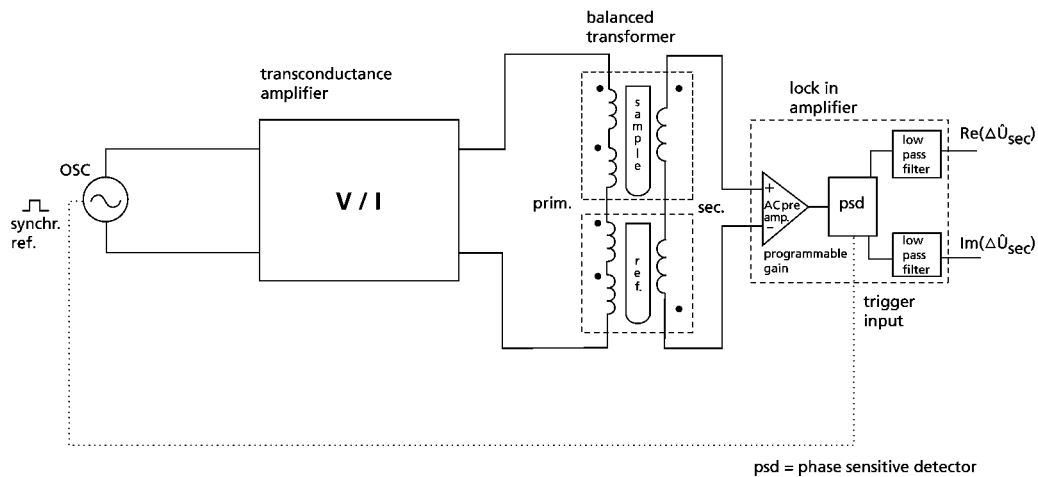
Figure 5.16. *Schematic drawing of frequency-dependent complex susceptibility meter.*

The measurement system

The AC signal is generated by an oscillator FG120 with a low distortion output option of Yokogawa. The voltage of this generator is converted to a current with a transconductance amplifier or V-I controller (figure 5.17). The primary coils form the inductive load of this current controller. To avoid undesired oscillation, a PD controller is part of the closed control loop. The amplifiers are high frequency precision operational amplifiers of type LM 318 of National Semiconductors. A shielded cabinet covers the electronic circuit. The circuit has one common earth point and the leads are shielded. The connections are stiff to avoid fluctuations of impedance of the leads. The difference between the secondary voltages of the coils is measured with the differential input of a dual phase EG&G PAR 5210 Lock In amplifier, which is triggered (locked) with a synchronization signal of the FG120 oscillator. The entire setup is computer controlled via an IEEE488 bus.
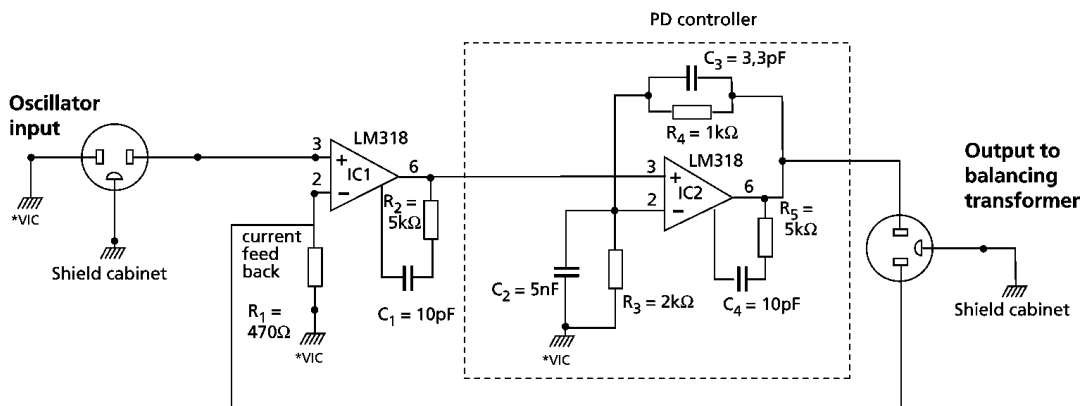

Figure 5.17. *Electronic circuit diagram of the transconductans (V-I) amplifier.*
VIC=common star point voltage to current converter.

The coil system

In figure 5.18, a schematic drawing of the primary and secondary coils in one branch is given. The dimensions of the coil systems were determined based on two criteria: 1) for phase separation experiments, the susceptibility should be measured *locally* in a tube; 2) for quantitative measurements, it is imperative that the magnetic field is homogeneous over the entire region where the susceptibility is measured. To meet the first criterium, the secondary coils should be as thin and as narrow as possible. The 220 turns were therefore wound around a temporary 8-mm thick cylindrical core, impregnated with GE varnish and baked, and removed from the core again to get narrow, self-supporting coils. The measurement range for these coils is about 12 mm above and below the coil. For the second criterium, the primary coils were wound in Helmholtz configuration. The distance between the coils is determined by the measurement range of the secondary coils, 30 mm in our case (1.2 times the measurement range).

The primary coils, consisting of 220 turns per Helmholtz pair, were wound around a transparent perspex support. The mechanical stability of the coils was enhaced by baking the transformer after fixing the windings with GE varnish. For both primary and secondary coils, 0.1-mm copper wire was used to avoid eddy currents. This is especially important at high frequencies. Each primary coil set has a self-inductance of 3.2 mH and a resistance of 80 Ω.
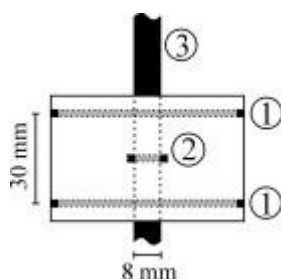

Figure 5.18. *Schematic drawing of one of the branches of the balanced transformer. The susceptibility meter consists of a sample branch and a reference branch, both of the type shown here. 1: Helmholtz coils, generating a homogeneous magnetic field of 100 Am^{-1}; 2: secondary coil, measuring χ_i; 3: sample tube.*

References

1   A. O. Tsebers, *Magnetohydrodynamics* **18**, 137 (1982).

2   K. Sano and M. Doi, *J. Phys. Soc. Jpn.* **52**, 2810 (1983).

3   H. Zhang and M. Widom, *Phys. Rev. E* **49**, 3591 (1994).

4   K. I. Morozov, A. F. Pshenichnikov, Y. I. Raikher, and M. I. Shliomis, *J. Magn. Magn. Mater.* **65**, 269 (1987).

5   Y. A. Buyevich and A. O. Ivanov, *Physica A* **190**, 276 (1992).

6   M. E. van Leeuwen and B. Smit, *Phys. Rev. Lett.* **71**, 3991 (1993).

7   J. J. Weis and D. Levesque, *Phys. Rev. Lett.* **71**, 2729 (1993).

8   J.-C. Bacri, R. Perzynski, D. Salin, V. Cabuil, and R. Massart, *J. Colloid Interface Sci.* **132**, 43 (1988).

9   V. Cabuil, E. Dubois, S. Neveu, J.-C. Bacri, E. Hasmonay, and R. Perzynski, *Progr. Colloid Polym. Sci.* **98**, 23 (1995).

10 E. Dubois, R. Perzynski, F. Boué, and V. Cabuil, *Langmuir* **16**, 5617 (2000).

11 E. Dubois, V. Cabuil, F. Boue, J.-C. Bacri, and R. Perzynski, *Progr. Colloid Polym. Sci.* **104**, 173 (1997).

12 V. Cabuil, R. Perzynski, and J. Bastide, *Progr. Colloid Polym. Sci.* **97**, 75 (1994).

13 See chapter 4 of this thesis.

14 J. C. Bacri and D. Salin, *J. Physique* **43**, L649 (1982).

15 E. A. Peterson and D. A. Krueger, *J. Colloid Interface Sci.* **62**, 24 (1977).

16 R. W. Chantrell, J. Sidhu, P. R. Bissell, and P. A. Bates, *J. Appl. Phys.* **53**, 8341 (1982).

17 P. R. Bissell, R. W. Chantrell, G. W. D. Spratt, P. A. Bates, and K. D. O'Grady, *IEEE Trans. Mag.* **20**, 1738 (1984).

18 M. S. Dababneh and N. Y. Ayoub, *IEEE Trans. Magn.* **31**, 4178 (1995).

19 S. Asakura and F. Oosawa, *J. Chem. Phys.* **22**, 1255 (1954).

20 H. N. W. Lekkerkerker, W. C.-K. Poon, P. N. Pusey, A. Stroobants, and P. B. Warren, *Europhys. Lett.* **20**, 559 (1992).

21 G. A. van Ewijk, G. J. Vroege, and A. P. Philipse, *J. Magn. Magn. Mater.* **201**, 31 (1999).

22 S. W. Charles, *Chem. Eng. Comm.* **67**, 145 (1988).

23 P. C. Scholten, *Chem. Eng. Comm.* **67**, 331 (1988).

24 V. M. Buzmakov and A. F. Pshenichnikov, *J. Colloid Interface Sci.* **182**, 63 (1996).

<div align="right">

6

</div>

Phase behavior of magnetic colloids-polymer mixtures:

influence of magnetic field

Abstract

This chapter describes experiments demonstrating that the stability of mixtures of oleic acid grafted magnetite particles and a non-adsorbing polymer can be lowered by applying a magnetic field. In a field of $28 \, kAm^{-1}$, the minimum amount of polymer needed to induce phase instability is decreased by about 20%, which agrees quite well with the mean field theory presented in chapter 4. In absence of polymer, the ferrofluid appeared to be stable in a field up to al least $28 \, kAm^{-1}$.

6.1   Introduction

Magnetic colloids distinguish themselves from other colloids by the anisotropic nature of their mutual interaction, i.e. the interaction between two magnetic particles depends not only on the distance between them, but also on the orientation of the magnetic dipole moments embedded in the particles. Because the orientation of these dipole moments can be influenced by applying a magnetic field, several macroscopic properties of magnetic colloids can be modified literally by turning a knob.

One such property is the thermodynamic stability. For example, in a common ferrofluid comprised of oleic acid grafted magnetite particles dispersed in an apolar solvent, it has often been observed that applying a magnetic field can induce phase separation [1-6]. This process manifests itself as the appearance of micron-sized, fluid droplets of high concentration, which can be seen with an optical microscope. The droplets can be elongated along the direction of the external field by increasing the field strength.

Although field-induced phase separation can be understood theoretically [7-11] and is also observed in simulation of dipolar hard sphere fluids [12], theoretical predictions and experimental observations are by no means quantitatively comparable. The strength of dipolar interaction in real systems is significantly lower than any theoretically obtained minimum strength of interaction needed to get field-induced phase separation. The discrepancy has been attributed to the presence of large particles that drive the phase transition [1,13]. Furthermore, the presence of small aggregates (~10 particles) in ferrofluids is well established [14-16], but their influence on the phase behavior is unknown [17].

In this chapter we investigate the stability of a fairly monodisperse, cluster-free magnetic fluid in a magnetic field. As in refs. [18-21], we employ a magnetic sensing coil to detect phase instability and measure the particle concentration in the dilute phase. Contrary to other observations [1-6], our ferrofluid could not be destabilized by a magnetic field. The destabilizing effect of magnetic interaction is nevertheless observed in mixtures of ferrofluid and non-adsorbing polymer. The polymer induces an effective isotropic attraction and can cause colloidal gas-liquid phase separation. In these mixtures, magnetic interaction is seen to decrease the minimal amount of polymer needed to induce phase separation. The decrease is comparable to results obtained with the mean field theory described in chapter 4.

6.2   Experimental

6.2.a   Magnetization measurements

Magnetization measurements were carried out as described in chapter 3. The magnetic core size of particles was calculated using the low-field approximation of the Langevin equation with an aditional diamagnetic term:

$$\chi_{\mathrm{i}} = M_{\mathrm{s}} \frac{\mu_{\mathrm{o}} m}{3kT} + \chi_{\mathrm{dia}} = M_{\mathrm{s}} \frac{\mu_{\mathrm{o}} M_{\mathrm{s,Fe3O4}} \pi d^{3}}{18kT} + \chi_{\mathrm{dia}} \tag{6.1}$$

with $M_{\mathrm{s,Fe3O4}}$ the saturation magnetization of bulk Fe_3O_4 (4.8 10^5 Am^{-1}) and d the magnetic core diameter.

6.2.b   Description of experimental setup

All phase separation experiments were carried out in the setup, which is schematically drawn in figure 6.1. The setup consists of a long cylindrical electromagnet, capable of generating magnetic fields up to 30 kAm^{-1}. In the electromagnet's core, a thermostat controls the temperature of the sample with an accuracy of 0.1°C. The concentration of magnetic particles is measured by moving the sample tube through a magnetic sensing coil.

The magnetizing coil is made of copper wire (1.08 mm) wound around a PVC tube and segmented by 1-mm thick copper cooling plates. These plates are placed at intervals of 11 mm and allow for fast radial transport of heat to the perimeter of the coil. Heat is dissipated by air convection, but the cooling plates allow for forced cooling in future, enabling higher magnetic field strengths than currently attainable.

A heterogeneous distribution of the number of windings per segment was chosen, with the following criteria in mind. First, the volume over which the field can be considered homogeneous should be as large as possible. This requires an increasing number of windings towards both ends of the coil. Second, because the experiments rely on the gravitational settling of concentrated droplets or aggregates, magnetic field gradients that obstruct settling must be absent. The maximum gradient ∇H can be calculated by comparing the gravitational and magnetic force on a droplet with volume V, density ρ and magnetization M:

$$\mu_0 V M \nabla H < V (\rho - \rho_{\mathrm{s}}) g \tag{6.2}$$

ρ_{s} is the solvent density, μ_0 the permeability of vacuum, and g the earth's gravitational acceleration. Assuming equal densities of the grafting layer and the solvent, the density
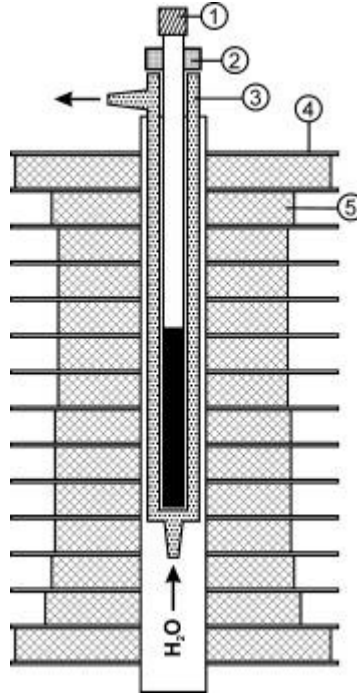
Figure 6.1. *Schematic drawing of the setup used for phase separation experiments.*
(1):sample tube; (2):magnetic sensing coil; (3):water-cooled thermostat;
(4):copper cooling plates; (5):copper windings

difference in Eq. (6.2) simply becomes $\varphi_m(\rho_m - \rho_s)$, with ρ_m the density of the magnetic material and φ_m the volume fraction of magnetic material. To obtain the smallest estimate for ∇H, we take the droplet to be fully magnetized to its saturation value $\varphi_m M_{s,m}$ ($M_{s,m}$ is the bulk saturation magnetization of the magnetic material). With these assumptions, Eq. (6.2) becomes

$$\nabla H < \frac{(\rho_m - \rho_s)g}{\mu_0 M_{s,m}} \qquad (6.3)$$

For magnetite, the upward gradient should therefore be less than $7\,10^4\,\mathrm{Am}^{-2}$ everywhere in the sample. For our setup, the number of windings was distributed in a way that should give a gradient of $10^4\,\mathrm{Am}^{-2}$ downward at the maximum field of $30\,\mathrm{kAm}^{-1}$. Because both the gradient and the sample length are small, the homogeneity of the field is only slightly affected.

The principle of operation of the magnetic sensing coil has been described in detail in ref. [18] and in the previous chapter of this thesis. Therefore, only a brief summary will be given here. The sensing coil is a part of a Colpitts oscillation circuit, oscillating at a frequency f_0. If a tube containing magnetic material is inserted into the coil, the frequency of the circuit changes by an amount $\ddot{A}f$, which is related to the susceptibility of the sample according to

$$\chi_i \propto F \equiv \left(\frac{f_o}{f_o + \Delta f} \right)^2 - 1 \tag{6.4}$$

The sensing coil measures the susceptibility locally, with a response that decreases with increasing distance from the coil center. The smeared out $F(z)$ profile of a susceptibility profile containing a step at $z=z_0$ appeared to be very accurately described by the empirical equation

$$F(z) = \frac{A}{1 + \exp\left[\pm \frac{(z - z_o)}{w} \right]} \tag{6.5}$$

The instrumental constant w can be seen as the length scale over which the profile is smeared out.

Eq. (6.5) is used to check if the boundary between a dilute and a concentrated phase is sharp, and if so, to find its position. With the position of the boundary, the volume of both phases can be calculated.

6.2.c   Materials

A cyclohexane-based dispersion of magnetite grafted with purified oleic acid was used. Particles were analyzed by transmission electron microscopy (Philips CM10). Analysis of the micrographs by computer yielded an average particle (core) size of 9.1 nm and a standard deviation of 26%. A magnetic core diameter of 11.3 nm was obtained from magnetization measurements (d^3 in Eq. (6.1) equals $<d^6>/<d^3>$ for polydisperse systems, which explains the higher diameter with respect to TEM results).

Poly(dimethylsiloxane) (PDMS, ACBR) with $M_w=41500$ and a radius of gyration of approximately 8.5 nm was used as depletion agent.

6.2.d   Phase separation experiments

Samples for phase separation experiments were kept in closed glass tubes with an internal diameter of 6 mm. Each sample was prepared by adding a known amount of dried magnetic fluid to a weighed tube, which already contains a known amount of polymer. The composition of the sample was thereafter changed by adding cyclohexane, or removing it by evaporation.

Unless otherwise stated, experiments were carried out at 295.9 K. After equilibrating the sample at the specified temperature, the magnetic field was turned on, and the sample was left undisturbed for at least one day. Just before each measurement, the field was switched off, and the sample (being in a metastable state) was carefully moved

through the sensing coil. In most cases where a concentrated phase appeared, this phase occupied only a small portion of the sample volume. Therefore, the concentration in the dilute phase could be measured immediately without interference of the concentrated phase. Occasionally, a susceptibility profile was recorded by moving the sample through the sensing coil in 1-mm steps.

Four ferrofluid samples were investigated: one without polymer and three mixtures of ferrofluid and PDMS, with compositions m_{PDMS}/m_{ff}=0.14, m_{PDMS}/m_{ff}=0.057 and m_{PDMS}/m_{ff}=0.039 (m_{ff} denotes the dried mass of magnetic particles including oleic acid). Without an external magnetic field, the PDMS/ferrofluid mixtures phase separate at magnetic particle concentrations of approximately 300 gl^{-1}, 560 gl^{-1}, and 750 gl^{-1}, respectively [22].

6.3   Results and discussion

6.3.a   Stability of a ferrofluid without polymer in a magnetic field

At all concentrations tested (from 5% to 30% by volume), the magnetic fluid sample without added polymer remained homogeneous in a magnetic field of 30 kAm^{-1}. This seems to contradict several literature reports on the phase separation of similar systems [1,3,5,6], where magnetic fluids generally destabilize below fields of 10 kAm^{-1}. However, as Pshenichnikov has experimentally demonstrated [1] and Ivanov has argued [13], phase separation in these systems is strongly promoted by the presence of a small fraction of large particles. The system used here has a lower polydispersity than reported elsewhere (with the exception of ref. [3]) and apparently lacks the large particles causing phase separation.

In addition, SAXS measurements in chapter 3 show that clusters are absent in FFR, which may also explain the higher stability. Furthermore, the presence of free oleic acid may be disadvantageous for ferrofluid stability [23,24]. Contrary to the ferrofluids used in [5] and [6], our ferrofluid underwent several precipitation/redispersion cycles to remove free oleic acid. Refs. [1] and [3] do not contain information from which the presence or absence of free oleic acid may be derived.

6.3.b   Stability of ferrofluid-polymer mixtures in a magnetic field

The general conclusion from the mean field calculations in chapter 4, namely that addition of a non-adsorbing polymer promotes field-induced phase separation, agrees with the experimental results plotted figure 6.2. These plots show the effect of an external magnetic field on PDMS/ferrofluid mixture with several compositions. If the
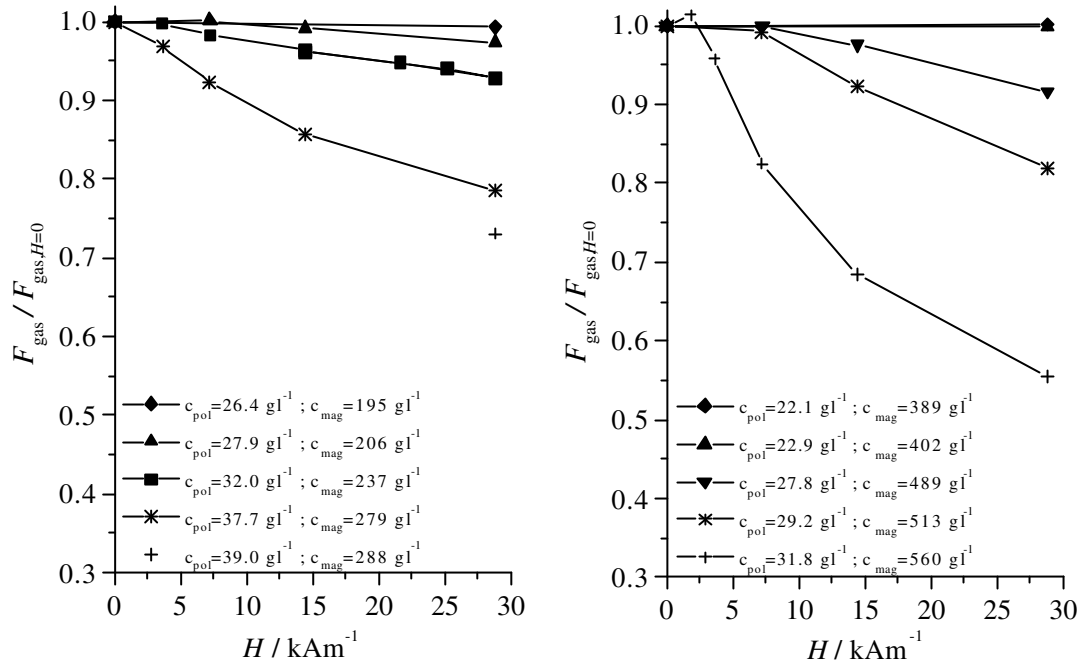
Figure 6.2. *Influence of an external magnetic field on the stability of PDMS/Fe$_3$O$_4$ mixtures with a high (left) or low (right) PDMS/Fe$_3$O$_4$ ratio. The plots shows the susceptibility of the dilute phase at a given field strength relative to the susceptibility of the dilute phase without a field.*

polymer concentration is low, no instability is observed even at 30 kAm^{-1}. However, as the polymer concentration is increased, field-induced instabilities start to appear at lower field strengths. The onset of phase separation, obtained from figure 6.2 by linear extrapolation, is plotted in figure 6.3 for both samples. The points in figure 6.3 seem to indicate that if the magnetic field causes an instability, the onset is below 15 kAm^{-1}.

That application of a magnetic field shifts the coexistence curve in the ferrofluid-polymer plane, can be seen in figure 6.4, where concentration lines in a field of 28 kAm^{-1} are plotted together with similar lines in zero field (see previous chapter). At both colloid/polymer ratios, applying a field of 28 kAm^{-1} lowers the minimal polymer concentration at which phase separation occurs by about 20%. This value agrees well with the mean field calculations in chapter 4 for $\alpha=3$ and $\lambda\approx1$. The relative decrease nevertheless strongly depends on λ, the effective value of which is difficult to obtain for the polydisperse ferrofluid used here. Moreover, in chapter 5 it was shown that phase separation caused severe fractionation of magnetic particle sizes. Fractionation is not considered in the mean field calculations, but can be expected to have a noticable influence on the phase behavior.
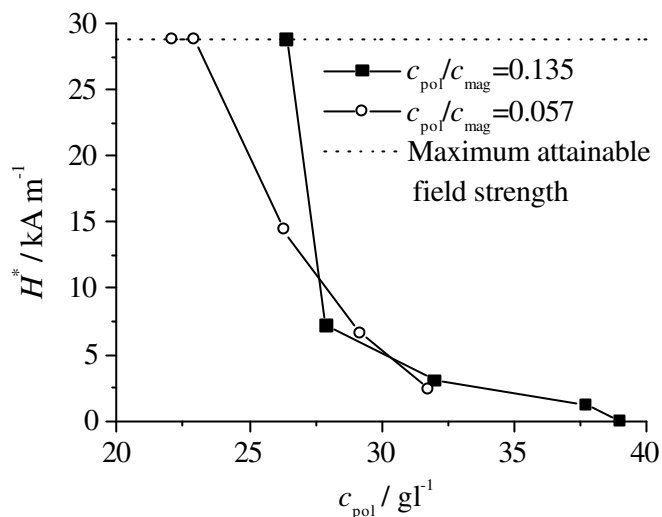
Figure 6.3. *Minimal field strength needed to induce an instability as a function of polymer concentration for two sample with different polymer/magnetite ratio.*
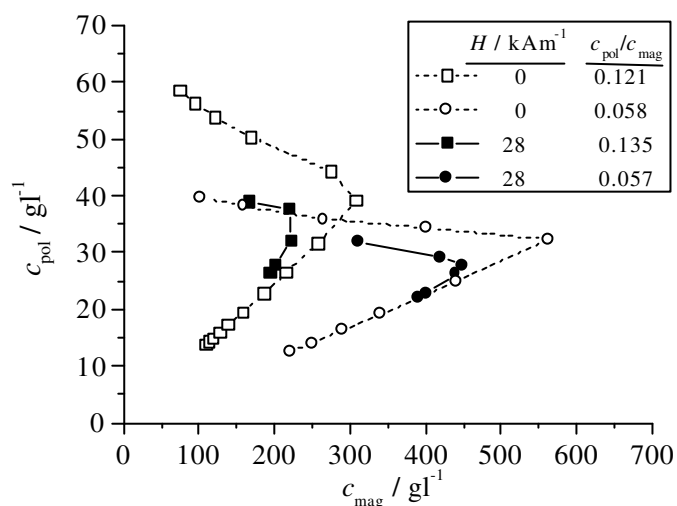
Figure 6.4. *Comparison of concentration lines in a constant magnetic field of 28 kAm^{-1} with previous experiments in zero field [22].*

6.4   Conclusions

The influence of a magnetic field on the stability of ferrofluid-polymer mixtures has been experimentally investigated using a magnetic sensing coil. An increase of magnetic field strength lowers the concentration of polymer needed to induce phase separation, but the decrease is not enough to give phase separation in a ferrofluid without polymer. The decrease in this critical polymer concentration agrees well with mean field calculations, despite the fact that polydispersity has not been taken into account in these calculations.

Acknowledgements

Bonny Kuipers is acknowledged for building the experimental setup.

References

1   A. F. Pshenichnikov and I. Y. Shurubor, *Izv. Akad. Nauk SSSR, Ser. Fiz.* **51**, 1081 (1987).

2   P. K. Khizenkov, V. L. Dorman, and F. G. Bar'yakhtar, *Magnetohydrodynamics* **1**, 30 (1989).

3   R. E. Rosensweig and J. Popplewell, in 'Electromagnetic Forces and Applications', ed. J. Tani and T. Takagi, Elsevier Science Publishers, Amsterdam (1992), p. 83.

4   H. Wang, Y. Zhu, C. Boyd, W. Luo, A. Cebers, and R. E. Rosensweig, *Phys. Rev. Lett.* **72**, 1929 (1994).

5   C.-Y. Hong, I. J. Jang, H. E. Horng, C. J. Hsu, Y. D. Yao, and H. C. Yang, *J. Appl. Phys.* **81**, 4275 (1997).

6   H.-E. Horng, C.-Y. Hong, W. B. Yeung, and H.-C. Yang, *Applied Optics* **37**, 2674 (1998).

7   A. O. Tsebers, *Magnetohydrodynamics* **18**, 137 (1982).

8   K. Sano and M. Doi, *J. Phys. Soc. Jpn.* **52**, 2810 (1983).

9   K. I. Morozov, A. F. Pshenichnikov, Y. I. Raikher, and M. I. Shliomis, *J. Magn. Magn. Mater.* **65**, 269 (1987).

10 Y. A. Buyevich and A. O. Ivanov, *Physica A* **190**, 276 (1992).

11 H. Zhang and M. Widom, *Phys. Rev. E* **49**, 3591 (1994).

12 D. Wei, *Phys. Rev. E* **49**, 2454 (1994).

13 A. O. Ivanov, *Colloid Journal* **57**, 321 (1995).

14 S. W. Charles, *Chem. Eng. Comm.* **67**, 145 (1988).

15 P. C. Scholten, *Chem. Eng. Comm.* **67**, 331 (1988).

16 V. M. Buzmakov and A. F. Pshenichnikov, *J. Colloid Interface Sci.* **182**, 63 (1996).

17 S. W. Charles, *Romanian Rep. in Phys.* **47**, 249 (1995).

18 E. A. Peterson and D. A. Krueger, *J. Colloid Interface Sci.* **62**, 24 (1977).

19 R. W. Chantrell, J. Sidhu, P. R. Bissell, and P. A. Bates, *J. Appl. Phys.* **53**, 8341 (1982).

20 P. R. Bissell, R. W. Chantrell, G. W. D. Spratt, P. A. Bates, and K. D. O'Grady, *IEEE Trans. Mag.* **20**, 1738 (1984).

21 M. S. Dababneh and N. Y. Ayoub, *IEEE Trans. Magn.* **31**, 4178 (1995).

22 See chapter 5 of this thesis.

23 E. Dubois, 'Stabilité des solutions colloidales magnétiques (ferrofluides) [In French]', PhD Thesis, Universite Pierre et Marie Curie, Paris (1997).

24 See chapter 4 of this thesis.

Anomalous attraction between colloidal magnetite and silica spheres in apolar solvents

Abstract

The existence of anomalous attraction between small (9 nm) oleic acid grafted magnetite particles and octadecanol grafted silica spheres (420 nm) in apolar solvents was demonstrated. This attraction leads to irreversible adsorption of magnetite particles onto silica spheres, with surface coverages up to 30%. The adsorption process appears to be very slow, proceeding over a period of weeks. Because this is orders of magnitudes slower than a diffusion-limited absorption process, the adsorption is not likely due Van der Waals attraction or Coulomb attraction between pre-existing charges. Instead, proton transfer between magnetite and silica was proposed as the cause for adsorption. This mechanism explains the strong attraction, slow adsorption kinetics and desorption in solvents with a higher dielectric constant.

7.1   Introduction

The interaction between colloidal particles is of paramount importance for the stability of colloidal dispersions, and is therefore one of the main topics in colloid science. In polar media, such as water, the interaction between colloids is often well described by the DLVO theory, combining Van der Waals attraction between particles and repulsion due to overlap of the ion clouds surrounding the particles. Although this theory succesfully explains the stability of many colloidal systems, the existence of so-called non-DLVO forces, such as hydrophobic interactions, has been frequently demonstrated [1].

Colloids can also be sterically stabilized by chemically or physically attaching polymers to the particle surface [2]. In good solvents or theta solvents for the polymer, colloids repel each other when overlap of their polymer layers forces the polymers into entropically unfavorable conformations. In contrast to the wealth of papers on non-DLVO forces, reports on anomalous interactions between sterically stabilized colloids are scarce, even though such colloids are widely applied and studied. One example of a yet unexplained attraction concerns stearylalcohol-grafted silica spheres in a good solvent. Although dispersions of monodisperse stearyl-silica spheres in cyclohexane behave as hard-sphere fluids [3], deviations from the hard-sphere character emerged in studies on *bidisperse* mixtures. Several techniques, such as rheology [4], phase separation experiments [5], small-angle neutron scattering [6], and sedimentation experiments [7] indicate a significant attraction between spheres with widely different sizes, even though interactions between particles with similar sizes were demonstrated to be purely repulsive. This phenomenon does not seem to be limited to silica mixtures. Recently, an indication for attraction between small sterically stabilized magnetite (Fe_3O_4) particles and large silica spheres was found [8]; the attraction seemed to be large enough for magnetite to irreversibly adsorb onto the silica surface.

Because only indications for this anomalous attraction in bidisperse mixtures of sterically stabilized colloids have been obtained so far, we decided to investigate this phenomenon in detail, focusing on demonstrating the existence of the attraction and quantifying adsorption of the small particles on the larger colloids. The mixture studied here consists of 9-nm oleic acid grafted magnetite particles and 420-nm stearyl-grafted silica spheres in cyclohexane. Its ferromagnetic properties make magnetite easy to quantify with magnetization measurements without interference by silica. Moreover, visual observations are facilitated by the deep black color of magnetite.

The results of this investigation indeed show that there is indeed an unexpectedly strong attraction between the magnetite and silica colloids, despite the fact that the separate silica and magnetite dispersions are colloidally stable. The attraction manifests itself in irreversible adsorption of magnetite onto silica, resulting in colloidally stable decorated

silica spheres with a surface coverages up to 30%. The adsorption process proceeds over a period of weeks, which is orders of magnitudes slower than a simple diffusion limited adsorption. Such slow kinetics is inconsistent with adsorption due to Van der Waals attraction or due to Coulomb attraction between pre-existing charges. A proton transfer mechanism is proposed, which explains all peculiarities found in the experiments.

7.2   Experimental

7.2.a   Description of dispersions

The silica (SiO_2) dispersion consists of silica spheres (diameter 420 nm) grafted with octadecanol, dispersed in cyclohexane. A detailed description of the preparation and characteristics of these particles can be found elsewhere [9]. The stock dispersion, coded SS, contained 164.3 gl^{-1} of solid material.

The Fe_3O_4 dispersion, coded FFS, contained particles (diameter 9.1 nm) grafted with purified oleic acid and dispersed in cyclohexane. The solid content of FFS was 126.3 gl^{-1}.

A second Fe_3O_4 dispersion ('FF2S'), consisted of particles grafted with octadecanoic acid [10].

Table 7.1 contains particle characteristics of SS, FFS and FF2S. All dispersions contained solvents of analytic quality, and were freed of unreacted octadecanol or oleic acid. The separate silica and magnetite dispersions were stable; no sign of aggregation was observed in any dispersion over a period of more than a year. Moreover, sedimentation experiments (section 7.3.b) confirm the hard-sphere characteristics of SS described elsewhere [9].

Table 7.1. Characteristics of dispersions.

Sample	d_{TEM} /nm [a]	σ_{TEM} /nm [a]	d_M /nm [b]	ρ /kg m^{-3}
SS	420	46		1781
FFS	9.1	2.3	11.3	2900
FF2S	14	4.2	13.6	

[a] Diameter and standard determined from electron micrographs

[b] Diameter obtained from magnetization measurements (section 7.2.b)

7.2.b Magnetization measurements

The amount and size of magnetite particles in a sample was measured with a MicroMag 2900 Alternating Gradient Magnetometer (AGM, Princeton Measurements Corp.). Samples were contained in glass cups with internal dimensions of $4 \times 3 \times 0.4$ mm, sealed with a cover glass glued over the open end. All measurements were performed at room temperature.

The saturation magnetization M_s and diamagnetic susceptibility χ_{dia} were determined by fitting the magnetization curve at high fields (up to $1.2\ 10^6$ Am^{-1}) with the Langevin function [11] with an added diamagnetic contribution:

$$M = M_s \left\{ \coth(\alpha) - \frac{1}{\alpha} \right\} + \chi_{dia} H \quad ; \quad \alpha = \frac{\mu_o m H}{kT} \tag{7.1}$$

where H is the applied field strength, m the magnetic moment of particles, μ_o the permeability of vacuum and kT the thermal energy.

Combined with the initial susceptibility χ_i, i.e. the slope of the magnetization curve at low field strength ($H < 10^3$ Am^{-1}), M_s and χ_{dia} yield the magnetic core diameter d of particles when substituted in the low-field approximation of (7.1) [11]:

$$\chi_i = M_s \frac{\mu_o m}{3kT} + \chi_{dia} = M_s \frac{\mu_o M_{s,Fe3O4} \pi d^3}{18kT} + \chi_{dia} \tag{7.2}$$

$M_{s,Fe3O4}$ is the saturation magnetization of bulk Fe$_3$O$_4$ ($4.8\ 10^5$ Am^{-1}). Eqn. (7.2) was only applied on dilute samples with a solid content below 10 gl^{-1}, so that magnetic interaction between particles is negligible.

Because the AGM actually measures the magnetic moment $M_s V$ of a sample, the inaccuracy in the small sample volume (2.5 µl) inhibits the precise determination of M_s. Therefore, AGM results were combined with susceptibility measurements performed on a Kappabridge KLY-3 susceptibility meter (Agico). The AGM data were used to calculate the reduced initial susceptibility ($\chi_{i,AGM} - \chi_{dia,AGM}$)/$M_{s,AGM}$, which is independent of the sample volume. Using this value, the saturation magnetization was obtained from

$$M_s = \frac{\chi_{i,\kappa b} - \chi_{dia,\kappa b}}{\left(\chi_{i,AGM} - \chi_{dia,AGM} \right) / M_{s,AGM}} \tag{7.3}$$

The subscripts *AGM* and κb in (7.3) refer to measurements done with the AGM and Kappabridge, respectively.

7.2.c Initial adsorption experiments

The anomalous behavior of mixtures of sterically stabilized silica and magnetite in a good solvent (cyclohexane) was illustrated by mixing 5 ml SS with 1.2 ml FFS. Free magnetite was then removed by centrifugating the sample at 1000 rpm in a Beckmann table centrifuge and replacing the supernatant with fresh solvent after each step. This procedure was repeated until the supernatant remained colorless.

The purified dispersions were examined visually and on a Philips CM10 transmission electron microscope. TEM samples were prepared by dipping formvar-coated copper grids in a dilute dispersion and drying them in air.

The influence of the chemical nature of the grafting layer on stability of magnetite-silica and magnetite-magnetite mixtures was qualitatively investigated as follows. An excess of FF2S, magnetite grafted with stearic acid, was added to SS. After one hour, free magnetite was removed. FF2S was also mixed with FFS in a one-to-one mass ratio of the two colloids. The stability of both mixtures was examined visually.

7.2.d Sedimentation experiments

The stability of silica spheres in the presence of magnetite particles was studied with sedimentation experiments in the earth's gravity field. Samples were kept in 20-cm long glass tubes with 5 mm internal diameter. Temperature fluctuations were minimized by performing the experiments in a thermostated room (294.7 K) and immersing the sample tubes in a large water bath. To minimize any influence of vibrations, the water bath was put on a heavy marble table [7].

Sedimentation rates were obtained by measuring the height of the sedimentation boundary with respect to the bottom of the tube at varying time intervals after the samples were homogenized. Using a Zeiss Ni-40 leveling instrument connected to a Mutiyoto AT-11-N linear scale system, the height could be measured with an accuracy of approximately 0.01 mm. During measurements, samples were illuminated at 90° with a slide projector to obtain enough contrast to see the boundary between the dispersion and supernatant. The time of illumination was reduced to a minimum to avoid any convection which can be caused by absorption of light by iron oxide [12].

Samples were prepared by diluting 1.00 ml of SS with 1.00 ml of cyclohexane, followed by adding a small amount (between 0 and 80 µl) of FFS. In addition, two dilute samples were prepared in tubes with 10 mm internal diameter by mixing 0.50 ml SS with 9.50 ml cyclohexane. 40 µl FFS was added to one of the dilute samples. All sample tubes were shaken thoroughly before each measurement.

7.2.e   Quantification of adsorption

The samples used in sedimentation experiments were characterized using magnetization measurements (section 7.2.b). Prior to characterization, free magnetite particles were removed by repeated centrifugation steps (see section 7.2.c).

The amount of adsorbed magnetite was calculated by combining the saturation magnetization of a sample and that of a calibration sample with known magnetite concentration. Magnetization curves of the removed supernatant were also recorded to examine if adsorption is size-selective. Particle sizes were calculated using eqn. (7.2).

7.2.f   Adsorption kinetics

The time-dependence of adsorption was investigated by preparing three tubes containing 1.00 ml of SS, 1.00 ml cyclohexane and 50 µl FFS, and one tube with the same silica concentration but twice as high a magnetite concentration. After different periods of time, samples were purified from free magnetite and analyzed following the procedure described in section 7.2.e. Samples were gently shaken every day to keep the silica concentration homogeneous.

For reference, the maximum amount of desorption was determined by sedimenting 5.00 ml SS and replacing the supernatant with 5 ml FF. The sample was analyzed after one month. During the adsorption process, the sample was regularly shaken.

7.2.g   Solvent variation

To study desorption, if any, in other solvents, silica with adsorbed magnetite was transferred to other solvents by centrifugation and redispersion. The following solvents were used: n-hexane, n-dodecane, n-hexadecane, p-xylene, toluene and chloroform. All solvents were of analytical grade.

Adsorption in toluene and chloroform was also examined. Particles were transferred to the other solvent before mixing: SS was transferred by centrifugation/redispersion, FFS by drying/redispersion. Samples were prepared according to the procedure used in section 7.2.f: 1.00 ml silica dispersion was mixed with 1.00 ml solvent and 50 µl magnetite dispersion. After 50 h, the mixtures were purified and analyzed as described in section 7.2.e.

7.3   Results and discussion

7.3.a   Initial adsorption experiments

Due to the large extinction coefficient of magnetite in the entire visible light spectrum, traces of this material can be easily detected visually. The brownish color which was observed in silica spheres freed from non-adsorbed magnetite was therefore a first evidence that magnetite adsorbs on silica. The supernatant remained almost colorless for weeks, indicating that desorption hardly took place. On the time scale of months, the supernatant became yellow, indicating that some desorption occurred, albeit at a very low rate.

The fact that a significant amount of magnetite adsorbs on silica was also evident from the migration of concentrated dispersions of magnetite-silica particles in the field gradient of a permanent magnet.

A representative TEM picture of dried silica spheres with adsorbed magnetite is shown in figure 7.1. Free magnetite had been removed prior to preparing the TEM samples. The surfaces of the spheres look smooth except at sites were they touch other spheres. At contact points between silica spheres there is an accumulation of magnetite particles. Local accumulation of small particles is also visible in previous work [7], and may be due to capillary forces of the solvent-air interface, and to convective flux towards narrow spaces [13] (if solvent evaporates from a narrow space, capillary suction draws other solvent from the surroundings, causing a net solvent flux).

Accumulation of magnetite also occurred between the silica spheres and the polymer coating of the TEM grid. Figure 7.2 shows a TEM picture of a sample from which some silica spheres were removed by gently wiping the grid with a piece of tissue paper, thereby exposing rings of magnetite particles that lay below the spheres.
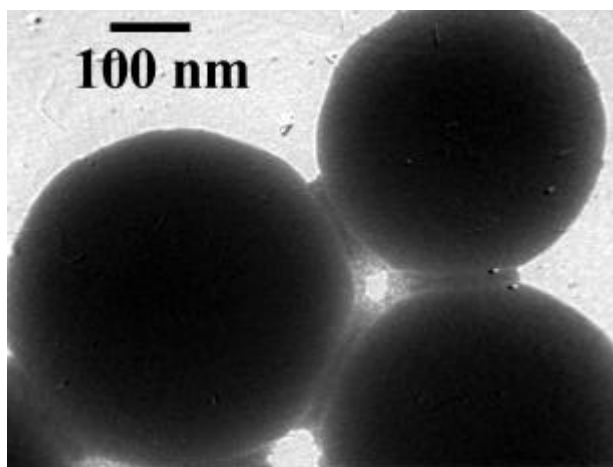

Figure 7.1. *TEM picture of silica spheres coated with magnetite particles. The coating is accumulated in the most narrow spaces, whereas the rest of the silica surface contains almost no magnetite.*
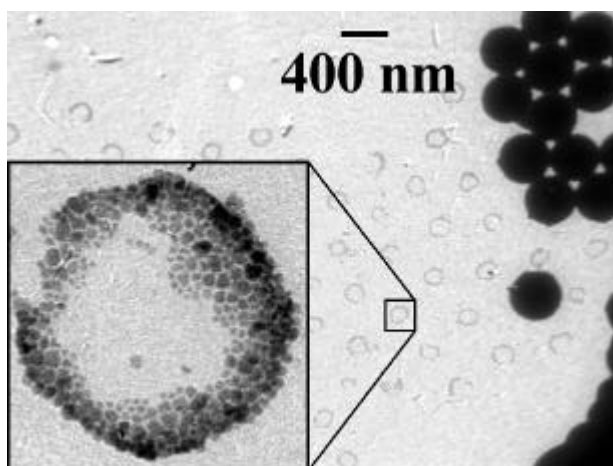
Figure 7.2. *TEM picture of a grid with coated silica spheres. Some silica spheres have been removed by gentle wiping with tissue paper, making rings of magnetite particles visible (enlargement) that had accumulated between the silica sphere and the grid.*

The experiments described here clearly demonstrate that there is attraction between sterically stabilized magnetite and silica, which is strong enough to lead to irreversible adsorption of magnetite on silica. This anomalous attraction is not limited to this particular mixture; magnetite, grafted with octadecanoic acid (FF2S) instead of oleic acid also adsorbs on silica. No instability was observed in the mixture of octadecanoic acid grafted magnetite and oleic acid grafted magnetite, demonstrating that the attraction is not due to a difference in the nature of the grafting layer but rather to a difference of particle size or core material.

7.3.b Sedimentation experiments

The colloidal stability of the silica spheres was expected to be influenced by the presence of magnetite. In particular, since magnetite is bound irreversibly to silica, bridging flocculation was expected to occur at small amounts of magnetite. Surprisingly, bridging flocculation was not observed, as can be seen in figure 7.3. This graph shows the sedimentation rate of silica as a function of the maximum surface coverage θ that could be reached, given the amount of magnetite added. The surface coverage is calculated considering magnetite particles as discs adsorbed on the surface of a sphere:

$$\theta = \frac{N_{Fe_3O_4} \frac{1}{4}\pi d^2_{Fe_3O_4}}{N_{SiO_2}\pi d^2_{SiO_2}} = \frac{m_{Fe_3O_4}\rho_{SiO_2}d_{SiO_2}}{4m_{SiO_2}\rho_{Fe_3O_4}d_{Fe_3O_4}} \tag{7.4}$$

N is the total number of particles, d the particle diameter including the grafting layer (13 nm for Fe_3O_4, 420 nm for SiO_2), m the total mass and ρ the particle density (see table 7.1).
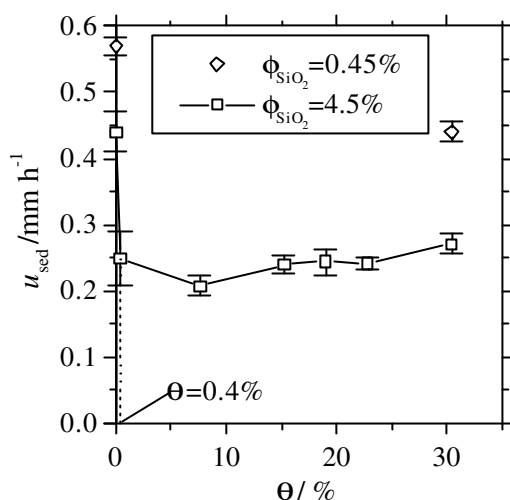
Figure 7.3*. Sedimentation rate of silica spheres as a function of the amount of magnetite added (θ denotes the surface coverage of silica with magnetite if all magnetite would adsorb). Despite the strong attraction between magnetite and silica, bridging does not occur: even the smallest amount of magnetite reduces the sedimentation rate.*

According to figure 7.3, even the smallest addition of magnetite results in a significant decrease in sedimentation rate, whereas bridging would have led to an increase thereof. The decrease is most likely due to an increase of the friction factor of silica spheres [7] upon adsorption of magnetite particles. Further evidence for the repulsive character of magnetite covered silica spheres follows from the decrease of sedimentation rate with increasing silica concentration [14] (see figure 7.3).

The sediment volume in the sample with bare silica spheres corresponds to a silica volume fraction of 54.3%. In the samples containing magnetite, the silica volume fraction was 46.6% ± 1.5% with no particular dependence on the amount of magnetite. Assuming that the lower packing density of coated silica spheres can be ascribed to an larger effective radius, the increase in radius is 11 nm, which is close to the diameter of adsorbed particles (13 nm).

The high sediment densities are a strong indication that the colloids are (nearly) uncharged. In nonpolar solvents, such as cyclohexane (ε_r=2.0), electrostatic screening is not operative [15] and the interaction between charged spheres can be described by Coulomb's law [16]. The high sediment density requires the Coulomb repulsion at closest contact to be smaller than kT, corresponding to a number of charges per sphere of at most 4.

7.3.c   Quantification of adsorption

Magnetization measurements on the samples used in sedimentation experiments reveal that a significant amount of magnetite is adsorbed (figure 7.4). Because the adsorption is irreversible, it was expected that initially all magnetite would adsorb and that the coverage θ remains constant after the surface has been saturated. Indeed, all magnetite was adsorbed at low magnetite concentration (θ=0.4%), but neither complete adsorption nor saturation were found at higher concentrations.

Of course, incomplete adsorption could be explained if only a fraction of the polydisperse magnetite particles is able to adsorb, and according to Table 7.2 there is indeed such a size-selectivity towards the larger particles (size differences are small, but significant; note that d^3 is measured in magnetization measurements, which is very sensitive to variations in d). However, this explanation disagrees with complete adsorption at low magnetite content, and the non-linear relation between adsorbed and added magnetite.

Another possibility is that the adsorption process is so slow that it is still in progress at the time of quantification, i.e. seven weeks after mixing. This would also explain the absence of bridging flocculation (previous section) in mixtures where the surface is far from saturated, because bridging is simply too slow to be observed within the duration of the sedimentation experiments.
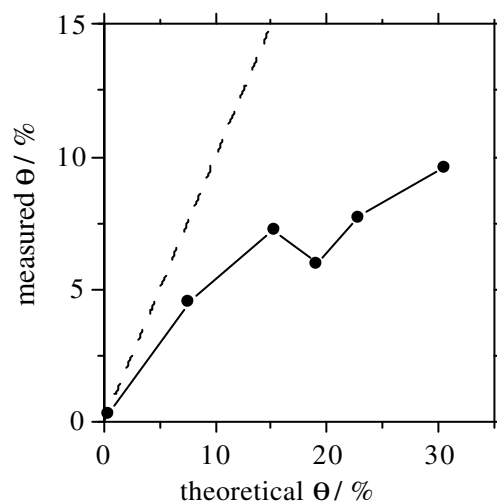

Figure 7.4. *Measured surface coverage of magnetite on silica versus theoretical coverage, i.e. the coverage in case all magnetite adsorbs. Complete adsorption (dashed line) is only seen in the sample with* θ=0.4%.

Table 7.2. Size of *non*-adsorbed particles in sedimentation samples.

$\theta^{(s)}$ / %	d_M (free Fe_3O_4)/nm
7.6	9.8
30.5	10.3
FFS	11.3

[a] Maximum surface coverage at given magnetite/silica ratio

7.3.d   Adsorption kinetics

The suggestion made in the previous section that the adsorption process is very slow, is confirmed by the kinetics measurements in figure 7.5. The plot clearly shows that, at constant amounts of magnetite and silica, the amount of adsorbed magnetite increases over a time span of at least five days. The point at $t=1175$ h (=7 weeks) was a sample used in sedimentation experiments, added to demonstrate that the adsorption process is certainly not complete after five days. The adsorption kinetics also depends on magnetite concentration: doubling it almost doubles the surface coverage at $t=120$ h.

It is interesting to note that Van Duijneveldt *et al.* [5] reported a similar time dependence; they observed that a mixture of small and large stearyl-silica spheres in cyclohexane, which initially exhibited aggregation or phase separation, sometimes became homogeneous again after a few days.

Such slow kinetics as seen in figure 7.5 cannot be explained by diffusion limitation only. This can be shown by calculating the steady state collision frequency Z of magnetite particles on a silica sphere with radius R_{SiO2} [17]:

$$Z = 4\pi R_{SiO_2} D_{Fe_3O_4} n_{Fe_3O_4} \tag{7.5}$$

where D_{Fe3O4} and n_{Fe3O4} are the diffusion coefficient and number density of magnetite particles. Using Stokes' equation, $D=kT/(6\pi\eta_0 R)$, we find a collision frequency of $3 \cdot 10^6$ s^{-1} for our samples. If the rate of adsorption would be limited purely by diffusion, each sphere would be completely occupied within a millisecond. This is clearly not the case: the experimental adsorption rate is roughly eight orders of magnitude smaller than the rate calculated with eqn. (7.5). Blocking of available surface can slow down adsorption [17], but certainly not enough to explain such slow kinetics as seen here. Besides, the maximum coverage we found was $\theta=0.30$, which means that in figure 7.5 a large part of the surface is still available for adsorption.
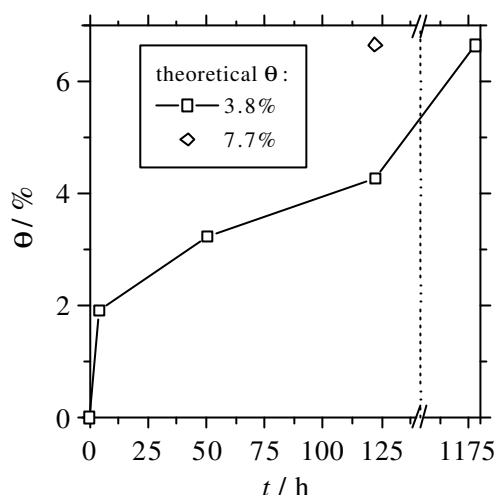
***Figure 7.5**. Amount of magnetite adsorbed on silica as a function of time (note the axis break). The adsorption process proceeds over a time span of weeks, which is about six orders of magnitude slower than a diffusion limited process would be.*

Hindrance of adsorption by an (electrostatic) energy barrier can have a strong effect on the kinetics [17]. If particles have to cross an energy barrier ψ in order to reach the surface, the particle flux towards the surface is reduced by roughly a factor $\exp(\psi/kT)$. A barrier of $20\,kT$ is already sufficient to slow kinetics down by a factor of 10^8, and could in principle explain our measurements. Such a barrier would, however, require a charged silica surface, which was already excluded by sedimentation experiments. Moreover, only charged magnetite particles would be hindered by the electrostatic barrier, hence *all* magnetite particles must be charged in order to explain the slow kinetics with an energy barrier. Given the magnetite concentration in these experiments, $1.5\ 10^{-6}$ mole l^{-1}, the counterion concentration must be at least this large. Such a high ionic concentration in cyclohexane can not be reached without the addition of a surfactant, such as AOT [16]. We therefore conclude that the slow kinetics are not due to the crossing of particles over an energy barrier. More likely, adsorption is preempted by some chemical or physical process, and this process limits the rate of adsorption.

7.3.e   Solvent variation

Magnetite remained adsorbed on silica in most solvents, which followed from the colorless appearance of the supernatant after sedimentation. However, desorption was observed in chloroform and toluene. An attempt was made to completely remove magnetite by replacing the supernatant repeatedly by solvent. In chloroform, almost complete desorption was found after 10 solvent refreshments. In toluene, only a fraction of the adsorbed material was released. Figure 7.6 shows that in toluene $\chi_i V$, a measure
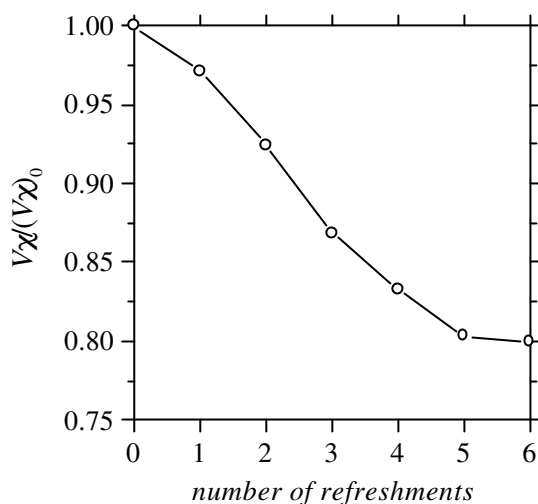
Figure 7.6. *The amount of magnetite adsorbed on silica (measured as V÷) is decreased by successive replacement of the supernatant by fresh toluene.*

for the absolute amount of magnetite, decreases after each of the first five refreshments of the supernatant. Subsequently, desorption ceases.

The amount of magnetite removed with each toluene refreshment did not depend noticeably on the desorption time, indicating that the system is in adsorption-desorption equilibrium. This is confirmed by an adsorption experiment in toluene. In toluene, and also in chloroform, magnetite readily adsorbs on silica. After fifty hours, the surface coverages in toluene and chloroform are 10% and 22%, respectively, which is significantly more than coverage of 3.2% found in cyclohexane under equal conditions. The difference is likely due to a difference in adsorption kinetics. In connection to this, it interesting to note that the magnetite+silica mixture in chloroform immediately flocculated upon mixing, whereas the separate dispersions in chloroform were stable. The postulation of slow kinetics as a reason for the absence of bridging flocculation of magnetite and silica in cyclohexane (section 7.3.b), agrees with this observation.

7.3.f General discussion

All experiments presented in this article clearly demonstrate that small sterically stabilized magnetite particles adsorb onto large silica spheres in various organic solvents. However, which mechanism underlies the attraction is unclear. Whatever mechanism is proposed, it must at least explain: 1) strong attraction, in the order of $10\,kT$ or more, which only acts between silica and magnetite and not between similar particles; 2) slow adsorption kinetics, roughly eight orders of magnitude slower than diffusion limited adsorption; and 3) absence of a significant amount of charges on bare as well as magnetite-covered silica spheres. In this section, some mechanisms will be

discussed and compared with our experimental data.

As Van der Waals attraction plays an important role in the stability of colloids, this is the first option we consider. The energy between two smooth spheres with radii r_1 and r_2 separated by a distance H between their surfaces is approximately [2]

$$U_{LW} \approx -\frac{A}{6} \frac{r_1 r_2}{H(r_1 + r_2)} \qquad (7.6)$$

The Hamaker constant A for the interaction between magnetite (subscript 'F') and silica ('S') in cyclohexane ('c') can be estimated with

$$A_{FcS} \approx \left(A_{FcF} A_{ScS} \right)^{1/2} \qquad (7.7)$$

Substitution of the Hamaker constants $A_{FcF} \approx 10\,kT$ and $A_{ScS} = 0.15\,kT$ gives $A_{FcS} \approx 1.2\,kT$. The Van der Waals interaction at closest approach ($H = 3$ nm) is then $U_{LW} = -0.3\,kT$, which is much too small to explain the almost irreversible adsorption observed in cyclohexane. As put forward in ref. [7], the surface-to-surface distance can be smaller at spots with low grafting density, but the large number of such spots needed to cover 30% of the silica surface with magnetite is incompatible with the well-documented high grafting density of alkyl chains on silica [3]. Moreover, Van der Waals attraction would lead to instantaneous adsorption upon collision, and hence a diffusion-limited adsorption rate. This is also contradicted by our experimental results.

In toluene, Van der Waals forces may even counteract adsorption; because the refractive index of the solvent (1.496) is in between the refractive indices of silica and magnetite (1.44 and 2.4, respectively) the Hamaker constant in toluene is expected to be negative, giving rise to Van der Waals *repulsion*. Repulsion between magnetite and silica may be an explanation why some magnetite desorbs in toluene and not in other apolar solvents.

Van der Waals forces between the grafting layers can under some conditions, such as low solvent quality, also give rise to attraction. However, since cyclohexane is a good solvent for both stearyl- and oleyl-chains, attraction between the grafting layers is not expected in the experiments described here. This argument is supported experimentally by the absence of any sign of attraction in mixtures of stearyl- and octadecyl-grafted magnetite (section 7.3.a).

Another possible source of attraction is due to the presence of surface charges. Especially in apolar solvents, like cyclohexane, Coulomb attraction can be considerable. For example, the interaction between two elementary charges at 3 nm distance is about $10\,kT$, which would be high enough to explain irreversible adsorption. It is quite inconceivable that each silica sphere carries enough charges beforehand to adsorb up to 1000 oppositely charged magnetite particles (this is the number of magnetite particles that corresponds to a surface coverage of 30%). That many charges would correspond to the unrealistic surface potential of 3.4 V, and is, moreover, contradicted by the high

sediment density found in sedimentation experiments (section 7.3.b).

Nevertheless, the possibility of Coulomb attraction is not completely ruled out. Suppose that a charge, in the form of a proton for example, is transferred between the silica and magnetite surface. Proton transfer between inorganic particles has, to our knowledge, not been reported yet, but proton transfer between pigment particles and dispersants in apolar media is known [18] and has been held responsible for charging of pigment particles. After a charge transfer between silica and magnetite, the particles bear opposite charges and will attract each other, but the resulting silica-magnetite sphere will still be charge neutral. And because adsorption involves a charge transfer in addition to the diffusion of magnetite to the silica surface, the adsorption kinetics can be much slower than that of a proces which is limited by diffusion only. Also, magnetite desorption in toluene is consistent with Coulomb attraction: due to the higher dielectric constants of toluene (2.4) compared to cyclohexane (2.0), the most weakly adsorbed particles can desorb. In chloroform, which has an even higher dielectric constant (4.8), almost complete desorption of magnetite was observed. In conclusion, the charge transfer hypothesis is consistent with the experimentally observed features of the anomalous adsorption of magnetite on silica, described in this chapter.

7.4   Conclusions

In contrast to the colloidal stability of separate dispersions of small oleyl-grafted magnetite colloids and large stearyl-coated silica colloids in cyclohexane, an unexpectedly strong attraction appears to be present between these magnetite and silica colloids. It was shown with several independent techniques that magnetite particles adsorb irreversibly on silica spheres. The amount of magnetite adsorbed is significant: up to 30% coverage of the silica surface was found.

Surprisingly, despite the strong attraction between magnetite and silica, no bridging flocculation was observed, not even under conditions where the silica surface was far from saturated with magnetite. This suggested that the decorated silica spheres are kinetically stable due to a low adsorption rate of magnetite on silica. Indeed, adsorption kinetics measurements confirmed the low rate: the absorption process appears to proceed over a period of weeks, whereas a diffusion limited adsorption process would have been completed in milliseconds.

The slow kinetics are likely due to a chemical or physical process other than diffusion, which precedes adsorption. A proton transfer mechanism was proposed to account for the low adsorption rate. This mechanism also explains the strong attraction between magnetite and silica in cyclohexane. Moreover, the observed desorption of magnetite in toluene and chloroform is consistent with the weakening of electrostatic attraction in solvents with a higher dielectric constant.

Acknowledgements

We thank prof. J. Dhont, prof. C. de Kruif and prof. A. Vrij and prof. A. van Blaaderen and Dr. J. Groenewold for many valuable discussions and suggestions.

References

1　B. W. Ninham, *Adv. Colloid Interface Sci.* **83**, 1 (1999).

2　J. Israelachvili, 'Intermolecular & Surface Forces', Academic Press Ltd., London (1992).

3　A. K. van Helden and A. Vrij, *J. Colloid Interface Sci.* **78**, 312 (1980).

4　A. T. J. M. Woutersen and C. G. de Kruif, *J. Rheol.* **37**, 681 (1993).

5　J. S. van Duijneveldt, A. W. Heinen, and H. N. W. Lekkerkerker, *Europhys. Lett.* **21**, 369 (1993).

6　M. H. G. Duits, R. P. May, A. Vrij, and C. G. de Kruif, *J. Chem. Phys.* **94**, 4521 (1991).

7　D. M. E. Thies-Weesie, A. P. Philipse, and H. N. W. Lekkerkerker, *J. Colloid Interface Sci.* **177**, 427 (1996).

8　B. J. de Gans, C. Blom, A. P. Philipse, and J. Mellema, *Phys. Rev. E* **60**, 4518 (1999).

9　A. P. Philipse and C. Pathmamanoharan, *J. Colloid Interface Sci.* **159**, 96 (1993).

10　G. A. van Ewijk, G. J. Vroege, and A. P. Philipse, *J. Magn. Magn. Mater.* **201**, 31 (1999).

11　R. E. Rosensweig, 'Ferrohydrodynamics', Cambridge University Press, Cambridge (1985).

12　D. M. E. Thies-Weesie and A. P. Philipse, *Langmuir* **11**, 4180 (1995).

13　N. D. Denkov, O. D. Velev, P. A. Kralchevsky, I. B. Ivanov, H. Yoshimura, and K. Nagayama, *Langmuir* **8**, 3183 (1992).

14　A. P. Philipse, *Curr. Opin. Colloid Interface Sci.* **2**, 200 (1997).

15　P. C. van der Hoeven and J. Lyklema, *Adv. Colloid Interface Sci.* **42**, 205 (1992).

16　A. Kitahara, in 'Electrical Phenomena at Interfaces. Fundamentals, Measurements and Applications', ed. A. Kitahara and A. Watanabe, Marcel Dekker (1984).

17　Z. Adamczyk, B. Siwek, M. Zembala, and P. Belouschek, *Adv. Colloid Interface Sci.* **48**, 151 (1994).

18　F. M. Fowkes, H. Jinnai, M. A. Mostafa, F. W. Anderson, and R. J. Moore, in 'Colloids and Surfaces in Reprographic Technology', ed. M. Hair and M. D. Croucher, American Chemical Society, Washington D.C. (1982), p. 307.

Summary

In this thesis, we have studied the thermodynamic stability of magnetic fluids, also called ferrofluids. These consist of spherical colloids of typically 10 nm, coated with a monolayer of oleic acid and dispersed in cyclohexane. The core material, Fe_3O_4, is ferrimagnetic and because of its small size, the core consists of a single magnetic domain with a permanent magnetic moment. An easy preparation method for such colloids is described in chapter 2.

The question how interactions between magnetic colloids affect the stability of magnetic fluids is one of practical as well as fundamental interest. Some applications require the magnetic fluid to remain monophasic under working conditions; others need phase separation of the magnetic fluid in order to work. To predict under which conditions a ferrofluid becomes unstable, it is often modeled as a dipolar hard sphere fluid (DHS fluid). Actually, theories for DHS fluids had been developed even before ferrofluids came up. Most of them aimed at describing the dielectric constant of polar liquids in terms of the properties of polar molecules. To assess the applicability of these theories on magnetic fluids, the magnetic susceptibility as a function of concentration and interaction strength of high quality ferrofluids has been studied in chapter 3. The variation of interaction strength was accomplished by separating a polydisperse ferrofluid into fractions with different mean particle sizes, ranging from 8 to 15 nm. None of the prevailing theories describes the measured susceptibilities accurately, although three theories (the Mean Spherical Model, Perturbation Theory and Onsager's theory) are in fair agreement with the experimental data.

In chapter 4, two theories are described that are used to predict the stability of ferrofluids against liquid-gas phase separation. The theories show that phase separation in magnetic fluids may be induced by applying a magnetic field, if magnetic interactions between the colloids are sufficiently strong, about 3 kT. In ferrofluids, however, the interaction strength is only 1 kT, though due to polydispersity there will be a small fraction of large particles with much stronger interaction. Even though magnetic interactions alone may be too weak to enable phase separation in magnetic fluids, they will influence the stability of ferrofluids destabilized by other factors, for example by the presence of non-adsorbing polymer. Even without magnetic interactions, non-adsorbing polymer can induce colloidal gas-liquid phase separation in a colloidal dispersion. In chapter 4, a mean field theory for the phase behavior of colloid-polymer mixtures is extended to take magnetic interactions into account. Calculations with this modified theory show that magnetic interactions decrease the stability of colloid-polymer mixtures, and moreover, that the decrease in stability is stronger when a magnetic field is

applied. As oleic acid can also be considered as a small polymer, removal of excess oleic acid, which is not always done after the synthesis of magnetic fluids, can improve the stability of magnetic fluids.

In chapters 5 and 6, the stability of magnetic fluids containing poly(dimethylsiloxane), a non-adsorbing polymer, is studied experimentally. In chapter 5, it is set out in detail how phase separation is detected and quantified using a susceptibility meter based on a Colpitts oscillator. This instrument can make local measurements of the susceptibility in a sample tube; hence, the colloid concentration in each phase can be measured in a quick and non-destructive way. Moreover, the locations of phase boundaries and therefore the volumes of separate phases can be accurately determined. Chapter 5 also describes a method to obtain the polymer concentration in each separate phase by combining susceptibility measurements of samples with different colloid/polymer ratios. In principle, susceptibility measurements allow for the determination of the full phase diagram of colloid-polymer mixtures, including nodelines. In practice, however, translation of susceptibilities to concentrations was obscured, because phase separation is shown to be accompanied by strong size fractionation, and the susceptibility is very sensitive to changes in particle size.

The influence of a magnetic field on the stability of ferrofluid-polymer mixtures is investigated in chapter 6, using the same susceptibility meter as used in chapter 5 and a thermostated electromagnet. Without polymer, the ferrofluid is stable at all attainable field strengths (up to 30 kAm^{-1}) and all concentrations. This is inconsistent with many reports in literature, but may be due to the fact that a high quality ferrofluid was used here, i.e. without excess oleic acid and clusters. With polymer, the phase behavior in a magnetic field clearly deviates from the behavior in zero field. The decrease in stability caused by the magnetic field is somewhat stronger that predicted by the theory described in chapter 4, but still of the same order of magnitude. An open question is how the stability is affected by the considerable polydispersity (26%) of the magnetic colloids.

That magnetic colloids do not always behave as dipolar hard spheres is demonstrated in chapter 7. Using several experimental techniques, the existence of a strong, anomalous attraction between sterically stabilized magnetite particles and silica spheres was demonstrated. The attraction resulted in irreversible adsorption of magnetite particles, covering up to 30% of the silica surface. The adsorption kinetics appeared to be orders of magnitudes slower than that of a diffusion limited adsorption. Based on this and other observations, proton transfer mechanism was proposed as a possible mechanism to account for the strong attraction.

Samenvatting voor niet-vakgenoten

1.1 Inleiding

Zoals bij veel proefschriften het geval is, is de inhoud van dit proefschrift abstract en specialistisch, zodat weinigen hem zullen begrijpen. In het eerste hoofdstuk, de algemene inleiding, heb ik al een poging gedaan om het beschreven onderzoek uit te leggen aan vakgenoten met een ander specialisme. Deze samenvatting is speciaal bedoeld voor lezers zonder al te veel kennis van scheikunde en natuurkunde. Om mijn onderzoek een beetje te kunnen plaatsen, leg ik eerst iets uit over de dynamische 'microwereld' die bepaalde scheikundigen en natuurkundigen bezighoudt.

1.2 Stoffen onder de loep

Wat gebeurt er als je een klontje suiker doormidden breekt, beide delen weer breekt, en nog eens breekt, etc? Kun je daarmee tot in het oneindige doorgaan, of houdt het een keer op? Het laatste is het geval. Als je een suikerklontje vaak genoeg breekt, hou je een ondeelbaar suikerdeeltje over, een suiker *molecuul*. Zo'n molecuul is heel klein, ongeveer een tienmiljoenste deel van een millimeter groot. Dat is veel te klein om met het oog of zelfs met een gewone microscoop te zien, maar er bestaan inmiddels apparaten waarmee ze wel waargenomen kunnen worden.

Veel stoffen, of ze nou vast, vloeibaar of gasvormig zijn, bestaan uit moleculen; soms maar één soort molecuul (suiker bijvoorbeeld, of puur water), soms een mengsel van moleculen (zoals koffie). De hoedanigheid van een stof wordt bepaald door de onderlinge afstand tussen de moleculen en hun ordening (zie figuur 1). In een gas bijvoorbeeld, zitten de moleculen ver van elkaar; ertussen zit niets, vacuüm. Door die grote leegtes in een gas kun je meer lucht in een fietsband pompen, zonder dat de inhoud toeneemt. Bij een vloeistof is dat anders; als een fles water eenmaal vol zit, kun je er niet nog meer water in krijgen. Dat komt omdat in een vloeistof de moleculen zo dicht op elkaar gepakt zitten, dat er nauwelijks plaats is voor meer moleculen. In een vaste stof, tenslotte, zitten de moleculen ook dicht gepakt, maar zijn ze ook nog eens geordend.

Als je zo'n sterke microscoop zou hebben dat je moleculen kon zien, zou je de ordening zoals geschetst in figuur 1 kunnen zien. Maar je zou ook nog iets anders zien: moleculen bewegen en botsen onophoudelijk, en des te hoger de temperatuur, des te wilder de bewegingen. Het

enige dat voorkomt dat moleculen direct de wijde wereld in vliegen is hun onderlinge aantrekkingskracht.   Zonder   die   aantrekking   zouden   de
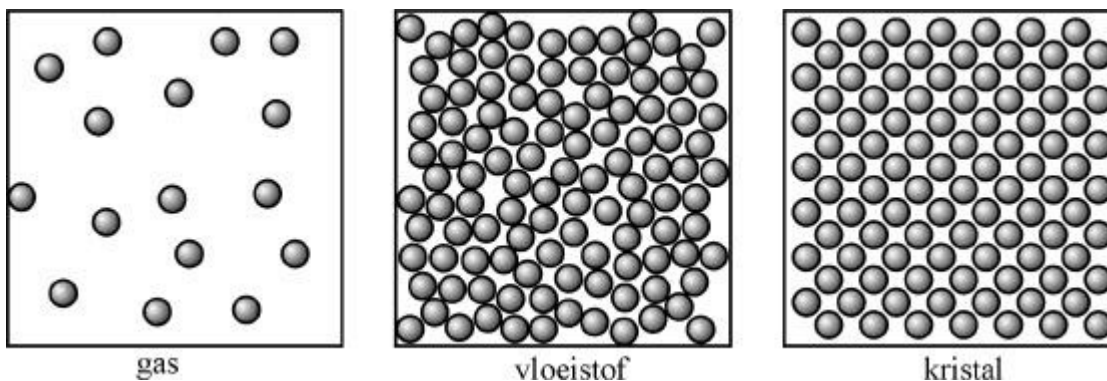
Figuur 1. *Schematische voorstelling van een gas, een vloeistof en een kristal, waarin moleculen (of colloïden) zijn voorgesteld als bolletjes.*

oceanen droog staan en zouden planten en dieren verdampen.

Nu is ook duidelijk wat er gebeurt bij het verhitten van een stof: de molecuul bewegingen worden sneller, totdat een temperatuur wordt bereikt waarbij de aantrekkingskracht de moleculen niet meer bij elkaar kan houden. De stof gaat dan over in een andere *fase* (hoedanigheid); eerst van de vaste naar de vloeibare fase (smelten), vervolgens van de vloeibare naar de gasfase (verdampen). Tijdens de overgang komt de stof in twee fasen met verschillende concentraties voor (fase evenwicht); de overgang vordert doordat de hoeveelheid nieuwe fase toeneemt ten koste van de oude fase.

1.3   Colloïden

Iets groter dan moleculen zijn *colloïden*, deeltjes met een afmeting tussen een miljoenste millimeter en een duizendste millimeter, meestal zwevend in een vloeistof. Het geheel van colloïden en oplosmiddel wordt een *dispersie* genoemd. Colloïden zijn alom aanwezig, bijvoorbeeld in de vorm van eiwitten en vetdruppeltjes in melk, kleine pigmentkorreltjes in verf, of rode bloedcellen in bloed. Onder invloed van de zwaartekracht zakken colloïden wel naar de bodem (of drijven ze naar boven), maar door hun kleine afmeting gaat dat heel langzaam.

Door de continue botsingen met vloeistofmoleculen zijn colloïden, net als moleculen, ook steeds in beweging. Maar anders dan bij moleculen, zijn de grillige bewegingen van colloïden wèl met een microscoop te zien. Deze zogenaamde *Brownse beweging* is vernoemd naar Robert Brown, die de beweging al in 1827 waarnam in suspensies van stuifmeelkorrels in water. Het was Albert Einstein die later de Brownse beweging in verband bracht met de

botsingen met moleculen.

De overeenkomst tussen moleculen en colloïden gaat verder dan beweging. Colloïden trekken elkaar ook aan, en afhankelijk van hun beweeglijkheid en aantrekkingskracht kunnen ze ook voorkomen in de verschillende fasen die in figuur 1 geschetst zijn. Het 'gas' is bij colloïden wat paradoxaal, omdat de dispersie als geheel is een vloeistof. De aanduiding 'gas' zegt alleen maar iets over de colloïden en hun onderlinge afstand. Tussen de colloïden zit vloeistof, wat een colloïdaal gas vloeibaar maakt. Naast de drie geschetste fasen zijn er nog meer hoedanigheden mogelijk. Als de aantrekkingskracht sterk genoeg is, kunnen colloïden een 'gel' vormen, waarin de colloiden een vertakt netwerk vormen, enigszins vergelijkbaar met een spons.

Het onderzoek naar fase overgangen in colloidale dispersies is vanuit meerdere perspectieven interessant. Voor toepassingen is het vaak van belang om de fase waarin colloïden voorkomen te beheersen. Een schilder wil verf met een homogene samenstelling, en zal dus niet tevreden zijn met een verf die uit twee fasen bestaat. Bij kaas moeten de colloïden elkaar juist sterk aantrekken zodat ze een gel vormen. Colloïdale dispersies worden ook gebruikt om meer inzicht te krijgen in de factoren die een rol spelen bij fase overgangen. Dus door naar colloïden te kijken, kun je meer te weten komen over het gedrag van moleculen. Er zijn meerdere redenen waarom je zulk onderzoek doet met colloïden in plaats van moleculen. Ten eerste zijn colloïden makkelijker op microscopische schaal te bekijken (bv. met een microscoop), omdat ze veel groter zijn dan moleculen en veel langzamer bewegen. Bovendien kan de aantrekkingskracht tussen colloïden gevarieerd worden, wat een onderzoeker in staat stelt om het effect van aantrekkingskracht los van andere factoren te bekijken. En als laatste hebben colloïden een bekende, vaak eenvoudige vorm, wat de verklaring van waargenomen effecten vereenvoudigt.

1.4 Onderzoek beschreven in dit proefschrift

Ik heb onderzoek gedaan aan zogenaamde *magnetische vloeistoffen*, vloeistoffen met sterk magnetische eigenschappen. Zo wordt een magnetische vloeistof zo sterk door een magneet aangetrokken, dat hij er ondersteboven aan kan blijven hangen. Hiervan wordt gebruik gemaakt onder andere bij de toepassing van magnetische vloeistof als smeermiddel voor harddisks; door de as van de harddisk magnetisch te maken, blijft de (magnetische) olie netjes op zijn plek en dicht het de binnenkant van de harddisk stofvrij af.

Een magnetische vloeistof is een dispersie van magnetische colloïden, meestal magnetiet deeltjes (magnetiet is een ijzer bevattend magnetisch mineraal) van ongeveer een honderdduizendste millimeter groot in een benzine-achtig oplosmiddel, cyclohexaan. Zonder

tegenmaatregelen zou de aantrekking tussen de deeltjes zo sterk zijn, dat ze onmiddellijk aan elkaar zouden plakken en snel op de bodem zouden liggen: einde magnetische vloeistof. Om dat te voorkomen, is elk deeltje bedekt met een dun laagje vetzuur (zie hoofdstuk 1, figuur 1.3) waardoor ze elkaar niet meer kunnen raken. Een procedure voor het bedekken staat beschreven in hoofdstuk 2.

Bij veel colloïden is de aantrekkingskracht in alle richtingen gelijk. Magnetische colloïden vormen daarop een uitzondering. De magnetietdeeltjes zijn kleine magneetjes met een noord- en een zuidpool, en hun onderlinge aantrekking of afstoting hangt af van hun oriëntatie: als twee deeltjes met de noorpolen (of de zuidpolen) tegen elkaar aanliggen, stoten ze elkaar af. Twee ongelijke polen trekken elkaar juist aan. Wat doet dat met een magnetische vloeistof: zorgt de aantrekking voor een fase overgang? Dit is de centrale vraag in dit proefschrift.

Het antwoord op deze vraag is op twee manieren onderzocht. Allereerst is in hoofdstuk 4 een theorie beschreven waarmee voorspellingen kunnen worden gedaan over het al dan niet optreden van een fase overgang in magnetische vloeistoffen. Het bijzondere van magnetische colloïden is dat de orientatie van de magneetjes wordt beïnvloed door een uitwendig magnetisch veld. Net als een kompasnaald draaien de magneetjes zich naar de richting van het magnetisch veld, wat leidt tot een versterking van de gemiddelde aantrekkingskracht tussen de deeltjes. Een magnetisch veld kan op die manier een fase overgang teweeg brengen. Het blijkt dat voor de meest gebruikte magnetische vloeistoffen de magnetische aantrekkingskracht te zwak is om een fase overgang te veroorzaken, zelfs in een sterk magneetveld. Die conclusie lijkt in strijd met wat experimenteel vaak gevonden is, namelijk dat een magnetisch veld wel een fase overgang veroorzaakt. De oorzaak van die discrepantie kan de aanwezigheid van vervuiling in magnetische vloeistoffen zijn. Inderdaad volgt uit de berekeningen dat een vervuiling, hier in de vorm van een polymeer, het experimenteel gevonden gedrag kan verklaren.

Om die conclusie te testen, zijn er ook experimenten gedaan, waarbij een gecontroleerde hoeveelheid polymeer aan een 'schone' magnetische vloeistof werd toegevoegd. Omdat een magnetische vloeistof te zwart is om er doorheen te kunnen kijken, moest iets anders bedacht worden om te bepalen of hij uit één of meerdere fasen bestaat. Een soort metaaldetector, waarmee eenvoudig de concentratie bepaald kon worden, bleek uitermate geschikt (zie hoofdstuk 5, figuur 5.1). Het optreden van de fase overgang bij voldoende hoge vervuiling werd daarmee ook experimenteel gevonden. Het is ook gebleken (hoofdstuk 6) dat een magnetisch veld inderdaad een fase overgang kan veroorzaken, maar alleen in de aanwezigheid van voldoende polymeer, zoals de theorie voorspelde.

Dankwoord

Eén proefschrift, één naam. Eigenlijk doet het geen recht aan al die mensen die hebben bijgedragen aan dit proefschrift. Gelukkig is er nog plaats voor een dankwoord.

Allereerst bedank ik Albert, mijn promotor voor de vrijheid die je me hebt gegeven tijdens het onderzoek, en het vertrouwen en enthousiasme dat ik kreeg voor nieuwe onderzoeksplannen. En ondanks de strakke planning van je eigen werkzaamheden stond je deur nagenoeg altijd open en *maakte* je altijd tijd voor discussie. Ik heb ook veel waardering voor de snelheid en grondigheid waarmee je teksten nakeek, iets wat dit proefschrift zeker ten goede is gekomen.

Naast Albert heeft Gert Jan, mijn co-promotor, een enorme bijdrage geleverd aan mijn proefschrift. Gert Jan, ik mag alleen maar hopen dat ik iets van je grondigheid bij het bekijken van theorie *en* experimentele resultaten heb overgenomen. Je snelle inzicht bij het bespreken van werkelijk alle resultaten heeft mij zeer geholpen.

Op het instrumentele vlak ben ik Bonny zeer erkentelijk. Je hebt altijd met volle inzet en zelfstandigheid gewerkt aan apparatuur die voor mijn onderzoek zeer essentieel zijn geweest. Wat had ik zonder jou moeten doen?

Ook de glasblazers Igno, Peter, Piet en Maarten en instrumentmakers Kees en Gerard hebben vele steentjes en stenen bijgedragen aan dit boekje, waarvoor dank. Op het Van 't Hoff lab werd het werk vergemakkelijkt door de secretariële ondesteuning van Marina, Hanneke en Mieke, de computerhulp van Carel en de chemische ondersteuning van Haran.

De studenten Rick, Marco, Jilles, Stan, Sanne en Ben hebben veel initiërend werk verricht, waarop bijna altijd is voortgebouwd. Mooi werk! Marco, molte grazie.

Voor posters, de kaft van dit proefschrift, en veel andere hulp ben ik het team van de audio-visuele dienst, Jan, Ingrid en Aloys, dank verschuldigd. Henk Pluijgers en Pim van Mourik zijn altijd zeer behulpzaam geweest bij het bedienen van de electronenmicroscoop. Het engelengeduld van Maarten Terlou kwam goed van pas bij het analyseren van TEM foto's.

De niet-stoffelijke bijdrage aan dit proefschrift komt van de vele collega's die voor de zeer aangename, amicale sfeer zorg(d)en, zowel op het Van 't Hoff lab als daarbuiten. Ik zal blij zijn als dit proefschrift af is, al is het alleen maar om de gezelligheid bij de koffiepauzes weer mee te maken. Mijn (ex-)kamergenoten Willem, Liesbeth, Tjerk en Karen zorgden ook nog eens voor een levendige sfeer op de kamer.

Pa en ma, jullie geloof in de juistheid van mijn keuzes en steun in alles wat ik heb gedaan hebben me enorm geholpen.

Marjolein, jij hebt de eindsprint van dit promotieonderzoek aanzienlijk veraangenaamd, meer dan je zelf denkt. Nog even, en dan mag je zelf promoveren. Ik hoop dat ik je net zoveel rust kan aanpraten als je bij mij hebt gedaan.

Curriculum vitae

De schrijver van dit proefschrift werd op 22 november 1971 geboren in Zeist. Nadat hij in 1990 zijn VWO diploma had behaald aan het Revius Lyceum in Doorn, begon hij in datzelfde jaar aan de studie Scheikunde aan de (toenmalige) Rijksuniversiteit Utrecht. In januari 1996 studeerde hij af, na bijvakken chemische informatica en thermodynamica, een afstudeeronderzoek bij anorganische chemie en een stage bij Gastec B.V. in Apeldoorn te hebben afgerond. Vanaf augustus 1996 werkte hij voor de Universiteit Utrecht als Assistent In Opleiding bij het Van 't Hoff Laboratorium voor Fysische en Colloïdchemie, en verrichtte het onderzoek wat heeft geleid tot dit proefschrift. Van augustus 2000 tot oktober 2001 zal de schrijver als post doc onderzoek doen bij het Van 't Hoff Laboratorium.

List of publications

G. A. van Ewijk, G. J. Vroege, A. P. Philipse, "Convenient preparation methods for magnetic colloids", *J. Magn. Magn. Mater.* **201**, 31 (1999).

G. A. van Ewijk, A. P. Philipse, "Preparation and properties of silica core-magnetite shell colloids" (in preparation).

G. A. van Ewijk, G. J. Vroege, A. P. Philipse, "Magnetic susceptibility of fractionated ferrofluids" (in preparation).

G. A. van Ewijk, G. J. Vroege, B. W. M. Kuipers, "Phase behavior of magnetic colloid-polymer mixtures: a magnetic sensing coil study" (in preparation).

G. A. van Ewijk, G. J. Vroege, B. W. M. Kuipers, "Phase behavior of magnetic colloid-polymer mixtures: influence of magnetic field" (in preparation).

G. A. van Ewijk, A. P. Philipse, "Anomalous attractions between colloidal magnetite and silica spheres in apolar solvents", *Langmuir* (submitted).